POLITECNICO DI MILANO

Facoltà di Ingegneria
Dipartimento di Chimica, Materiali ed Ingegneria Chimica
"Giulio Natta"
Corso di Laurea Specialistica in Ingegneria dei Materiali

ORGANIC LUMINESCENT SOLAR CONCENTRATOR DEGRADATION AND PHOTOVOLTAIC PROPERTIES

Relatori: Prof. Stefano TURRI
Prof.ssa Mirella DEL ZOPPO
Correlatori: Dott. Gianmarco GRIFFINI
Dott. Luigi BRAMBILLA

Tesi di Laurea Specialistica di
Antonio Massimo Sguazzini
Matr. 751758

Anno Accademico 2010-2011

ESTRATTO IN LINGUA ITALIANA
Concentratore Solare Luminescente Organico
Studio del processo di degradazione e proprietà fotovoltaiche

Introduzione

La radiazione solare incidente la superficie terrestre rappresenta un'incredibile fonte di energia rinnovabile. La tecnologia disponibile, in grado di convertire l'energia solare in energia elettrica, è limitata. I dispositivi che convertono direttamente la luce solare in energia elettrica, le celle fotovoltaiche, possono convertire solo una frazione di questa radiazione dal momento che sono composti da materiali che possono assorbire solamente un definito range di lunghezze d'onda.
Per superare questo limite aumentando la quantità di fotoni che possono essere assorbiti dalle celle fotovoltaiche sono sfruttati i Luminescent Solar Concentrators (LSC). Tali dispositivi assorbono la porzione di radiazione solare non assorbita dalla cella, riemettendo per fenomeno di fluorescenza, fotoni energicamente più affini ai gap energetici dei materiali.
Nel caso di LSC realizzati con matrice organica e dye organico, si parla di Organic Luminescent Solar Concentrator (OLSC).
Questo lavoro focalizza la sua attenzione in parte sulla realizzazione di un dispositivo funzionante ottenuto dall'accoppiamento di un OLSC a film sottile con una cella fotovoltaica, dall'altro lo studio della fotodegradazione del materiale attivo luminescente.

Parte sperimentale

I film sottili impiegati nello studio di degrado e per la realizzazione del dispositivo OLSC sono stati realizzati deponendo per spincoating una soluzione di PMMA e Lumogen F Red 305 in cloroformio con PMMA al 10% rispetto al cloroformio.
Nello studio del degrado inoltre sono stati studiati anche film sottili di solo dye e di solo PMMA, per studiare separatamente gli effetti della radiazione UV sui materiali che compongono il materiale attivo dell'OLSC.
Lo studio del degrado si è avvalso delle tecniche spettroscopiche FTIR, UV-vis e di fluorescenza, con lo scopo di identificare un processo di degrado.
L'OLSC è stato realizzato deponendo per spincoating su un substrato di vetro le soluzioni di materiale luminescente. Il concentratore così realizzato è stato quindi accoppiato alla cella fotovoltaica. Per studiare il miglioramento di efficienza che si verifica grazie all'accoppiamento del concentratore, misure I-V sono state effettuate su diversi set di celle fotovoltaiche prima dell'applicazione e successivamente all'incollaggio del concentratore. Attraverso il confronto delle medie dei valori raccolti è stato possibile definire un miglioramento di efficienza. È stata quindi valutata la dipendenza dell'efficienza del dispositivo accoppiato dalla concentrazione di dye disciolto in matrice, ed è stato effettuato uno studio preliminare sulla dipendenza dell'efficienza rispetto allo spessore del materiale luminescente.

Risultati e discussione

Studio di degrado

Lo studio del degrado del materiale luminescente si è concentrato sugli effetti causati dall'esposizione alla radiazione UV a campioni di sola matrice polimerica, di solo dye, e infine sul materiale luminescente (in questa sezione chiamato PL6, dove 6 è relativo alla concentrazione di dye, al 6% rispetto al PMMA). Tali effetti sono stati valutati dall'analisi degli spettri raccolti attraverso le tecniche spettroscopiche UV-vis, FTIR e di fluorescenza.
Dall'analisi degli spettri di assorbimento UV-vis di campioni di PMMA degradato si

osserva un aumento di intensità nella regione tra i 250 e i 350 nm. Il picco principale centrato a 230 nm nello spettro pristino, subisce un blue-shift crescente all'aumentare del tempo di esposizione. A un iniziale incremento di intensità di assorbimento del picco, probabilmente dovuta a una variazione di proprietà ottiche della superficie, segue una graduale riduzione dell'intensità del picco che può essere dovuta a una parziale perdita di materiale.

La degradazione del PMMA èstata quindi monitorata attraverso la spettroscopia FTIR. Sebbene in tutto lo spettro si verifichi una generalizzata riduzione delle intensità, si osserva la formazione di due bande. In particolare a 3500 cm^{-1} e dall'allargamento del picco centrato a 1731 cm^{-1} e attribuito alla vibrazione del legame C=O. All'aumentare del tempo di esposizione alla radiazione UV, l'intensità del picco a 1731 cm^{-1} decresce gradualmente ma contemporaneamente si definisce un nuovo picco fra 1754-1760 cm^{-1} che può essere atttribuito a specie ossidate.

Lo spettro di assorbimento UV-vis del dye organico mostra due principali bande di assorbimento. Attraverso il confronto con lo spettro di assorbimento di una molecola simile (Perilendiimide, PDI) è stato possibile attribuire il picco più energetico centrato a 445 nm ai sostituenti laterali e il picco strutturato centrato a 568 nm all'assorbimento del core perilenico. Attraverso questa identificazione è stato possibile monitorare separatamente la degradazione dei due gruppi della molecola. Dal confronto tra i due andamenti non si osserva una marcata differenza nei due andamenti. Si può appena intuire una maggiore rapidità di scomparsa dei sostituenti laterali rispetto al core perilenico.

Dall'analisi dello spettro UV-vis del solo dye si è riscontrato inoltre un red-shift di 5 nm del picco principale, probabilmente dovuto a una perdita di coniugazione della molecola.

Sono stati quindi raccolti gli spettri di emissione da campioni di solo dye. Le strutture degli spettri di emissione del dye eccitato con lunghezze d'onda 445 nm e 540 nm mostrano la stessa struttura, lasciando intuire l'assenza di fenomeni di emissione contrastanti. Dallo studio della degradazione attraverso la fluorescenza non si sono riscontrati andamenti differenti, in accordo con la teoria.

Infine il dye è stato analizzato per mezzo della spettroscopia infrarossa. Attraverso il confronto con molecole simili, alcuni picchi caratteristici dello spettro FTIR del dye sono stati attribuiti al core perilenico (1586 cm^{-1} e 1342 cm^{-1}) oppure ai sostituenti laterali (877 cm^{-1}).

La spettroscopia è stata quindi sfruttata per l'analisi di campioni di PL6. Dagli spettri di fluorescenza si riscontra, come avvenuto per l'analisi degli spettri di emissione del solo dye, l'assenza di fenomeni di emissione contrastanti poiché i due spettri di emissione ottenuti eccitando il materiale a 445 nm e 540 nm presentano struttura identica.

Gli spettri di assorbimento UV-vis dei campioni PL6 pristini mostrano una struttura del tutto simile a quelli ottenuti dai campioni di solo dye. Si verifica però uno spostamento del picco principale da 568 nm in solo dye, a 576 in PL6.

Gli spettri di PL6 esposto a radiazione UV mostrano una graduale riduzione delle intensità di assorbimento, con una cinetica nettamente più rapida rispetto a quella riscontrata dallo studio attraverso spettroscopia UV-vis dei campioni di solo dye. Inoltre si osserva un red-shift di 8 nm del picco principale. Dal confronto dell'andamento della degradazione del picco centrato a 445 nm rispetto all'andamento del picco a 576 nm, si osserva che il picco centrato a 445 nm decresce più rapidamente. Questa differenza di cinetica lascia intuire una più rapida degradazione dei sostituenti laterali rispetto al core perilenico.

Simile osservazione si intuisce dallo studio dei campioni di PL6 attraverso spettroscopia infrarossa.

Inoltre, dal confronto fra gli andamenti di fotodegradazione del dye nel caso di campioni di solo dye e di PL6, si osserva che il dye risulta essere marcatamente più sensibile e instabile alla radiazione UV nel caso in cui è disciolto in matrice. Per studiare la stabilità del dye in campioni di solo dye sono state effettuate prove di calorimetria DSC e prove 1H-NMR. Entrambe verificano l'ipotesi di stabilità.

Risultati e discussione

Dispositivo OLSC

L'OLSC è stato realizzato mediante la deposizione mediante spincoating di un film di

materiale luminescente (PMMA e Lumogen) su un substrato di vetro, il cui spessore si comporta da guida d'onda per la luce raccolta. L'OLSC è stato quindi accoppiato a una cella fotovoltaica attraverso uno dei suoi bordi. La cella è stata accuratamente scelta perchè le dimensioni della superficie attiva risultassero molto simili a quelle del bordo del substrato di vetro.
La realizzazione del dispositivo ha mostrato in fase di assemblaggio diverse difficoltà. Al fine di ottenere una buona ripetibilità nei risultati elettrici, è stato definito un metodo standard di assemblaggio. Una squadra di acciaio posta su una piastra riscaldante ha operato da guida per ottenere perpendicolarità tra il concentratore e la cella, garantendo contemporaneamente una buona conducibilità termica necessaria a riscaldare il materiale adesivo (Krystalflex PE 399) utilizzato per legare la cella al concentratore.
Le valutazioni dell'efficienza del concentratore sono state effettuate mediante misurazioni I-V, e l'efficienza del concentratore è stata valutata in relazione a due parametri: la concentrazione del dye e lo spessore del film.
Per valutare il guadagno in efficienza di ogni singolo dispositivo, le prove elettriche prima sono state effettuate sulle sole celle e, dopo la fase di assemblaggio, sono state ripetute sul dispositivo montato. Per ogni condizione imposta sono state effettuate più prove al fine di considerare dei valori medi e di avere quindi una maggiore affidabilità.
Nel caso della concentrazione di dye variabile è stata effettuata un'analisi completa. In corrispondenza della concentrazione di dye al 12% rispetto al PMMA, il dispositivo mostra un guadagno di efficienza negativo. L'andamento di efficienza mostra due trend differenti. Per basse concentrazioni di dye l'efficienza aumenta fino a raggiungere un massimo in corrispondenza del 5% rispetto al PMMA. Per concentrazioni superiori invece l'efficienza mostra un andamento negativo.
È stato infine effettuato uno studio preliminare sulla dipendenza dell'efficienza del dispositivo dallo spessore del materiale luminescente, mantenendo la concentrazione di dye ottimale trovata nel caso dello studio della concentrazione di dye. Sono stati studiati dispositivi realizzati da soluzioni con concentrazioni di PMMA al 1%, 5% e 10% rispetto al cloroformio. La concentrazione di PMMA al 10% rispetto al cloroformio risulta ancora quella in corrispondenza della quale si riscontra il massimo guadagno in efficienza.

Conclusioni

L'analisi dei risultati ottenuti dagli spettri di assorbimento e di emissione permette la formulazione di alcune ipotesi sui meccanismi di degrado. In prima osservazione si può ipotizzare che la decomposizione dei sostituenti laterali sia più rapida del core perilenico. Questo si osserva soprattutto negli studi effettuati sui campioni PL6.
Le analisi spettroscopiche inoltre suggeriscono la stabilità del dye alla radiazione UV quando è esposto in campioni di solo dye e la sua instabilità quando è disciolto nella matrice polimerica. Le ipotesi di stabilità del dye nei campioni di solo dye è inoltre supportata dalle analisi calorimetriche effettuate e dagli spettri 1H-NMR. Il motivo dell'instabilità del dye quando è disciolto in matrice può essere l'assenza di ordine cristallino. Infatti, la fase amorfa presente in grandi quantità in campioni PL6 può subire una degradazione molto più rapida. Contrariamente, grazie ad un elevato grado di cristallinità, i campioni di solo dye mostrano un'elevata stabilità all'esposizione alla radiazione UV.
Inoltre, dal confronto fra le cinetiche di degrado di campioni di solo PMMA e di PL6, si può supporre che il dye si comporti da assorbitore di radiazione UV, proteggendo la matrice polimerica dal momento che i campioni di PMMA degradano molto più velocemente rispetto ai campioni di PL6.

Lo studio delle efficienze dei dispositivi OLSC è stato limitato a causa di una scarsa ripetibilità dei valori ottenuti. La ripetibilità delle misure elettriche è risultato molto limitato a causa delle scarsa qualità mostrata dalle celle a disposizione (elevati valori di deviazione standard nel caso di Fill Factor e V_{OC}). Nonostante gli alti valori di errore riscontrati, le misure ottenute hanno dimostrato che è comunque possibile l'individuazione di massimi di efficienza.

Index

Premise

The Luminescent Solar Concentrator (LSC) is a solar cell supporting device. It collects the solar spectrum and converts a portion poorly absorbed by Silicon solar cells of the sun light to radiation in the absorption spectrum of Si cells. It permits an increase of the cell efficiency while it is bound to the cell through its edge.

LSC technology adopts luminescent materials. Quantum dots or equally luminescent organic dyes are used in LSC technology. These two different concentrators rely to different light conversion principles and, on the other hand, present different performances and different stability when exposed to solar radiation.

The stability to sun light and to outdoor degradation are the mostly studied causes of aging. LSC coupled to solar cells are then studied by means of power conversion and of increase in electrical efficiency.

The purpose of the research performed during this thesis was the development of an efficient Organic Luminescent Solar Concentrator (OLSC), realized by mixing an organic luminescent dye into a polymeric carrier matrix.

OLSCs can be developed in the shape of plates or thin films. In the present work, thin film OLSC were realized.

Materials were chosen in order to comply with the requirements of thin film OSLC technology. The luminescent material was realized by mixing Lumogen F Red 305 dye in a carrier matrix (PMMA). Lumogen F Red 305 is a commercial available high efficient lumescent dye. The chosen binder shows a refractive index matching with the refractive index of the glass substrate adopted as carrier for emitted photons.

Through spectroscopic analyses, optical and molecular properties of the adopted materials were defined. In order to define the resistance of the thin film OLSC to light exposure, accelerated aging process were performed through the exposure of deposited samples under an UVB radiation emitted by a 500W UV lamp.

A degradation process was defined by means of optical and molecular variations, collected by UV-vis, fluorescence and FTIR spectroscopies. In order to prevent the identified degradation process, preliminar studies of protective materials were carried out.

Secondly, thin film OLSCs were mounted on Silicon solar cells, and electrical measurements were performed in order to calculate variations in efficiency. The fabrication of the OLSC mounted device was performed by linking an edge of the OLSC to the active

surface of the solar cell. In order to reduce as possibile reflections occurring at the interface between the OLSC and the active area of the cell, a supporting material with refractive index matching with the glass refractive index was chosen. OLSC was coupled to the PV cell through a thermosoftening organic material.

Although, the fabrication can present several realization inaccuracies. In order to ensure repeatability in the efficiency calculations, PV cells need to be high quality products. In addition, the bonding stage need to ensure perfect perpendicularity between the OLSC and the cell active surface in order to reduce photon losses due to reflections at the interface.

Several OLSC parameters can be independently studied in order to optimize the electrical efficiency of the OLSC mounted device. The dependence of the efficiency on the dye concentration represent a key feature in the OLSC device optimization, as theoretically two divergent phenomena occur. Low dye concentration convert few photons and electrical efficiencies are low in values. In high dye concentrated films, reabsorption losses are amplified, leading to low efficiency values. Therefore, a maximum in efficiency can be found related to the optimized dye concentration.

In addition, the electrical efficiency of the OLSC device depends on the film thickness, the active surface area of the OLSC and on many geometrical and fabrication features, such as reflecting coatings on the edges which are not linked to the cell and backreflector side coatings.

In this work, electrical measurements were evaluated in dependence of the dye concentration in the dye-doped luminescent material and the film thickness.

Chapter I
Introduction

Presently, the world energy consumption is 10 terawatts (TW) per year, and by 2050, it is projected to be about 30 TW. The world will need about 20 TW of non-CO_2 emitting energy to stabilize CO_2 in the atmosphere by mid-century. The simplest scenario to stabilize CO_2 by mid-century is one in which photovoltaics (PV) and other renewables are used for electricity (10 TW), hydrogen for transportation (10 TW), and fossil fuels for residential and industrial heating (10 TW) [3,4]. Thus, PV will play a significant role in meeting the world future energy demand.

The PV effect was discovered in 1839 by Becquerel while studying the effect of light on electrolytic cells. A long period was required to reach sufficiently high efficiency. Solar cells developed rapidly in the 1950s owing to space programs and used on satellites. The energy crisis of the 1970s greatly stimulated research and development for PV.

Solar cells based on compound semiconductors were first investigated in the 1960s. At the same time, polycrystalline Si (pc-Si) and thin-film solar cell technologies were developed to provide high production capacity at reduced material consumption and energy input in the fabrication process, and integration in the structure.

I.1 Renewable Energy Sources

The renewable energy sources available are largely covered by hydropower, biomass energy, solar energy, wind energy, geothermal energy, and ocean energy.

When comparing all these technologies according to the theoretical potential (how much energy there is available), the technical potential (how much we can extract), and the current use, it quickly becomes apparent that solar energy is used little, while there is a massive theoretical and technical potential for its use. Therefore solar energy is a renewable energy with a large potential. This is the motivation for many scientists working in this field.

I.2 Solar Energy

We receive plenty of energy from the sun and the challenge is simply to make use of it. The side of the earth that is exposed to the sun receives approximately 1.2×10^5 TW from the sun continuously [1]. Even with the projected doubling of our energy consumption over the next 50 years, there is plenty of energy available from the sun alone. The plentitude is such that we can easily accommodate for energy conversion factors well below 100% and we still have to cover only a fraction of the earth's surface with energy extraction devices such as solar cells. There are obvious logistical problems associated with solar energy because the energy we receive and convert into electricity is lost if it is not used as it is generated.

The photovoltaic (PV) cell is the main important solar energy conversion device, as it converts solar energy in electricity.

I.3 Photovoltaic Cell

The archetypical photovoltaic device is a silicon-based pn-junction. Since its first fabrication, the silicon solar cell has taken many forms and is by far the most exploited photovoltaic technology.

In order to overcome silicon-based photovoltaic cells limits, PV technology has studied several inorganic and organic materials and compounds.

I.3.1.Working principles of solar cells

Photovoltaic energy conversion in both inorganic and organic solar cells consists of two steps. First, absorption of light generates an electron-hole pair. The electron and the hole are then separated by the structure of the device thus generating electrical power.

I.3.1.1.Inorganic Solar Cells

Photodetection in semiconductors works on the general principle of the creation of electron-hole pairs under the action of light [21-25].

When a semiconductor material is illuminated by photons of an energy greater than or equal to its bandgap, the absorbed photons promote electrons from the valence band into excited states in the conduction band, where they behave like free electrons able to travel long distances across the crystal structure under the influence of an intrinsic or externally-applied electric field. In addition, the positively-charged holes left in the valence band contribute

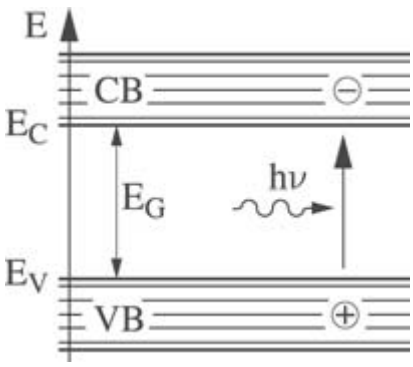

FigureI. 1-Radiative generation of an electron-hole pair

to electrical conduction by moving from one atomic site to another under the effects of the electric field (FigureI. 1). In this way the separation of electron-hole pairs generated by the absorption of light gives rise to a photocurrent, which refers by definition to the fraction of the photogenerated free charge-carriers collected at the edges of the material by the electrodes of the photodetecting structure, and whose intensity at a given wavelength is an increasing function of the incident light intensity.

Photovoltaic photodetectors use the internal electric field of a p-n or Schottky (metal-semiconductor) junction to achieve the charge separation. Photovoltaic photodetectors include photovoltaic structures consisting of a simple p-n junction, and p-i-n photodetectors which comprise a thin layer of semiconductor material between the p and n region which is not deliberately doped, as well as all Schottky junction photodetectors.

Solar cells are photovoltaic photodetectors (or photodiodes) characterized by wide absorbing surface as their aim is to generate high photocurrents. A photodiode is a p-n junction or p-i-n structure.

In p-n diodes, the interface between a region of a p-type doped semiconductor and a region of n-type doped-semiconductor forms a p-n junction, where the joining of the Fermi levels in equilibrium mostly occurs through a flow of charge between the n and p regions. In equilibrium we therefore find a region with no free charge carriers immediately around the junction, while there are, on the n side, positively ionized donors and, on the p side, negatively ionized acceptors. This region is known as the space charge region (SCR) or depletion region. The presence of charged donors and acceptors around the depletion region produces an electric field in that region which curves the energy bands and, in equilibrium, forms an energy barrier between the two regions: the bottom of the conduction band and the top of the valence band on the n side are below the corresponding levels on the p side (FigureI. 2).

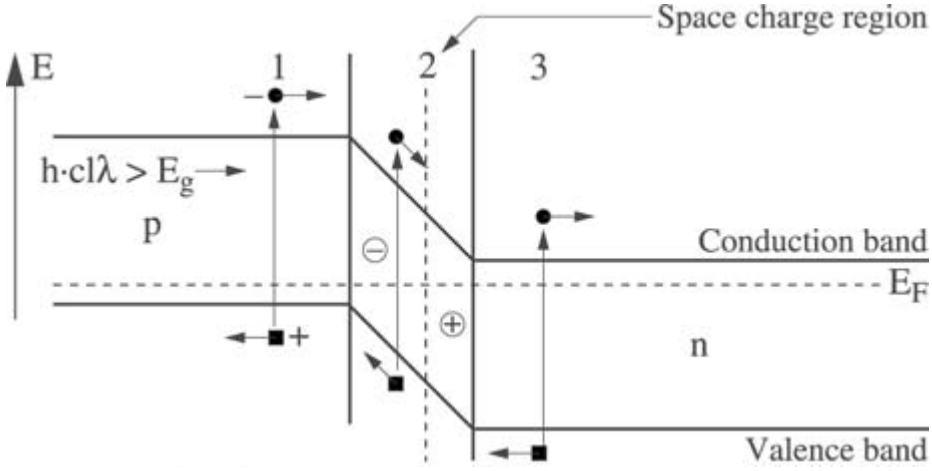

FigureI. 2 - Curvature of the energy bands and mechanisms of photocurrent generation in a p-n junction

The width of the SCR is a decreasing function of the level of doping in the material, while the height of the energy barrier is an increasing function of it. An electron-hole pair produced in this SCR (situation 2 in FigureI. 2) is therefore separated by the effect of the internal electric field of the junction, and so does not recombine. These are the charge carriers which contribute to the photocurrent, to which we can add, to some extent, those generated at a distance from the junction less than or equal to the diffusion length (situations 1 and 3 in FigureI. 2).

The band structure of the junction implies that the photocurrent will consist of minority charge carriers. For this reason, the photocurrent flows in the opposite direction to the bias on the diode, where the forward direction is defined as the direction of flow of the majority charge carriers (from the n to the p region in the case of electrons, and vice versa for holes). Moreover, the application of an opposing external electric field ($Vp–Vn < 0$) allows us to increase the height of the energy barrier in the vicinity of the junction, and also increase the spatial extent of the SCR, which significantly improves the efficiency of the separation of electron-hole pairs by increasing the electric field within the junction [21-24].

A simple means of increasing the spatial extent of the SCR is to introduce between the n and p regions a thin layer of intrinsic semiconductor material which is not intentionally doped: the structure is therefore referred to as p-i-n. Such a structure is interesting because it is possible to maintain high levels of doping in the n and p regions without significantly reducing the extent of the SCR, whose width is then largely determined by the thickness of the "i" layer [21-24].

I.3.1.2.Organic Solar Cells

In organic materials electrons are rather localised [1, 22]. This results in large effective masses, small mobilities and small diffusion coefficients [18]. Optical excitation leads to excited species called excitons, i.e. An electron-hole pair hightly bound with binding energies much larger than kT (where k is the Boltzmann constant and T is the absolute temperature). These excitons are stable against thermal ionisation at room temperature.

In addition electron states exist for free electrons which are more extended. They allow transport over large distances. Following semiconductor terminology, we call these states conduction states with a lower energy, these states may also be called LUMO (lowest unoccupied molecular orbital). Similarly conduction states for holes have an upper energy, also called HOMO (highest occupied molecular orbital) [19].

Like inorganic semiconductors, many organic materials can be doped n-type or p-type [20].

For nearly complete absorption of the incident light, a thickness of the absorber of 1 μm is sufficient. Nevertheless, this is much larger than the diffusion length of excitons and they will not be able to traverse the absorber.

For an electrical current the transport of electrons and holes is necessary. In the excitons generated by photon absorption in organic materials, electrons and holes are strongly bound. Since no energy supply is available to provide for the binding energy, free electrons and holes must be generated from excitons without additional energy. It is known that this may happen at interfaces between different materials [19].

A photon absorber material can be brought into contact with a second material in which the energy of a free electron is more negative because of a larger electron affinity. This enables the electron to tunnel from its bound state in the absorber into a free state in the adjacent material which we therefore call an electron acceptor.

The interface between the absorber and the electron acceptor serves two purposes: it generates free electrons and holes and in addition it separates them locally so that they can no longer recombine. The interface is the required selective contact for electrons and the electron acceptor must be a good electron conductor and should not provide any states for free holes to go from the absorber into this material.

There is a problem for the transport of the excitons. They are generated by photon absorption throughout the absorber and they all have to move towards the interface with the electron acceptor which must therefore be within a diffusion length of their point of generation. Since the diffusion length of excitons is typically in the nm range and much smaller than the penetration depth $1/\alpha$ of the photons in the absorber, efficient exciton transport and sufficient absorption seem to be incompatible.

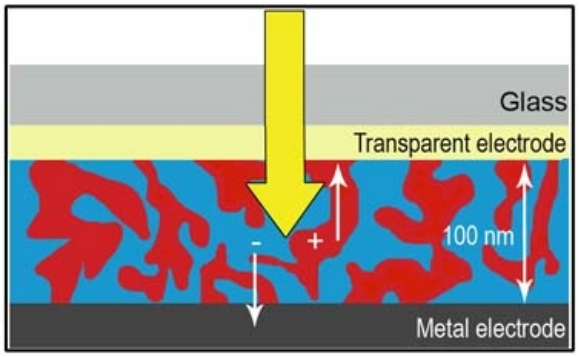

FigureI. 3 - Bulk Heterojunction: the p-type material is mixed with the electron acceptor

In the first hetero-junction solar cell, the exciton dissociation occurred at the interface between donor and acceptor materials incorporated in a planar bi-layer configuration [22]. An evolution of such configuration is represented by the FigureI. 3, in which the p-type absorber is mixed with an electron acceptor [47,48]. The bulk heterojunction is important because a large interfacial area between the donor and acceptor materials is created where charge separation can take place. The introduction of the BHJ concept in organic PV cells has allowed an increase in the efficiency to about 5–6% in standard systems [47,48].

I.3.1.3.I-V characteristics and definition of static parameters

When the solar cell (pn junction) is illuminated (FigureI. 4), electron-hole pairs are generated and acted upon by the internal electric fields, resulting in a photogenerated current [1, 21-25]. The generated photocurrent flows in a direction opposite to the forward dark current. Even in the absence of external applied voltage, this photocurrent continues to flow, and it is measured as the short circuit current (I_{SC}).

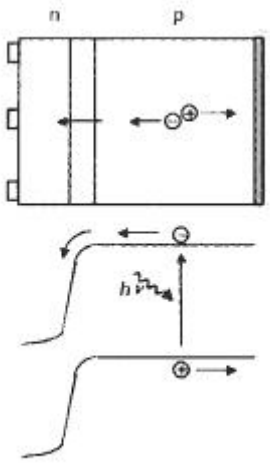

FigureI. 4- Schematic of pn junction

An ideal solar cell can be represented by a photogenerated current source (I_{ph}) connected in parallel with a rectifying diode, as shown in FigureI. 5. The corresponding I-V characteristic is described by the Shockley solar cell equation:

$$I = I_{ph} - I_0 \left(e^{\frac{qV}{k_B B}} - 1 \right)$$

where k_B is the Boltzmann constant, T is the absolute temperature, q (>0) is the electron charge and V is the voltage at the terminals of the cell. I_0 is the diode saturation current, serving as a reminder that a solar cell in the dark is simply a diode. The photogenerated current I_{ph} is closely related to the photon flux incident on the cell and its dependence on the wavelenght of light is discussed in terms of the quantum efficiency or spectral response.

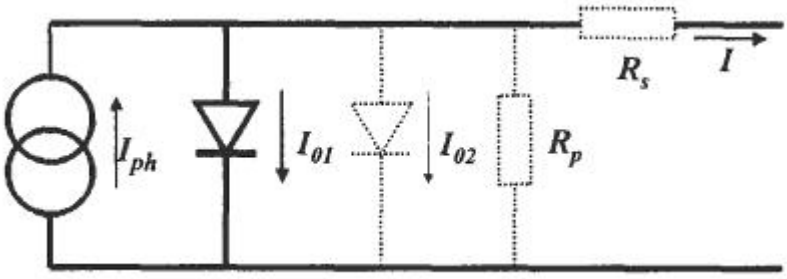

FigureI. 5- The equivalent circuit of an ideal solar cell (full lines). Non-ideal components are shown by the dotted line

In the ideal case, the short circuit current I_{SC} is equal to the photogenerated current I_{ph}, and the open circuit voltage V_{OC} is given by:

$$V_{OC} = \frac{k_B T}{q} \ln\left(1 + \frac{I_{ph}}{I_0}\right)$$

The cell generates the maximum power P_{max} at a voltage V_m and current I_m, and it is convenient to define the fill factor FF by:

$$FF = \frac{I_m V_m}{I_{SC} V_{OC}} = \frac{P_{max}}{I_{SC} V_{OC}}$$

The fill factor is a measure of sharpness of the knee in an I-V curve. It indicates how well a junction was made in the cell and how the series resistances has been made. It can be lowered by the presence of series resistance and tends to be higher whenever the open circuit voltage is high. It tends to 1, but in practice this value is impossible to obtain.

FigureI. 6 shows the I-V characteristic of an ideal solar cell.

The I-V characteristics of an ideal solar cell complies with the superposition principle: the functional dependence can be obtained from the corresponding characteristic of a diode in the dark by shifting the diode characteristic along the current axis by I_{ph}.

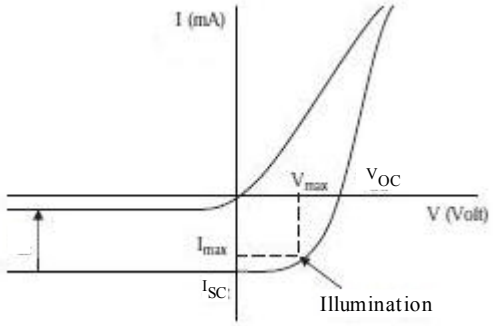

FigureI. 6- I-V characteristic of a solar cell

The I-V characteristic of a solar cell in practice usually differs to some extent from the ideal characteristic. The equivalent circuit of a solar cell in practice contains the diode and the resistances shown in dotted line in FigureI. 5. These non-idealities depend on different features while considering inorganic cells or organic cells. For a good solar cell, the series resistance, R_S, should be very small and the parallel resistance, R_P, should be very large. For commercial solar cells R_P is much greater than the forward resistance of a diode so that it can be neglected and only R_S is of interest.

The solar cell power conversion efficiency can be given as:

$$\eta = \frac{P_{max}}{P_{ph}} = \frac{I_{max} V_{max}}{Incident\ solar\ radiation * Area\ of\ the\ solar\ cell} = \frac{V_{OC} I_{SC} FF}{I(t) A_C}$$

where I_{max} and V_{max} are the current and voltage for maximum power, corresponding to solar intensity.

The photocurrent I_{ph} produced by a photodiode is proportional to the illumination across a large range of optical power P. The coefficient of proportionality is the response coefficient R (A/W) (responsivity):

$$R = \frac{I_{ph}}{P} = \frac{q}{h\upsilon} EQE$$

where q is the charge of an electron and $h\upsilon$ is the energy of a photon and EQE is the external quantum efficiency, which links the generated electron flux to the incident photon flux.

The External Quantum Efficiency (EQE) can be though of as the product of an internal quantum efficiency and an optical efficiency and also as the ratio of the photon flux entering

the device to the photons incident on its surface. The optical efficiency η_O is the ratio of the photon flux refracted at the surface to the photon flux reflected at the surface. At normal incidence, used as the reference situation, the Fresnel transmission coefficient determines the optical efficiency:

$$\eta_O = \frac{4n}{(n+1)^2}$$

which depends on the wavelength and the angle of incidence, where n is the refractive index.

The Internal Quantum Efficiency (IQE) is defined as the ratio of the electron-hole pairs generated to the absorbed photons. The electron-hole pairs created by the absorption of photons entering the device may, or may not, give rise to a current flow in the external circuit. In inorganic semiconductor junctions, the internal quantum efficiency depends therefore on where they are generated in the structure. If generation is in the depletion region, the electrons and holes are separated by the electric field leading to the passage of one electron for each absorbed photon: thus, the internal quantum efficiency is 100%. In the case of generation in the electrically neutral p and n regions, where the electric field is weak, only the electrons (or holes) generated less than one diffusion length away are transported into the depleted region, and the internal quantum efficiency is in most cases weak.

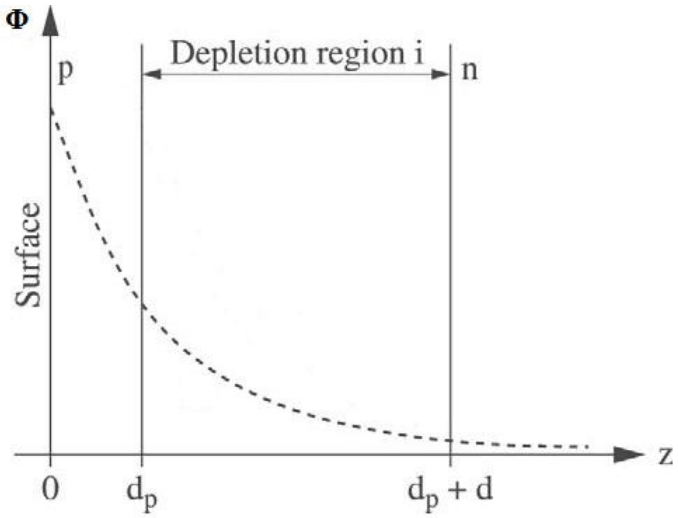

FigureI. 7 - Photon flux across the structure of p-i-n junction. The electron-hole pairs that generate photocurrent are generated in the depletion region [21]

It is therefore desirable to design a photodiode in such a way that the radiation should be entirely absorbed in the depleted region. FigureI. 7 shows a model which provides a good evaluation of the internal quantum efficiency of a PIN photodiode, as a function of the nature of the material on whose surface the radiation falls [21].

I.3.2. Materials and technologies

I.3.2.1 Silicon-based solar cells

The monocrystalline silicon solar cells show module efficiencies of up to 20% in the case of float zone–grown monocrystalline silicon. In terms of the best reported efficiencies for small-scale laboratory devices, crystalline silicon (25% efficiency) is only rivaled by gallium arsenide (GaAs, 25.1% efficiency) for single junction devices. Generally, photovoltaics based on the monocrystalline materials are costly and various thin film-technologies exist that offer lower cost both in terms of stock material and thermal budget. Amorphous silicon is perhaps the most well-known technology, and while it suffers from degradation under illumination, the technology offers stable efficiencies of around 5–10% [2].

Most commercial Si solar cells use boron-doped single-crystal wafers (around 400 μm thick) grown by the Czochralski (CZ) process. It is the standard process also used in the needs of microelectronic industry. CZ Si is free from lattice defects, but it contains residual impurities such as oxygen, carbon, and transition-metal ions [3].

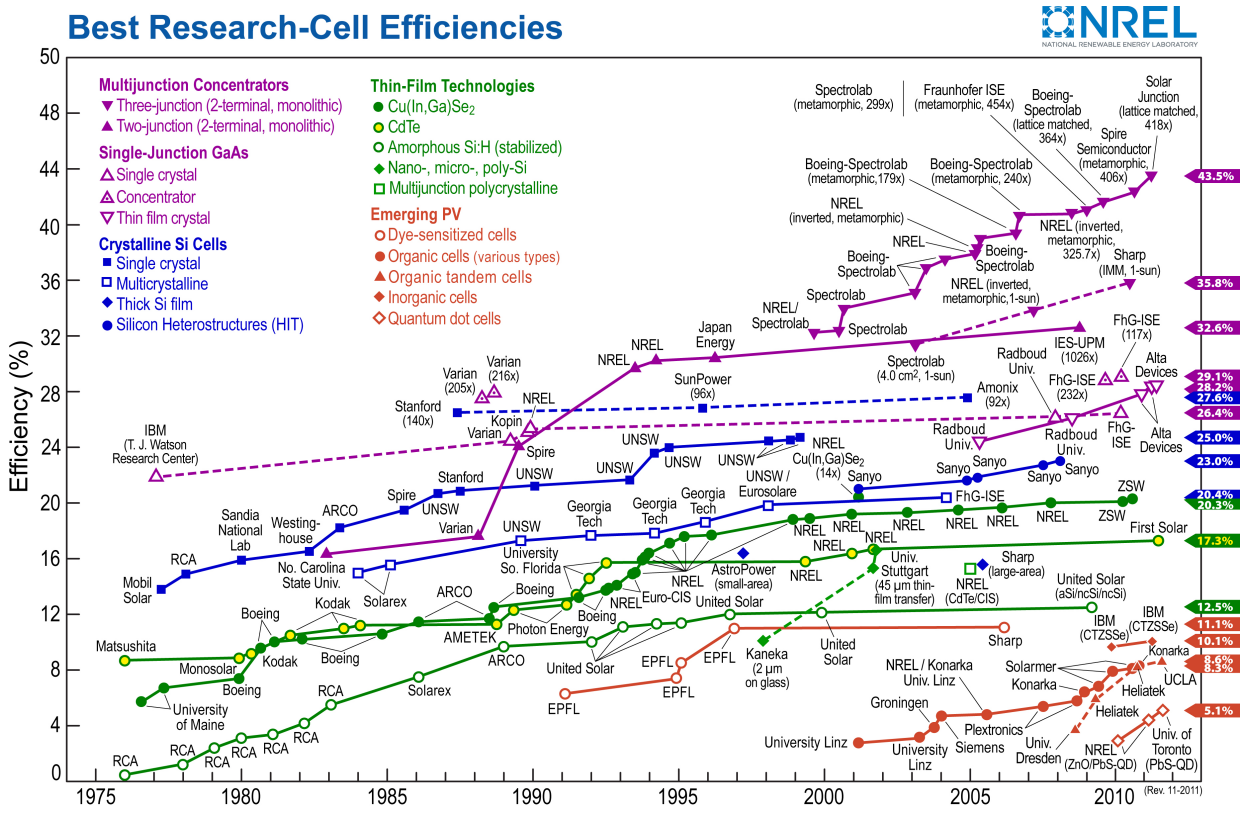

FigureI. 8 - Evolution of the conversion efficiencies of various types of research PV cells

The evolution of world-record efficiencies of laboratory semiconductor cells is shown in FigureI. 8. Si PV cell efficiency can be divided into four stages, with each stage corresponding to new solutions in technology or cell structure. In the beginning, the rapid progress of silicon technology allowed production of Si solar cells with 15% efficiency. In the

second stage (1970s), 17% efficiency Si solar cells were fabricated due to achievements in microelectronics. The most significant results have been obtained in the third (1980s) and fourth (2000+) stages, and Si cell efficiencies close to 25% have been achieved. These efficiencies were due to improved contact and surface passivation of the cell, along the front and rear surfaces, as well as an improved understanding of the significant role of light-trapping in Si devices.

Thin-film Si solar cells have three important advantages compared to crystalline cells: the thickness of Si can be drastically reduced down to 50 μm, thin films can be deposited on low-cost substrates, thin films can be fabricated on module-sized substrates and in integrally interconnected structures. Although Si films were developed in microelectronics many years ago, it has taken about 30 years to begin fabricating thin-film polycrystalline (pc-) Si solar cells with reasonable efficiency. In poly-Si films the average grain size is about 10–15 μm, corresponding to a grain size/thickness ratio of greater than 20.

Thin amorphous Si films usually contain a few percent of hydrogen to passivate dangling bonds that result from the random arrangement of the Si atoms and increase material quality. Plasma chemical vapor deposition (CVD) is widely used for fabricating these films. The layers may be deposited onto both rigid substrates (e.g. glass) and flexible substrates (e.g. thin metallic sheets and plastics), allowing for continuous production and diversity of use.

The hydrogenated amorphous Si is found to have a direct optical energy bandgap of 1.7 eV and an high optical absorption coefficient α for photons with energies greater than the energy bandgap. This means that only a few microns of material are needed to absorb most of the incident light, reducing materials usage and hence cost.

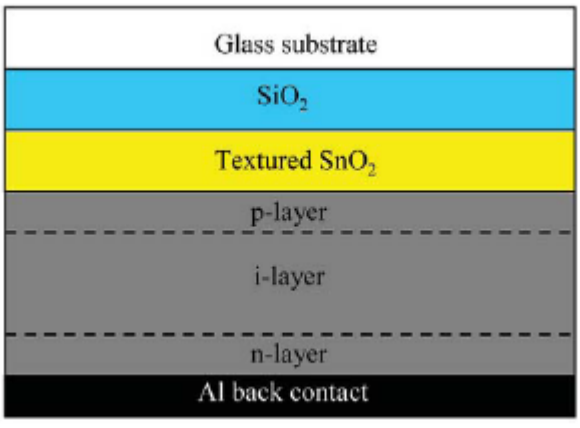

FigureI. 9- Cross-sectional view of a p-i-n single junction amorphous Si solar cell

The design of the cells optimizes the collection of current by having very thin n- and p-layers, with an intrinsic intermediate layer to give a p-i-n structure FigureI. 9. The thickness of the intrinsic intermediate layer is enough to absorb almost all the incident light. However, the physical properties of the i-layer degrade under illumination, because Si-H bonds are destroyed under visible light [8]. This effect can be reduced by careful control of the deposition process, decreasing the thickness of the i-layer, and using multiple junctions. The best initial efficiencies of 13.7% and 9.8% were

achieved on triple-junction cells and modules, respectively [5]. However, stabilized efficiencies still remain low: 6–7% for the best commercial modules [6]. Nevertheless, at present, about 8–10% of the worldwide PV production uses a-Si technology.

Amorphous silicon cells have been combined with nanocrystalline silicon-junction cells and cells of other materials, in order to develop the Heterojunction with Intrinsic Thin layer (HIT) solar cell [9]. In this device, layers of amorphous Si are deposited onto both faces of a textured wafer of single-crystal Si. The advantages of this structure include the potential for high efficiency, very good surface passivation, low-temperature processing, reduced energy payback time, and reduced cost relative to conventional Si devices.

I.3.2.2. Solar cells based on III-V and II-IV compouds

The compounds, such as GaAs, InP, and GaSb, have direct energy bandgaps, high optical absorption coefficients, and good values of minority carrier lifetimes and mobilities. This makes them excellent materials for high efficiency solar cells. The materials used most widely for making single-junction solar cells are GaAs and InP, as both have near optimum energy bandgaps of 1.4 eV. The highest conversion efficiencies confirmed under standard conditions are 25.8% for GaAs [10] and 21.9% for InP [11] single-junction cells. The disadvantage of using these compounds in photovoltaic devices is the very high cost of producing device-quality substrates or epitaxial layers of these compounds. Crystal imperfections, including unwanted impurities, severely reduce device efficiencies and alternative, lower cost deposition methods cannot be used. These materials are also significantly mechanically weaker than Si. The high density of the materials is also a disadvantage, in terms of weight, unless very thin cells can be produced to take advantage of their high absorption coefficients. These drawbacks have led to these compounds not being considered as promising materials for single-junction solar cells. Their development has been undertaken primarily because of their potential for space applications.

In a single-junction Si solar cell, 56% of the available energy is lost because photons with energies less than the bandgap are not absorbed, and photons with energies greater than the bandgap ‘thermalize’, such that the excess energy over the bandgap is lost as heat. A range of studies have shown that using multijunction solar cells (sometimes referred to as tandem solar cells), such losses can be minimized

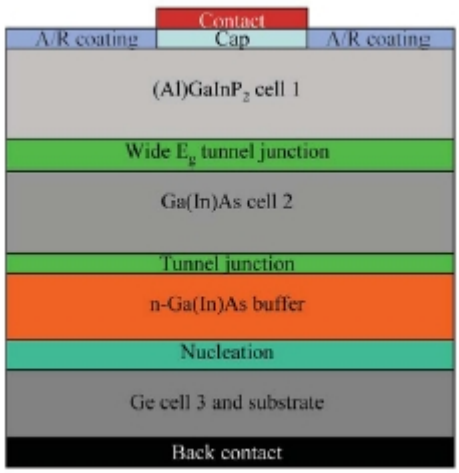

FigureI. 10 - Cross-sectional view of a multijunction device grown on a Ge substrate with 39.3% efficiency

leading to much higher efficiency devices. A landmark achievement demonstrating this concept was the development in 1990 of a GaAs/GaSb stacked cell with an efficiency greater than 30%41. A cross-sectional view of a device with an efficiency >39% is given in FigureI. 10.

In addition, solar cells based based on II-IV compounds have been developed, such as the CdTe solar cells. Cadmium telluride (CdTe) is a direct-bandgap material. Its bandgap energy of 1.45 eV is quite favorable for conversion of the solar spectrum into electricity with a single-junction solar cell. Its very high optical absorption and p-type conductivity make it an ideal material for PV applications. As with other II–VI materials, electronic doping is controlled by substitution of atoms at vacancy sites. Although n-type doping control is relatively easy, it is difficult to vary the doping concentration in p-type CdTe because of compensation effects.

I.3.2.3.Dye-sensitized solar cells (DSSCs)

Dye-sensitized solar cells (DSSCs) have been extensively studied for their reasonable photoelectric conversion efficiency, simple assembly technology, and potential low cost. The sensitization of wide-bandgap semiconductors, such as ZnO, by organic dyes was investigated by several research groups for photoelectrochemical (PEC) processes. The PEC approach to solar energy conversion then shifted toward the use of narrow-bandgap semiconductors (e.g., Si, GaAs, CdSe) in conjunction with electrolytes.

DSSCs based on liquid electrolytes have reached efficiencies as high as 11% under AM 1.5 [16]. However, the use of liquid electrolyte has created difficulties in sealing and the long-term photochemical stability of the device [14]. To overcome these problems, researchers have attempted to replace the liquid electrolytes with solid or quasi-solid charge-transport materials. However, the use of a liquid electrolyte and long-term stability remain as barriers to further technology development. The field of DSSC research gained significant worldwide interest after Graetzel et al. reported the use of a Ru-based dye to achieve higher efficiency in a cell made of TiO2 nanoparticles [15]. They achieved a major improvement in solar energy conversion efficiency of 11% in a dye-sensitized TiO2 thinfilm solar cell [16]. DSSCs exhibit energy conversion compatible to a-Si thin-film solar cells of about 10%, but can be produced at much lower cost.

I.3.2.4.Organic solar cells

With a theoretical efficiency that is the same as conventional semiconductor devices and a cost structure derived from plastic processing, organic PV cells offer the long-term

potential of achieving the goal of a PV technology that is economically viable for large-scale power generation. The first highly conductive polymer (chemically doped polyacetylene) was reported by Chiang et al. [17]. Organic molecules and semiconducting polymers are being increasingly used in optoelectronic devices.

Some key advantages for organic PV are that organic small-molecule and polymer materials are inherently inexpensive; they can have very high optical absorption coefficients that permit the use of films with thicknesses of only several hundred nanometers; they are compatible with plastic substrates; and they can be fabricated using high-throughput, low-temperature approaches that employ one of a variety of well-established printing techniques in a roll-to-roll process [49,50].

The ability to design and synthesize molecules and then integrate them into organic-organic and inorganic-organic composites provides a unique pathway in the design of materials for novel devices. Single-layer BHJ cells give efficiencies exceeding 8% [51]. A key issue faced by the organic electronics community in general is the stability of the organic materials.

Device degradation pathways stem largely from changes in morphology, loss of interfacial adhesion, and interdiffusion of components, as opposed to strictly chemical decomposition. Thus, careful design and materials engineering can substantially improve device lifetimes.

I.4 Luminescent Solar Concentrators

An interesting approach for conversion of light to electricity is the luminescent solar concentrator (LSC). The LSC consists of a transparent matrix containing luminescent species such as organic dyes or quantum dots that absorb part of the incident solar spectrum and re-emit it at a different wavelength. Part of the light emitted by the luminescent particles is guided towards the edges of the dye-doped transparent matrix by total internal reflection, where high efficiency solar cells are placed.

The device allows concentration of light entering through a large front surface onto a small photo active area. A fundamental difference of the luminescent solar concentrator compared to other concentrator approaches is that it concentrates diffuse light as well as direct light. Tracking of the sun, therefore, is not necessary. The main motivation for implementing an LSC is to replace the large area of expensive solar cells required in a standard flat-plate PV panel, with an inexpensive polymeric collector, thereby, reducing the cost of the module (in

dollars per watt) and also of the solar power (in dollars per kilowatthour).

The first publications on LSCs first appeared in the late 1970s [26, 27], and the technology was studied intensely through the early 1980s until limitations of fluorescent organic dyes hindered further development [28, 29]. The highest conversion efficiency achieved for a large-area LSC (40 cm× 40 cm × 0.3 cm) was η_{LSC} = 4.0% with a two-stack system consisting of a shorter wavelength emitting plate coupled to gallium arsenide (GaAs) solar cells and below that, a longer wavelength emitting plate coupled to silicon (Si) solar cells [30].

In recent years, there has been a renewed interest in LSCs due to the availability of new luminescent materials, such as semiconductor quantum dots (QDs) [31], rare earth (RE) materials [32], and semiconducting polymers [33].

The challenges faced in LSC development can be subdivided into those presented by the luminescent materials and those of the matrix materials used to fabricate devices.

Luminescent materials mostly used in LSC technology are inorganic QDs and organic dyes. Typically, organic and inorganic materials possess unique characteristics, both satisfying some but not all of the requirements in LSC technology.

QDs exhibit broad absorption spectra, high absorption coefficients, and emission peaks in the NIR region. However, commercially available PbS QDs exhibit low Fluorescence quantum yields of ~10% and are very unstable and expensive. On the other hand, RE materials exhibit superior stability, emission peaks at λ ~1000 nm, and high FQY values of ~90% have been reported [35]. Unfortunately, they have narrow absorption peaks with low absorption coefficients; therefore, high concentrations are required leading to increased cost.

Organic luminescent materials such as perylene-based dyes exhibit near-unity FQY [34] and have been demonstrated to be rather stable in a poly(methyl methacrylate) (PMMA) host. However, organic dyes exhibit narrow absorption bands. In addition, significant reabsorption losses occur with organic dyes, being lower in solution but increasing in solid host matrices.

There are four main criteria that should be met in order to comply OLSC technology requirements: absorption of all wavelengths λ < 950 nm with high absorption coefficients and an emission peak located within the absorption band of Silicon, minimum reabsorption losses due to overlap of absorption and emission spectra, near-unity fluorescence quantum yield (FQY), long-term outdoor stability.

Organic dyes present absorptions in the visible region and emissions at higher wavelengths in the Near Infrared region (300-900 nm), which is included in the broad

absorption band of Si solar cells.

The Stokes shift is the difference between positions of the band maxima of the absorption and emission spectra of the same electronic transition. If the fluorescent molecule presents a high Stokes shift, reabsorption losses are minimized.

The Fluorescence quantum yield gives the efficiency of the fluorescence process. It is defined as the ratio of the number of photons emitted to the number of photons absorbed.

$$\text{FQY} = \frac{photons\ emitted}{photons\ absorbed}$$

The theoretical maximum fluorescence quantum yield is 1, which means that every photon absorbed results in an emitted photon.

Many organic dyes exhibit FQY values close to 1 in certain solvents, but it is their FQY within the LSC carrier matrix that is actually required to be near unity. The FQY of a luminescent species in a host matrix is strongly affected by the matrix material and the concentration of luminescent material used.

In the region where the absorption spectrum of a luminescent species overlaps with the emission spectrum, emitted light can be reabsorbed by another luminescent species.When this occurs, the light may be lost through the escape cone of the LSC, or if the luminescent species does not have 100% FQY, the light may not be re-emitted due to radiationless relaxation [52]. Reabsorption losses are represented by decreasing emission intensity and redshifts in emission spectra. The effects of reabsorption are intensified with increasing pathlength and with high concentrations of luminescent species [52]. Reabsorption can be minimized by usingmaterials with a large Stokes shift. Calculation of the optimum concentration is also beneficial, balancing the need for sufficient absorption of incident light and minimum reabsorption.

Self-absorption losses can be quantified also using a ratio S, defined as the ratio of the absorption coefficients at the absorption and emission maxima. To reduce concentration quenching, M. J. Currie [53] adopted phosphorescent dyes. Compared with conventional fluorescent dyes, an advantage of phosphorescent dyes is that the emissive state is only weakly absorptive. Thus, phosphors typically exhibit large Stokes shifts. The ratio S for LSCs realized with phosphorescent materials results an order of magnitude higher comparated to the ratio S calculated on typical dyes suitable for LSC technology.

Optical properties of the LSC depends also on its fabrication procedure. A typical design consists of a polymer matrix doped with a luminescent material. The matrix material needs to fulfill several requirements: high transparency, good photostability and mechanical and chemical resistance. The carrier matrix is also responsible of the total internal reflection

of the emitted light and it is required to have low absorption coefficient over a very wide wavelength range (from 350 to 1000 nm). The light scattering within the matrix is an important feature and this is related to the total internal reflection of the light within the matrix. Total internal reflection will occur in a medium with refractive index n when light strikes the matrix to air boundary at angles greater than the critical angle. The critical angle is determined by the following formula [38]:

$$\theta_c=\sin^{-1}(1/n)$$

while the amount of light thet will be totally internally reflected in an LSC plate (L) is given by

$$L=\frac{(n^2-1)^{1/2}}{n}$$

As an example, for a material with n=1,5, 74,5% of emitted light would be trapped inside the plate, leading to a significant loss of 25,5% of incident light [38].

OLSC thin-film devices consist of a layer characterized by a thickness in the order of μm of luminescent material deposited onto a thicker transparent plate, ideally of the same refractive index. They offer the possibility of reducing reabsorption effects by confining all the absorption and emission to the thin film while trapping and reflection events occur primarily in the clear matrix [37]. This configuration offers more flexibility in the choice of the substrate and cheaper fabrication methods such as spincoating. It has also been suggested as a way to reduce losses due to reabsorptions.

Light emitted into the undoped layer will travel to the plate edges by TIR with a greatly reduced chance of being reabsorbed. Absorption by the host material can also be minimized since pure materials with high optical clarity can be used.

In conclusion, a mathematical explanation of OLSC basis phenomena can be dealt.

The efficiency of re-emission is given by the photoluminescent efficiency of the dye, η_{PL}. Ideally, photons re-emitted within the LSC are trapped in the waveguide by total internal reflection and guided to the edge of the transparent substrate. The fraction of photons confined within the waveguide is the trapping efficiency, η_{trap}. As a photons propagates within an OLSC it may be re-absorbed by other dye molecules when a finite overlap exists between the absorption and emission spectra of the dyes. For N re-absorption events in the waveguide the OLSC efficiency scales as $(\eta_{PL}\ \eta_{trap})^N$. OLSC performance consequently depends on three key parameters: η_{PL}, η_{trap}, and N. Many dyes already exhibit $\eta_{PL} = 1$ especially in the visible range, while N depends on geometrical gains and on the concentration of the dye within the matrix. Conventional OLSCs employ randomly aligned dyes that collectively emit photons

isotropically. This yields a trapping efficiency of η_{trap} = 0,75 for a waveguide that presents a refractive index of n = 1,5. C.L. Mulder et al. [54.,55.] align the dyes vertically so their dipole couple more strongly into the waveguide.

By considering the efficiency η_{CELL} of the PV cell coupled to the OLSC, the External Quantum Efficiency, defined in theory as the ratio of the generated electrons to the photons incident on the surface, can be defined as [54]:

$$EQE = \eta_{CELL}\eta_{abs}\frac{\eta_{PL}\eta_{trap}(1-r)}{1-r\,\eta_{PL}\eta_{trap}}$$

where r is the average probability that an emitted photon will be reabsorbed, η_{abs} is the fraction of incident photons that are absorbed, η_{PL} is the photoluminescent yield of the OLSC and η_{trap} is the OLSC trapping efficiency.

The stability of the OLSC device still represents a key issue for commercial deployment of this technology. The stability of luminescent species is one of the main challenges in LSC development, as if high LSC efficiencies are achieved, it will not be commercially viable unless lifetimes greater than ten years are possible [38.]. In the initial period of study, stability of up to two years was measured [38.], while more recently, dye stability of many years under sunlight has been reported [38.,51.]. Techniques to improve the stability of LSC devices include choice of optimum matrix materials, use of specific casting and curing techniques.

T. Dienel et al [42.] studied LSC based on a thin dye-doped polymer film. Solution was made by dissolving in $CHCl_3$ both PMMA and Lumogen F305 Red. The solution was then deposited onto a microscopy slide, used as substrate, by the doctor blading technique. The samples were subjected to aging process due to exposure to a xenon lamp. Figure I.12 shows the optical spectra of degraded samples.

A decrease in intensity of both UV-vis absorption and fluorescence was observed. Thin film LSCs were characterized, demonstrating a good agreement between spectral and electrical analysis, and the parameters governing the efficiency could be addressed separately.

Similar degradation trends were observed in the works by Tanaka et al [45.] and by Earp et al.[46], althought different light sources were employed. In particular Tanaka exposed the sample under simulated sun light, while Earp to outdoor exposure.

Variations in solar cells performances were studied by comparing I-V characteristics of the cell alone and the OLSC mounted device. R.Kinderman et al. [40.] carried out I-V characterization of OLSC mounted devices obtained by LSC plate fabrication. An increase in electrical current is observed. In addition variations of the optical and electrical properties of

the plate were presented after exposure to simulated solar light.

Degradation studies have been carried out also by van Sark et al. [39]. In this work, van Sark exposed both LSC plates and LSC coatings to continuous illumination under a sulphur lamp and at outdoor conditions. The plate samples were realized by polymerization of MMA and dye solution, while the coatings were produced by deposition of a solution of PMMA and dye (Lumogen F Red 305).

In addition, I-V tests on OLSC mounted devices were performed in order to track the degradation effects of OLSC mounted device performance.

Both devices aged under sulfur lamp and in outdoor conditions showed a decrease of the current generated by the OLSC mounted device.

The lifetime was found to depend strongly on the dye molecule.The best concentrators exhibited an initial decrease in performance of 20% and stayed relatively stable thereafter. In particular, degradation of device performance was found also for samples stored in the dark, suggesting that light exposure is not the only responsible for device degradation.

Bibliographic References

1. F. C. Krebs “Polymer Photovoltaics A Practical Approach” Spie, (2008)
2. L.H. Slooff, T. Budel, A. R. Burgers, N.J. Bakker, A. Büchtemann, R. Danz, T. Meyer, A. Meyer “The Luminescent concentrator: stability issues”, Energy research Centre of the Netherlands (2008)
3. T.M. Razykov, C.S. Ferekides, D. Morel, E. Stefanakos, H.S. Ullal, H.M. Upadhyaya “Solar photovoltaic electricity: Current status and future prospects” Solar Energy – (2011)
4. K. Zweibel “The Terawatt challenge for thin film PV” in: Poortmans, J., Archipov, V. (Eds.), “Thin Film Solar Cells: Fabrication, Characterization and Application”, John Wiley, pp. 18–22, 2005
5. S. Guha “Thin film silicon solar cells grown near the edge of amorphous to microcrystalline transition” Solar Energy 77, 887–892, (2004)
6. B. von Roedern, K. Zweibel, S.H. Ullal, “The role of polycrystalline thin-film PV technologies for achieving mid-term market-competitive PV modules” in: Proc. of the IEEE PVSC-31, Orlando, USA, pp. 1635–1638, (2005)
7. P.A. Basore “Simplified processing and improved efficiency of crystalline silicon on glass modules” in: 19th European Photovoltaic Solar Energy Conference, Paris, June, pp. 455–458, (2004)
8. C.R. Wronski, “Amorphous Si Solar Cells. In Clean Electricity from Photovoltaics” Archer, M. D., Hill, R. (eds.), Imperial College Press, London, UK, 199, (2001)
9. E. Maruyama et al., In Proceedings of the 4th World Conference on Photovoltaic Energy Conversion, Hawaii, 1455, (2006)
10. R.P. Gale et al., In Proceedings of the 21st IEEE Photovoltaic Specialists Conference, Kissimmee, Florida, 53, (1990)
11. C.J. Keavney, et al., In Proceedings of the 21st IEEE Photovoltaic Specialists Conference, Kissimmee, Florida, 141, (1990)
12. F.C.Krebs et al. “Strategies for incorporation of polymer photovoltaics into garments and textiles”, Sol. Energy Mater. Sol. Cells, **90**, pp. 1058–1067, 2006.
13. Nazeeruddin, et al. “Conversion of light to electricity by cis-X2 bis (2,20- bipyridyl-4,40-dicarboxylate) ruthenium (II) charge-transfer sensitizers on nanocrystalline titanium dioxide electrodes” Journal of American Chemical Society 115, 6382–6391, (1993)
14. Papageorgiou et al. “An iodine/triiodide reduction electrocatalyst for aqueous and

organic media" Journal of the Electrochemical Society 144, 876–884, (1997)

15. B. O'Regan, M. Graetzel, "A low-cost, high efficiency solar cell based on dye-sensitized colloidal TiO2 films", Nature 353, 737–740, (1991)

16. M. Gratzel "Solar energy conversion by dye-sensitized photovoltaic cells" Inorganic Chemistry 44 (20), 6841–6851, (2005)

17. C.K.Chiang et al. "Electrical conductivity in doped polyacetylene" Physical Review Letters 39, 1098–1101, (1977)

18. B. A. Gregg, S.-G. Chen, R. A. Cormier, Chem. Mater. 16, 4586, (2004)

19. P. Peumans, S. R. Forrest, Chem. Phys. Lett., 398, 27, (2004)

20. K. Walzer, B. Maennig, M. Pfeiffer, K. Leo, Chem. Rev., 107, 1233 (2007)

21. D. Decoster, J. Harari "Optoelectronic Sensors" Wiley ed., (2009)

22. O. Sergiyenko "Optoelectronics: devices and properties" InTech, (2011)

23. E. Rosencher, B. Vinter "Optoelectronics" Cambridge, (1998)

24. J. Gao "Optoelectronic integrated circuit design and device modeling" Wiley ed., (2011)

25. S.O. Kasap "Optoelectronics and photonics Principles and pactices" Prentice-Hall, (2001)

26. W. H. Weber, J. Lambe, "Luminescent greenhouse collector for solar radiation" Appl. Opt., vol. 15, no. 10, pp. 2299–2300, (1976)

27. A.Goetzberger, W. Greubel "Solar energy conversion with fluorescent concentrators" Appl. Phys., vol. 14, pp. 123–129, (1977)

28. A. M. Hermann, "Luminescent solar concentrators—A review," Solar Energy, vol. 29, no. 4, pp. 323–329, (1982)

29. P. S. Friedman, C. R. Parent "Luminescent solar concentrator development" SERI/STR-211-3149, (1980)

30. V. Wittwer, W. Stahl, and A. Goetzberger "Fluorescent planar concentrators" Sol. Energy Mater., vol. 11, no. 3, pp. 187–197, (1984)

31. K. Barnham et al., "Quantum-dot concentrator and thermodynamicmodel for the global redshift" Appl. Phys. Lett., vol. 76, no. 9, pp. 1197–1199, (2000)

32. M. H. V. Werts et al. "Fluorescein and eosin as sensitizing chromophores in near-infrared luminescent ytterbium(III), neodymium(III) and erbium(III) chelates" Chem. Phys. Lett., vol. 276, no. 3/4, pp. 196– 201, (1997)

33. V. Sholin, J. D. Olson, S. A. Carter "Semiconducting polymers and quantum dots in luminescent solar concentrators for solar energy harvesting" J. Appl. Phys., vol. 101,

no. 12, pp. 123114-1–123114-9, (2007)

34. G. Seybold and G.Wagenblast "New perylene and violanthrone dyestuffs for fluorescent collectors" Dyes and Pigments, vol. 11, no. 4, pp. 303– 317, (1989)

35. W. G. Quirino et al. "Effects of non-radiative processes on the infrared luminescence of Yb3+ doped glasses" J. Non-Cryst. Solids, vol. 351, pp. 2042–2046, (2005)

36. J. M. Drake et al. "Organic dyes in PMMA in a planar luminescent solar collector: A performance evaluation"Appl. Opt., vol. 21, no. 16, pp. 2945–2952, (1982)

37. R. Reisfeld, C. K. Jorgensen "Luminescent solar concentrators for energy conversion" Struct. Bond., vol. 49, pp. 1–36, (1982)

38. B. C. Rowan et al. "Advanced material concepts for luminescent solar concentrators" IEEE Journal of selected topics in quantum electronics, vol. 14, no. 5, (2008)

39. W.G.J.H.M van Sark et al. "Luminescent solar concentrators – A review of recent results" Optics Express 21792, vol.16, no.26, (2008)

40. R.Kinderman et al. "I-V performance and stability study of Dyes for Luminescent plate concentrators" Journal of Solar Energy Engineering, vol 129/277, (2007)

41. L.H. Sloof et al. "A luminescent solar concentrator with 7.1% power conversion efficiency" phys. stat. sol. (RRL) **2**, No. 6, 2008

42. T Dienel et al. "Spectral-based analysis of thin film luminescent solar concentrators" Solar Energy 84 1366-1369 (2010)

43. T.J.J. Meyer, T.Markvart "The chemical potential of light in fluorescent solar collectors"Journal of applied physics, 105, 063110, (2009)

44.

45. N.Tanaka "Photodegradation of polymer-dispersed perylene di-imide dyes" Optical Society of America (2006)

46. A.Earp "Absorption tails and extinction in luminescent solar concentrators – Solar Energy Materials and Solar Cells" Volume 95, Issue 4, Pages 1157-1162, (2011)

47. Thompson, Frèchet, Angew. Chem. Int. Ed. 47 58-77 (2008)

48. Heeger et al., Science 270 1789-1791 (1995)

49. F.C.Krebs, Sol. Energy Mater. Cells 93 394-412 (2009)

50. Manceau, Krebs et al., Organic Electronics 12 566 (2011)

51. A. A. Earp et al., "Optimisation of a three-colour luminescent solar concentrator daylighting system," Sol. Energy Mater. Sol. Cells, vol. 84, no. 1–4, pp. 411–426, (2004).

52. R. W. Olson, R. F. Loring, M. D. Fayer, "Luminescent solar concentrators and the

reabsorption problem," Applied Optics, 20, 2934–2939, (1981)

53. M. J. Currie, J. K. Mapel, T. D. Heidel, S. Goffri, M. A. Baldo "High efficiency organic solar concentrators for photovoltaics", Science 321, 226 (2008)

54. C.L. Mulder, P.D. Reusswig, A.M. Velazquez, H. Kim, C. Rotschild, M. A. Baldo "Dye alignment in luminescent solar concentrators: I. Vertical alignment for improved waveguide coupling", Optical Society of America, 18 (2010).

55. C.L. Mulder, P.D. Reusswig, A.M. Velazquez, H. Kim, C. Rotschild, M. A. Baldo "Dye alignment in luminescent solar concentrators: II. Horizontal alignment for energy harvesting in linear polarizers", Optical Society of America, 18 (2010).

Chapter II

Materials and characterization techniques

II.1.Introduction

The present chapter is an overview of the materials and the characterization techniques employed in this work.

The research has been focused onto one polymeric material, poly(methyl methacrylate), and a perylene red fluorescent dye (Lumogen F Red 305).

One of the aims of this work has been the study of the degradation of the dye exposed to UV light, so its properties have been analyzed with different characterization techniques before and after UV irradiation.

The same characterization techniques were used to examine the properties of the coating obtained by depositing a solution of Poly(methyl methacrylate) and Lumogen in chloroform ($CHCl_3$) onto a rigid substrate during the exposure time. The coating was deposited onto glass substrates coupled to silicon solar cell and the electrical properties of the solar concentrator device so formed were examined under simulated solar light by using a multimeter.

II.2.Materials

II.2.1.Lumogen F Red 305

Lumogen F Red 305 is a perylene-based red fluorescent dye produced by BASF and its formula is shown in Figure II.1. It appears as a red powder, soluble in aromatic and chlorinated hydrocarbons and can be easily incorporated in polymer matrices such as Poly(methyl methacrylate), Polystyrene, Polycarbonate, Polyethylene therephthalate.

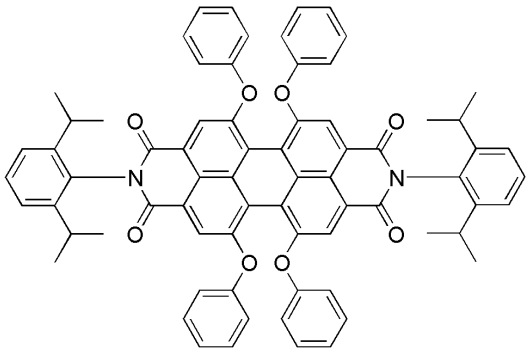

Figure II.1 - Lumogen F Red 305

The molecular structure of the dye consists of a perylene core and six lateral

substituents. Four aromatic rings are attached to the perylene core via C-O-C bonds. Each nitrogen atom in the core is linked to an aromatic ring bearing two isopropyl groups.

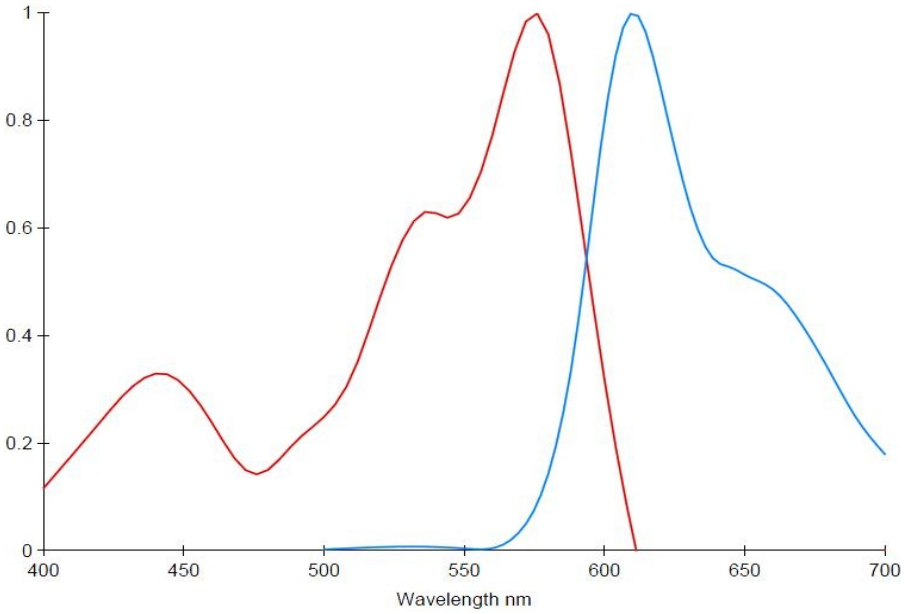

Figure II.2 - Absorption/Emission Lumogen in dichlorometane solution

The dye shows an absorption peak at 578 nm and an emission peak at 613 nm in dichloromethane solution and because its quantum yield is over 90%, this dye is suitable for fluorescent solar concentrators.

Figure II.2 shows the UV-vis absorption spectrum in the visible region and the emission spectrum of Lumogen F Red 305 together.

II.2.2.Poly(methyl methacrylate)

Poly(methyl methacrylate), known by the acronym PMMA, is a widely used termoplastic transparent polymer, with a glass transition temperature in the range 105-120°C.

The polymer consists of strongly polar, flexible ether side chains, weakly polar methyl groups and the unpolar polymer backbone. The molecular structure of its repeating unit is shown in Figure II.3.

PMMA is resistant to petrol and oil, diluted acids and bases. It is not resistant to aromatic and chlorinated hydrocarbons and it is soluble in chloroform, dichloromethane, trichloromethane, toluene, benzene, ethyl acetate and isobutyl ketone.

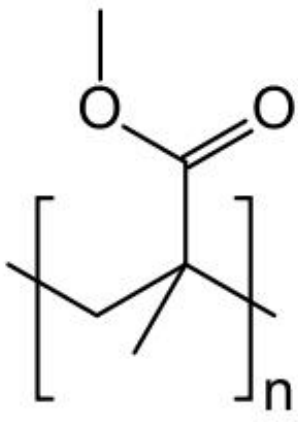

Figure II.3 - PMMA repeating unit

With regards to optical properties, PMMA is a highly transparent material in the visible and near-IR regions and its refractive index is about 1.5, which means it is a high bandgap dielectric material.

PMMA is inexpensive and can be easily doped.

PMMA is often preferred in comparison to other transparent polymers because of its good balance of properties,

easy handling and processing, and low cost. Sheets of PMMA are commonly used for glazing, lighting, signage, displays and sanitary ware. It is also used in optical fiber technology as plastic optical fiber used for short distance communication. In the electron beam lithography process PMMA aids as a resist. PMMA can be used as a dispersant for ceramic powders to stabilize colloidal suspensions in non-aqueous mediums.

Thanks to good chemical resistance, good sun exposure resistance, high refractive index and low cost, PMMA is eligible as matrix in laser dye-doped solid-state gain media for solid state dye lasers, and also in active layers in luminescent solar concentrator technology.

II.2.3.HALS

Sterically Hindered Amines (HALS) based on tetramethyl piperidine derivatives are excellent alkyl radicals scavengers. Scavenging alkyl radicals can help preventing autoxidation.

The operating mechanism of hindered amine light stabilizers can be explained by the reaction of alkyl radicals with the nitroxyl radicals. This reaction appears to be faster than that of alkyl radicals with oxygen. This process occurs leading to reformation of the nitroxyl radical until its complete destruction by side reactions. Hindered amine stabilizers are also highly efficient light stabilizers. Figure II.4 shows the schematic of the process of radical scavenging.

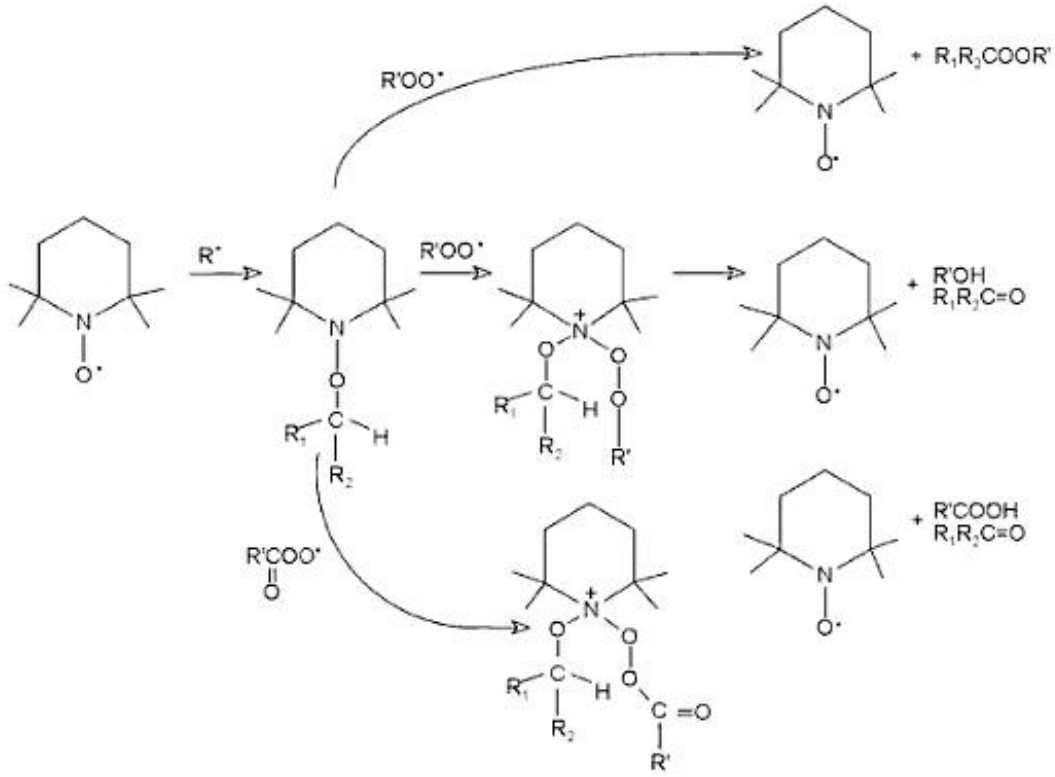

Figure II.4 - Process of radical scavenging by nitroxyl radicals

HALS are commonly used in the manufacture of surface coatings, plastics and printing inks to counteract the effects of long term degradation by exposure to weather and sunlight.

In this work Tinuvin 123 and Tinuvin 292 from Ciba were used.

Tinuvin 123 is used mostly in paints for the automotive industry. Its low basicity prevents possible interactions with acidic paint ingredients such as catalysts.

Tinuniv 292 is produced for coatings.

Both can be used for the protection of termoplastic acrylics, and therefore both were used as potential stabilizing agents for the polymeric binder employed in this work as OLSC matrix (PMMA).

II.2.4.PE 399 Krystalflex

PE 399 Krystalflex is a thermoplastic polyurethane adhesive.

Thermoplastic polyurethanes (TPU) are polymers that become soft and processable when heated, hard when cooled and capable of being reprocessed multiple times without losing structural integrity. TPU can be used either as a malleable engineering plastic or as a replacement for hard rubber. They are renowned especially for their high elongation and tensile strength, their elasticity, and to some extent, their ability to resist oil, grease, solvents, chemicals and abrasion.

PE 399 Krystalflex appears as a high performance aliphatic polyether film, and it is intended for processing by lamination with a range of glass and plastic components.

It has excellent laminated transparency, enhanced UV stability, good low temperature flexibility and contains adhesion promoter. Once heated over its glass transition temperature, about 120°C, it become transparent, with a refractive index of 1.49 which is similar to the refractive index of glass. Thanks to these properties it was chosen as optical contact between the Si solar cell and the luminescent solar concentrator fabricated on glass substrates.

II.3.UV-visible spectroscopy

Ultraviolet-visible spectroscopy [1-7] represents a type of absorbtion spectroscopy where electron excitation occurs in ultraviolet-visible spectral region.

The wavelength range of UV radiation starts at the blue end of visible light (about 400nm) and ends at approximately 200nm for spectrometers operating in air. As the radiation has sufficient energy to excite valence electrons in many atoms and molecules, UV radiation is involved with electronic excitation.

The wavelength range of visible light starts at approximately 800 nm and ends at 400

nm. Visible light acts in the same way as UV light, so it is also considered part of the electronic excitation region.

UV-vis spectrometers operate with wavelenghts between 800 nm and 200 nm.

The region from 200 nm down to X-ray region is called the vacuum UV region because oxygen, water vapour and other molecules in air absorb UV radiation below 200 nm, so the spectrometer light path must be free of air to observe wavelenghts below 200 nm.

In this work UV visible spectroscopy analyses were performed with a Jasco V-570 UV-VIS-Near Spectrophotometer.

II.3.1.Principles

The interaction of UV and visible radiation with matter can provide qualitative information on molecules and polyatomic species, including ions and complexes. Structural information about molecules and polyatomic species, especially organic molecules, can be aquired by observing the UV-vis spectrum. Most UV-vis absorptions by organic molecules are attributed to transitions involving non-bonding (n) electrons or electrons in molecular orbitals found in unsaturated molecules. Generally the absorption events are due to $n \leftrightarrow \pi^*$ and $\pi \leftrightarrow \pi^*$ transitions. Hence molecules with double bonds and especially conjugated double bonds (such as aromatic compounds) are strong absorbers.

UV-vis spectroscopy can also provide quantitative information when absorption intensity is considered. A higher absorption intensity at a given wavelenght can be attributed to a higher concentration of the molecular species generating that specific absorption event. Indeed concentrations of species in samples, especially solutions, are often measured using UV-vis absorption spectrometry. The measurement of concentration or changes in concentrations can be used to calculate equilibrium constants, reaction kinetics and stoichiometry for chemical systems.

II.3.2.Qualitative Information

The ultraviolet and visible spectra usually consist of a few broad peaks. This is due to the fact that electronic transitions dominate these spectral regions.

The absorption of a photon by a molecule promote an excitation of the molecule, that is the movement of the molecule from the ground state to a higher energy state.

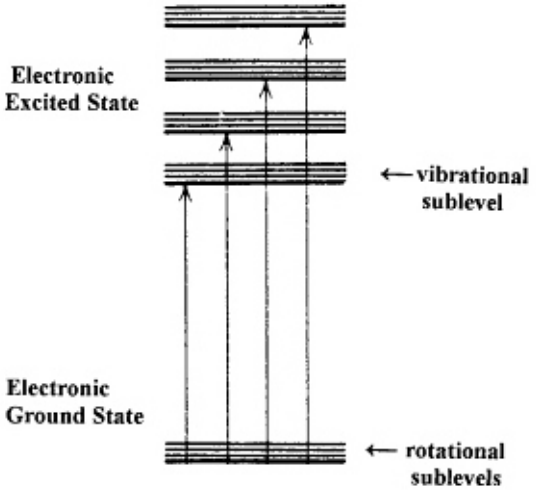

Figure II.5 - Schematic of electronic transitions

Figure II.5 shows a schematic of possibile electronic transitions promoted by photon absorptions. It is an electronic transition: the absorption of the photon promote an electron from the ground state to an occupied orbital. The frequency absorbed or emitted by the molecule and the energy of radiation are related by:

$$\Delta E = E_1 - E_0 = h\nu$$

where E_1 is the energy of the excited state, E_0 the energy of the ground state, ν the frequency absorbed or emitted by the molecule and h the Planck's constant.

In absorption and emission spectroscopy two important types of orbitals are considered: the Highest Occupied Molecular Orbital (HOMO) and the Lower Unoccupied Molecular Orbital (LUMO). Both refer to the ground state of the molecule.

Molecular groups that absorb visible or UV light are called chromophores.

II.3.3.Lambert Beer Law

The quantitative information that can be obtained by UV visible spectroscopy is ruled by the Lambert Beer Law [1-4, 7]**.** It relates absorbance of a sample to the path lenght and concentration of absorbing species.

$$A = abc = \varepsilon bc$$

where A is the absorbance, b the path lenght and c the concentration of the absorbing species. The proportionality constant, a, is the absorpitivity of the absorbing species. It defines how much radiation will be absorbed by that molecule at a given concentration and at a given wavelenght. If the concentration is expressed in molarity (mol/L), the absorbivity is defined as the molar absorbivity ε.

Commonly $\varepsilon = 10^4 – 10^5$ L mol^{-1} cm^{-1} for an allowed transition and it is on the order of 10 – 100 L mol^{-1} cm^{-1} for a forbidden transition. So the magnitude of the absorbivity is an indication of the probability of the electronic transition, if ε, b and c are known.

The molar absorbivity may be specified for any wavelenght, but is usually tabulated for the wavelenght at which maximum absorption of light occurs for a molecule.

Generally a spectrophotometer does not measure the absorbance directly. This quantity must rather be calculated by taking the negative logarithm of the fraction of light transmitted through the sample. Named P the power of the light passing through a sample and P_0 the power of light detected when the concentration of absorbing material is zero, the fraction of light transmitted is given by

$$T = P/P_0$$

where T is the transmittance. Absorbance is given by

$$A = -\log T = \log(P_0/P)$$

The quantities P and P_0 can be measured sequentially on sample and blank, or simultaneously with sample and blank in two identical cuvettes.

Lambert-Beer's law suggests a linear dependence between absorbance and the concentration of the species. Failure to obey the linear dependence of the absorbance on concentration may be due to aggregate formation at high concentrations or to the presence of other absorbing species.

Moreover P_0 may be reduced due beam reflections or absorption by the sample holder. Also scattering and possible absorption by the solvent when a solution is analyzed in a cuvette may reduce P_0. So practical use of the Lambert Beer law deserves attention.

II.3.4.UV-vis spectrophotometer

Depending on the region of the electromagnetic spectrum that is considered, different spectrophotometer components are used. Transmission optics in the UV region must be made of pure silica, reflection optics must have a special coating, the source is generally a deuterium lamp and the detector must be UV-enhanced. In fact the cross-over from the visible to the UV occurs at about 350nm, where the visible tungsten-halogen lamp stops emitting and the deuterium lamp is required.

The sensitivity in any region depends on the light source, the composition of the optical components and the response of the detector. Ideally accurate measurements of transmission should be possible from nearly 100% to as low as 10^{-3} to 10^{-4}, corresponding to absorbances between 0 and 3 or 4 units.

UV-vis spectrophotometers consist of a light source, a monochromator, a chopper (rotating sector mirror or rotating sector disc) to generate a sample and a reference beam as well as to recombine them, a sample and reference compartment and a detector (Figure II.6). Spectrophotometers which permit a synchronous measurement of sample and reference beams are as denoted double beam instruments. UV-vis spectra may also be obtained with single beam instruments. In single beam spectrophotometers the background and sample spectra are measured one after the other. Since a chopper and reference chamber are not needed, single beam instruments are usually cheaper than double beam instruments.

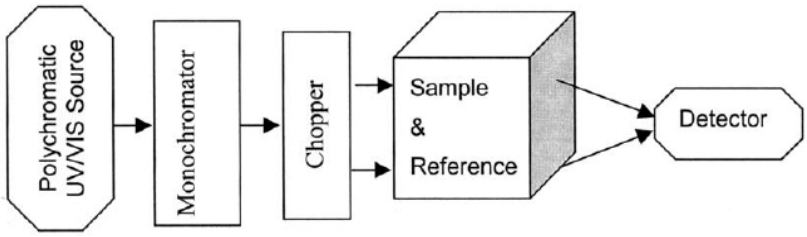

Figure II.6 - Block diagram of a UV visible spectrometer

II.3.4.1.Sources

A deuterium lamp is the primary source for a UV radiation. An electric discharge passing through the gas excites the deuterium atoms which then lose their excess energy as the characteristic radiation. High-pressure gas-filled arc lamps containing argon, xenon or mercury can be used to provide particularly intense source for specific UV regions. Tungsten-halogen lamps are usually used for the visible and NIR regions.

II.3.4.2.Wavelength selectors

The most commonly used wavelenght selectors for UV-VIS-NIR spectrophotometers are grating monochromators. However, filter instruments, and prism monochromators are sometimes used.

Monochromators in routine spectrometers usually have a prism or diffraction grating. The complete spectrum can be measured by turning the prism or grating. The spectral slit function (SST) is determined by the slit width and the dispersion of the monochromator. The spectral slit function of single monochromator does not extend below 5 nm. If a higher resolution is required, the use of double monochromators is necessary. Double monochromators improve the stray light rejection and allow measurement of samples with high optical density.

The radiation dispersed by prism monochromators is nonlinear and the resolution is not so good as with gratings. However prism monochromators are still in use. The easiest design is the Bunsen monochromator (Figure II.7). Light focused onto the entrance slit is collimated by the first lens and the parallel rays directed to a 60° glass prism. Light passing through the prism is refracted. Shorter waves are dispersed more strongly than longer wavelenghts (blue light is bent more than red). Then dispersed light is then focused by the second lens onto the exit slit. Different wavelenghts can be focused through the exit slit by moving the exit slit and lens.

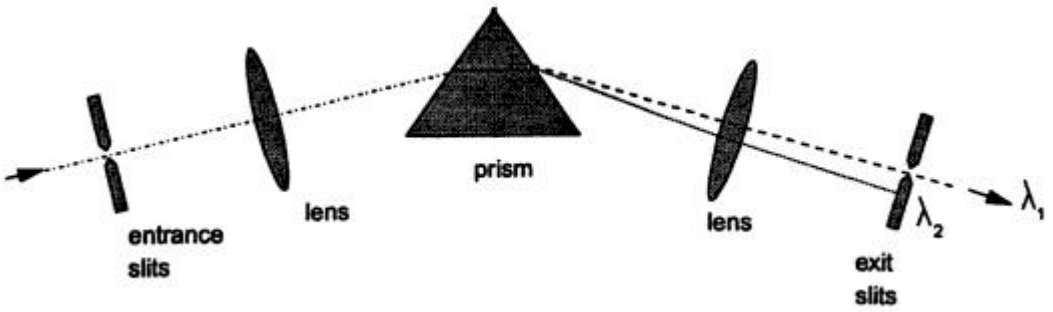

Figure II.7 - Optical diagram of Bunsen's prism monochromator

Diffraction gratings have become much less expensive and of improved quality in recent years. Gratings can be fabricated for either transmission or reflection applications. At present, replica gratings are made from a master that was scribed with the ruling engine on a very hard, optical flat, polished surface. The surface is made reflecting with a thin coating of aluminium or gold.

Replica gratings are now being replaced by holographic gratings. These are made using a pair of mutually interfering laser beams to develop a film of photo-resist on a glass surface. The sensitized regions of the photo-resist are etched away leaving grooved structure that can be coated with a reflective metallic film. Holographic gratings produce more perfect line shapes and provide spectra with reduced stray light, virtually free from the images or ghosts often found in their predecessors. The most frequent design for grating monochromator is the Czerny-Turner design (Figure II.8). This is a symmetric design with the entrance slit and concave collimating mirror on one side of the normal to the grating and the focusing mirror (identical to the collimating one) and exit slit on the other side. The Ebert design is similar, but the two mirrors are combined into a single mirror.

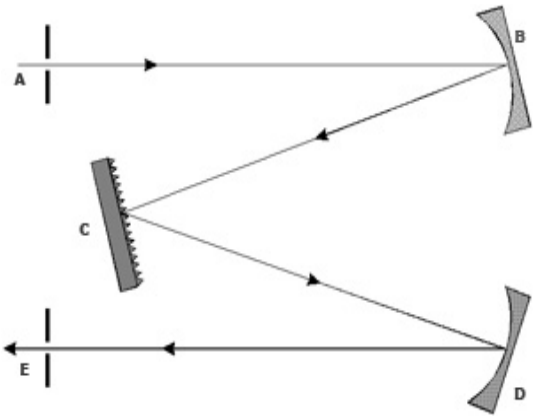

Figure II.8 - Czerny - Turner monochromator schematic, where A: entrance slit, B: collimating mirror, C: grating, D: focusing mirror, E: exit slit

II.3.4.3.Detectors

The earliest detector used for visible light spectroscopy was the human eye. There are still spectroscopes and color comparators designed for visual osbervation of color and intensity.

Modern instruments rely on photoelectric transducers, detection devices that convert photons into an electrical signal. Photoelectric transducers have a surface that can absorb

radiant energy. The absorbed energy either causes the emission of electrons, resulting in a photocurrent or moves electrons into the conduction band of solid semiconductor, resulting in an increase in conductivity. There are several common forms of detectors such as photomultiplier tubes, semiconductor detectors and barrier layer cells.

Photomultiplier tubes are monochannel detectors and are still popular. They consist of a photosensitive surface and a series of electrodes (dynodes), each at an increased potential compared to the one before. When a photon strikes the photosensitive surface, a primary electron is emitted and accelerates towards the first dynode. This electron impacts the dynode and causes the release of a number of secondary electrons, which hit the next electrode and so on until the signal is amplified many times over. Even extremely small signals can be detected.

Because of the increase of popularity of multichannel spectrometers, multichannel detectors are needed. These consist of arrays of diodes (photodiode array, charge-coupled device, charge-injection device). They have the advantage over photomultipliers of being able to measure many wavelenghts simultaneously. They need, therefore, a polycromator placed after the sample and before the detector. These multichannel detectors work by having hundreds of silicon photodiodes positioned side by side on a single collision crystal. Each photodiode has an associated storage capacitor that collects and integrates the photocurrent generated when the photons strike the photodiode. Periodically the capacitors are discharged and the current read. A spectrum can be recorded if radiation dispersed into its different wavelenghts falls on the surface of the diode array.

A charge-coupled device is also based on semiconductor technology. It is a two-dimensional array which stores photo-generated charge. The electrons are tranferred out for reading until the array has been fully read.

For detection of ultraviolet photons the preferred device is the photomultiplier tube because in the ultraviolet region of the spectrum the available light sources produce relatively few photons when compared to the visible light sources.

Light sources produce plentiful amounts of photons in the visible region and the photon energy is sufficient so that a simple phototube or phototransistor will generalte enought eletron flow to measure.

In the present work a Jasco V-570 was used. This instrument possesses a PbS photocell for the visible and near infrared region of the spectrum and a photomultiplier for the ultraviole region. PbS photocell is a photoresistor, a resistor whose resistance decreases with increasing incident light intensity.

II.3.4.4.Sample Holders

Samples for UV visible spectroscopy can be solids, liquids or gases. Different types of holders have been designed for these sample types.

The cuvettes used in UV absorption or emission spectroscopy must be transparent to UV radiation. The most common materials used are quartz and fused silica. They are also chemically inert to most solvents, which make them versatile during use. Quartz and fused silica are also transparent in the visible and int the NIR region, so they can be used in all regions in the UV and visible regions.

For spectrophotometric analysis in the visible region of the spectrum, glass or disposable plastic cells may be used. These are less expensive than quartz or fused silica but cannot be used at UV wavelenghts.

The absorption spectrum of thin films of solid materials, such as polymers, can be obtained by using a film holder. The simplest type of holder can be a paper slid mount with the sample taped to the slide mount.

II.3.4.5.Signal Processing

The PC collects the data, converts it from transmission to absorbance and displays the spectrum. It can often carry out baseline subtraction and smoothing and filtering tasks as well as qualitative and quantitative analysis. It may have other capabilities, such as the ability to compare a spectrum to those in a special library and to carry out peak purity checks.

As the absorbance is directly proportional to the concentration of the absorbing species according to the Lambert Beer law, UV-vis is a very quantitative technique. It has wide applicability and good sensitivity.

II.4.Fluorescence Spectroscopy

Molecular luminescence spectroscopy [1-3, 13-17] can be used for fundamental studies of molecular excited states as well as for selective and sensitive analysis of luminescent samples. Luminescence processes such as fluorescence and phosphorescence are emission processes, and as a result, luminescence techniques have dynamic ranges and detection limits that are several orders of magnitude better than molecular UV-vis absorption techniques for highly luminescent compounds. Selectivity can be derived from several sources. First, only certain groups of compounds that absorb UV visible radiation are likely to undergo de-excitation by luminescence. Second, selectivity among luminescent molecules can often be accomplished on the basis of excitation and emission spectral characteristics and

excited-state lifetimes.

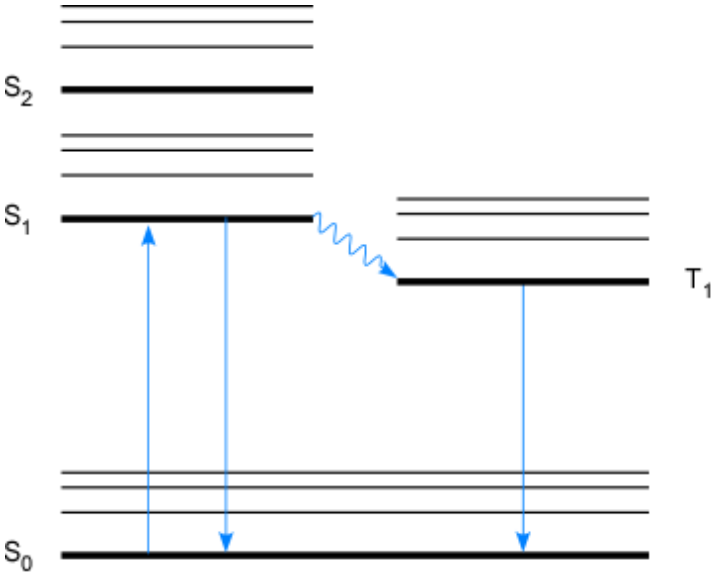

Figure II.9 - A Jablonski diagram showing electronic processes

II.4.1.Principles

Molecular absorption of photons in the ultraviolet-visible range causes the electronic transition from a lower energy level (S_0) to an excited singlet state (S_1). The emission phenomena can be explained with a Jablonski diagram, shown in Figure II.9. The molecule rapidly undergoes vibrational relaxation to the lowest vibrational level of the excited state, from which it may be de-excited by one of several competitive pathways. De-excitation directly back to the ground state can occur either by non-radiative processes or by emission of photons. The de-excitation by emission of photons is referred to as fluorescence. Alternatively under favorable conditions the molecule may undergo a forbidden transition to an overlapping triplet state (T_1) by a process know as intersystem crossing. Once in the triplet state, the molecule may undergo vibrational relaxation to the lower vibrational level of T_1 or return to S_1 by intersystem crossing. In the latter case, de-excitation by photon emission results in delayed fluorescence, which is spectrally identical to prompt fluorescence but exhibits the longer decay associated with phosphorescence. Phosphorescence generally occurs at longer wavelenghts than fluorescence since the triplet state is lower in energy than the overlapping excited singlet state.

II.4.2.Fluorescence Spectrometers

Instruments for measuring fluorescence and phosphorescence spectra have similar construction and should be called luminescence spectrometers. However the group of molecules that exhibit phosphorescence is by far smaller than that exhibiting fluorescence, hence the term fluorescence spectrometer is used.

The main spectral features of luminescence are the spectral distribution, the polarization and the radiation lifetime. For analytical purposes spectral distribution and polarization are mainly used. Measuring the lifetimes requires a rather sophisticated time-resolved spectroscopy technique.

Two types of spectra can be produced by a conventional fluorescence spectrometer. In the emission spectrum the wavelenght of the exciting radiation is held constant and the spectral distribution of the emitted radiation is measured. In the excitation spectrum the fluorescence signal is measured at a fixed wavelenght of the emission selector as the wavelenght of the exciting radiation is varied. An analyte can fluoresce only after it has absorbed radiation, and an excitation spectrum identifies the wavelenghts of light that che analyte can absorb. The excitation spectrum of a molecule, therefore, should be the same as its UV visible absorption spectrum.

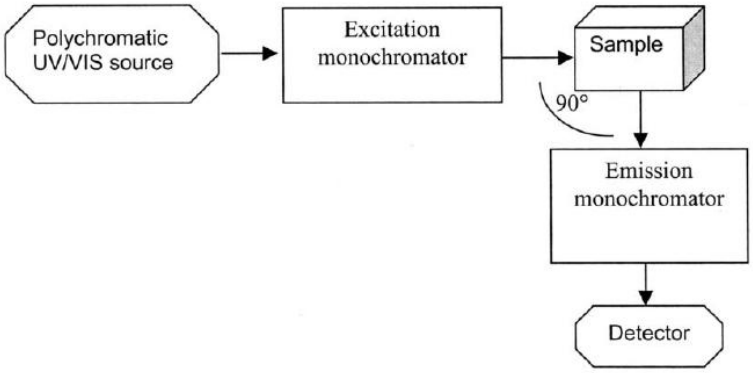

Figure II.10 - Diagram of a fluorescence spectrometer

The instrument contains the source of UV visible radiation, an excitation wavelenght selector, an emission wavelenght selector, a sample chamber and a detector. Basically it is a single beam instrument. The fluorescence emitted by the sample is usually measured at 90° in order to avoid disturbances by non-absorbed excitation radiation. If the sample is a film deposited onto a sample holder, the angle should be varied in order to focus the emitted radiation on the detector and prevent the reflected radiation to be collected.

A diagram of a fluorescence spectrometer is shown in Figure II.10.

The detectors are the same as those used for UV visible spectroscopy.

II.4.3.Application of Luminescence

Fluorescence occurs in molecules that have low energy transitions. Such molecules are primarily aromatic hydrocarbons and polycyclic aromatic compounds. Molecules with rigid structures exhibit fluorescence, because the rigidity decreases the probability of a radiationless deactivation. Some organic molecules increase their fluorescence intensity on complexation with a metal ion. The resulting complex structure is more rigid than the isolated organic molecule in solution.

A fluorometric analysis results in the collection of two spectra, the excitation spectrum and the emission spectrum. The excitation spectrum should be the same as the absorption spectrum obtained spectrophotometrically. Differences may be seen due to instrumental factors. Usually the excitation wavelenght chosen is the one that provides the most intense

fluorescence which matches with the highest peak in the absorption spectrum.

The advantages of fluorescence and phosphorescence for analysis of molecules include extremely high sensitivity, high specificity and a large linear dynamic range. The sensitivity is a result of the direct measurement of the fluorescence signal against a zero background signal. Specificity is a result of two factors: first, not all molecules fluoresce, so many molecules are eliminated from consideration, and second, two wavelenghts (excitation and emission) are used in fluorometry instead of one in spectrophotometry. It is not likely that two different compounds will emit at the same wavelenght, even if they absorb the same wavelenght. If the fluorescing compounds have more than one excitation or fluorescent wavelenght, the difference in either the emission spectrum or the excitation spectrum can be used to measure mixtures of compounds in the same solution.

Peaks may appear in the fluorescence spectrum that are due to other emission and scattering processes. Rayleigh, Tyndall and Raman scattering may be seen because of the high intensity of the light source used. Peaks due to fluorescent impurities may occur.

Reversal of fluorescence intensity or self-quenching at high concentration is a problem in quantitative analysis but can be eliminated by successive dilutions. Quenching by impurities can also occur and can cause significant problems during the analysis.

Photochemical decomposition or photochemical reactions may be induced by the intense light source used.

II.5.Infrared spectroscopy

II.5.1.Principles – Vibration in molecules

Infrared and Raman are vibrational spectroscopy techniques [1-3, 7-12]**.** They are extremely useful for providing structural information about molecules in terms of their functional groups, the orientation of those groups and information on isomers. They can be used to examine most kind of samples and are nondestructive. Infrared region covers the range 4000-400 cm^{-1} (2500 – 25000nm) and Raman radiation the range 4000 down to about zero cm^{-1}.

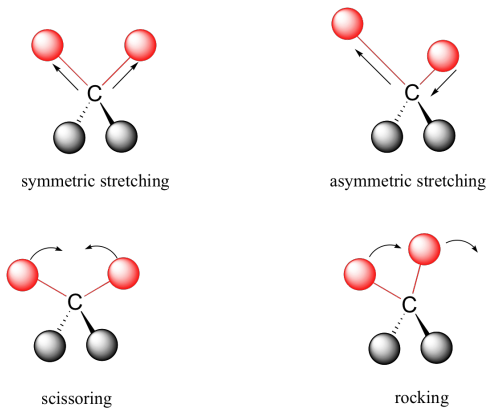

Figure II.11 - Some of the possible vibrations for a simple molecule upon absorption of infrared radiation

Infrared and Raman spectroscopies are similar as they both produce spectra because of vibrational transitions within a molecule and use the

same region of the electromagnetic spectrum. They differ in how observation and measurement are achieved, since IR is an transmission method and Raman is a scattering method. In Figure II.11 are shown some possible vibrations.

II.5.2.Infrared Spectroscopy

Molecules with covalent bonds may absorb IR radiation. It is a quantized absorption, so only certain frequencies of infrared radiation are absorbed. When the radiation is absorbed, the molecule moves to a higher energy state. Many molecules absorb IR radiation, which corresponds to the vibrational and rotational transitions of the molecules. For this absorption to occur, there must be a change in dipole moment of the molecule. IR radiation possesses a very low energy to excite electronic transition. There are a number of vibrations and rotations that the molecule can undergo which all result in absorption of IR radiation.

The IR region comprises fundamental vibrations of bound atoms. Whenever such bound atoms vibrate, they absorb infrared energy. The condition for a normal vibration *j* to be IR active is a change in molecular dipole moment μ during vibration:

$$\mu_j = \mu_0 + \left(\frac{\delta\mu}{\delta q_j}\right) q_j + \frac{1}{2}\left(\frac{\delta^2\mu}{\delta q_j^2}\right) q_j^2 + \ldots$$

where *q* is the normal coordinate describing the motion of atoms during a normal vibration.

For a vibration to give rise to the absorption of infrared radiation, it must cause a change in the dipole moment of the molecule, and the larger this change, the more intense the absorption band will be. Symmetrical molecules will have fewer infrared-active vibrations than unsymmetrical molecules. This leads to the conlcusion that symmetric vibrations will generally be weaker than asymmetrical vibrations, since the former will not lead to a change in dipole moment. It therefore follows that the bending or stretching of bonds involving atoms in widely separated groups of the periodic table will lead to intense bands. Vibration of bonds such as C–C or N=N will give weak bands. This again is because of the small change in dipole moment associated with their vibrations.

Molecule vibrations can be distinguished in stretching vibrations (changing of bond lenght) and deformation vibrations (changes of bond angles). Deformation vibrations can be subdivided into bending, torsion modes, wagging and rocking modes. Further subdivision refers to the simmetry of the vibration (symmetric/antisymmetric, in plane/out-of-plane).

The IR region can be divided in group frequencies corresponding to specific radiation absorptions by specific molecular bonds. The mid-infrared spectrum (4000-400 cm^{-1}) can be approximately divided into four regions: the X–H stretching region (4000-2500 cm^{-1}), the

triple-bond region (2500–2000 cm^{-1}), the double-bond region (2000-1500 cm^{-1}) and the fingerprint region (1500-600 cm^{-1}). The fundamental vibrations in the 4000-2500 cm^{-1} region are due to O–H, C–H and N–H stretching. N–H stretching is usually observed between 3400 and 3300 cm^{-1}. This absorption is generally much sharper than O–H stretching and may, therefore, be differentiated. C–H stretching bands from aliphatic compounds occur in the range 3000-2850 cm^{-1}. If the C–H bond is adjacent to a dougle bond or aromatic ring, the C–H stretching wavenumber increases and absorbs between 3100 and 3000 cm^{-1}.

Because of the high force constants, triple bond stretching absorptions fall in 2500-2000 cm^{-1} region. C≡C bonds absorb between 2300 and 2050 cm^{-1}, while nitrile group (C≡N) occurs between 2300 and 2200 cm^{-1}. C≡C is generally weak, while C≡N is of a medium intensity. In this region there are the most common absorptions. Some X–H stretching absorptions too, where X is a more massive atom such phosphorus or silicon. These absorptions usually occur near 2400 and 2200 cm^{-1} respectively.

In 2000-1500 cm^{-1} region are the principal bands due to C=C and C=O stretching. Carbonyl stretching is usually the most intense band in the spectrum and, depending on the type of C=O bond, occurs in the 1830-1650 cm^{-1} region.

It has been assumed that each band in an infrared spectrum can be assigned to a particular deformation of the molecule, the movement of a group of atoms or the bending or stretching of a particular bond. Many vibrations are not so well behaved and may vary by hundreds of wavenumbers, even for similar molecules. Figure II.12 shows the typical vibrational bands of polymers.

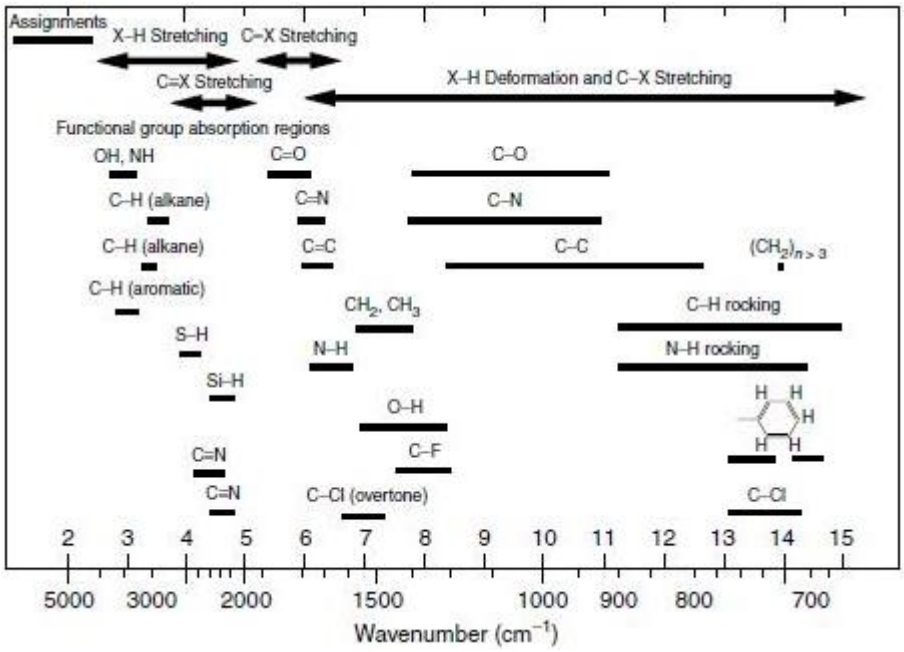

Figure II.12 - Infrared bands of polymers

This applies to most bending and skeletal vibrations, which absorb in the 1500-650 cm^{-1} region, for which small steric or electronic effects in the molecule lead to a charge shifts. In the subregion between 910 and 650 cm^{-1}, called aromatic region, are

mostly the out-of-plane aromatic C–H bending.

The absorptions observed in the near-infrared region (13000-4000 cm^{-1}) are overtones of combinations of the fundamental stretching bands which occur in the 3000-1700 cm^{-1} region. The bands involved are usually C–H, N–H or O–H stretching. The resulting bands in the near infrared are usually weak in intensity and the intensity generally decreases by a factor of 10 from one overtone to the next.

The region between 400 and 100 cm^{-1} is the far-infrared region. This region is more limited than the mid-infrared region for spectra-structure correlations, but does provide information regarding the vibrations containing heavy atoms, molecular skeleton vibrations, molecular torsions and crystal lattice vibrations. The standard format of an IR spectrum is transmittance (%T) versus wavenumber [cm^{-1}].

The features of an infrared spectrum (number of infrared absorpion bands, their intensity and shapes) are directly realated to the molecular structure of the compound under study. The IR spectrum, therefore, is the molecular fingerprint of a compound, since it represents a physical property of the molecule. So given a configuration, the main absorption bands may be predicted by energetic considerations.

The relation between measeured intensities and concentrations is expressed in the Lambert-Beer's law. It is possible, therefore, to carry out quantitative information by methods based on band heights or on integrated intensities.

II.5.2.1.Fourier Transform Infrared Spectrometer

Fourier-transform infrared (FTIR) spectroscopy is based on the idea of the interference of radiation between two beams to yield an interferogram. The latter is a signal produced as a function of the change of pathlength between the two beams. The two domains of distance and

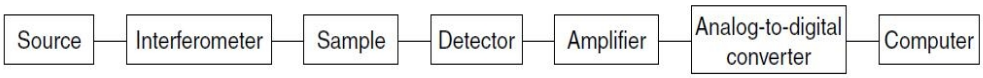

Figure II.13 - Scheme of a FTIR

frequency are interconvertible by the mathematical method of Fourier transformation. As shown in the scheme, the radiation emerging from the source is passed through an interferometer to the sample before reaching a detector (Figure II.13). Upon amplification of the signal, in which high-frequency contributions have been eliminated by a filter, the data are converted to digital form by an analog-to-digital converter and transferred to the computer for Fourier-transformation.

A radiation source for IR spectroscopy should comply with the requirements of an ideal radiation source: coninuity over the wavelenght range used,coverage of a wide wavelength range, constancy over long periods of time. For the mid-infrared region, Nerst glowers, globars and heated wires are the most common sources of IR radiation. These are heated sources that emit continuous radiation with a spectral output very similar to that of the blackbody. Normally they operate at about 1100 and 1500 K and the output range extends from near-IR to far-IR. The intensity is maximumin the mid-IT region from 4000 to 400 cm^{-1}.

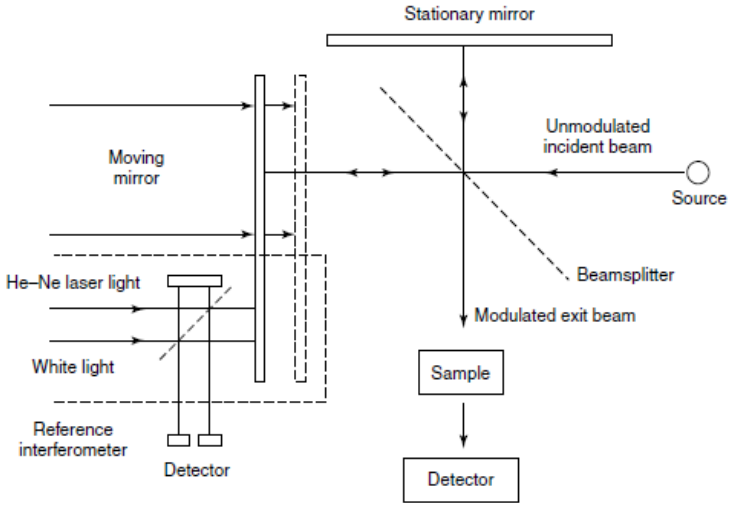

Figure II.14 - Shematic of a Michelson interferometer

The most common interferometer used in FTIR spectrometry is the Michelson interferometer (Figure II.14). It consists of two perpendicularly plane mirrors, one of which can travel in a direction perpendicular to the plane. A semi-reflecting film (beamsplitter) bisects the planes of these two mirrors. The beamsplitter material has to be chosen according to the region to be examined. Material such as germanium or iron oxide are coated onto an infrared-transparent substrate such as potassium bromide or caesium iodide to produce beamsplitters for the mid- near-infrared regions. Thin organic films such as poly(ethylene terephtalate) are used in the far-infrared region. If a collimated beam of monochromatic radiation of wavelenght λ (cm) is passed into an ideal beamsplitter, half of the incident radiation will be reflected to one of the mirrors while the other half will be transmitted to the other mirror. The beams are reflected from these mirrors, returning to the beamsplitter where they recombine and interfere. Ideally 50% of the beam reflected from the fixed mirror is transmitted through the beamsplitter while 50% is reflected back in the direction of the source. The beam which emerges from the interferometer at 90° to the input beam is called the transmitted beam and this is the beam detected in FTIR spectrometry.

The moving mirror produces an optical path difference between the two arms of the interferometer. Fot path differences of $(n + 1/2)\lambda$, the two beams interfere destructively in the case of the transmitted beam and constructively in the case of the reflected beam. The resultant interference pattern for a source of monochromatic radiation is a simple cosine

function but is of a more complicated form for a source of polychromatic radiation.

FTIR spectrometers use a Globar or Nernst source for the mid-infrared region, a high-pressure mercury lamp for the far-infrared region and a tungsten-halogen lamp for the near-infrared region.

Commonly for the mid-infrared region are employed DTGS and MCT as detectors. DTGS is a pyroelectric device incorporating deuterium tryglycine sulfate in a temperature-resistant alkali halide window, and MCT stands for mercury cadmium telluride. The former is preferred because MCT has to be cooled to liquid nitrogen temperatures, but it is better for more sensitive work. For far-infrared region are employed germanium or indium-antimony detectors, operating at liquid helium temperatures. For the near-infrared region generally lead sulfide photoconductors are used as detectors.

The essential equations for a Fourier-transformation relating the intensity $I(\delta)$ to the spectral power density at a particular wavenumber ν given by $B(\nu)$ are:

$$I(\delta) = \int_0^{+\infty} B(\nu)\cos(2\pi\nu\delta)\,d\nu$$

$$B(\nu) = \int_{-\infty}^{+\infty} I(\delta)\cos(2\pi\nu\delta)\,d\delta$$

The first shows the variation in power density as a function of the difference in pathlenght, which is an interference pattern. The second shows the variation in intensity as a function of wavenumber.

The moving mirrors is the crucial part of the interferometer, so it has to be accurately designed and must be capable of scanning two distances so that the path difference is knowable.

The interferogram is an analogue signal at the detector that has to be digitalized in order to have the Fourier-transformation in a conventional spectrum form. Having the Fourier-transform in a digitalized form it is useful to check if there are unwanted interference in the signal and if the mirrors are placed properly.

There are two conventional sampling techniques for IR spectroscopy: transmission and reflection methods.

II.5.2.2.Infrared Methods - Transmission

This technique is based on the absorption of infrared radiation at specific wavelenghts as it passes through a sample. It is possibile to analyse liquid, solid or gaseous samples. Depending on the range to be analyzed, several holder materials can be chosen as they have an useful range in wavenumbers: KBr can be used between 43500-400 cm^{-1}, NaCl between

40000-600 cm^{-1}, KCl 33000-400 cm^{-1}. Where water is used as a solvent, NaCl cannot be empoyed as a infrared window material as it is soluble in water. A drop of liquid may be sandwiched between two infrared plates, which are then mounted in a cell holder. Liquid films provide a quick method of examining liquid samples. Before producing an infrared sample in solution, a suitable solvent must be chosen. It has to dissolve the compound, it should be as non-polar as possible to minimize solute-solvent interactions and it should not absorb infrared radiation strongly.

Depending on the nature of the sample to be examined, in transmission-mode there are three methods used for examining solid samples: alkali halide discs, mulls and films. The use of alkali halide discs involves mixing a solid sample with a dry alkali halide powder. The most common alkali halide used is potassium bromide (KBr), which is completely transparent in the mid-infrared region. The mull method involves grinding the sample and then suspending in on to two drops of a mulling agent. This is not transparent in the infrared region, but known its spectrum, the sample spectrum is obtained by subtraction. Films are produced by solvent casting or by melt casting. In solvent casting the sample is dissolved in a solvent. Variations of concentration of the sample determines the thickness. The solvent chosen has to divvolve the sample and also to produce an uniform film. The film could be deposed straight onto the infrared window to be used.

II.5.2.3.Infrared Methods – Reflection

Attenuated totale reflectance (ATR) is useful for obtaining infrared spectra of difficult samples that cannot be readly examined by the normal transmission method. They are suitable for studying thick or highly absorbing solid and liquid materials. It requires little or no sample preparation for most samples and is one of the most versatile sampling technique.

ATR occurs when a beam of radiation enters from a medium with a higher refractive index to a medium with a lower refractive index. It utilizes the phenomenon of total internal reflection. A beam of radiation entering a crystal will undergo total internal reflection when the angle of incidence at the interface between the sample and the crystal is greater than the critical angle which is a function of the refractive indices of the two surfaces. The beam penetrates a very short distance beyond the interface and into the less-dense medium before the complete reflection occurs. This penetration is called the evanescent wave and typically is at a depth of a few micrometers. Its intensity is reduced (attenuated) by the sample in regions of the IR spectrum where the sample absorbs. The depth of penetration can be calculated by the following:

$$d_p = (\lambda/n_1)/\{2\pi[\sin\vartheta - (n_1 / n_2)^2]^{1/2}\}$$

where d_p is the depth of penetration, n_1 is the refractive index of the sample and n_2 is the refractive index of the more dense medium.

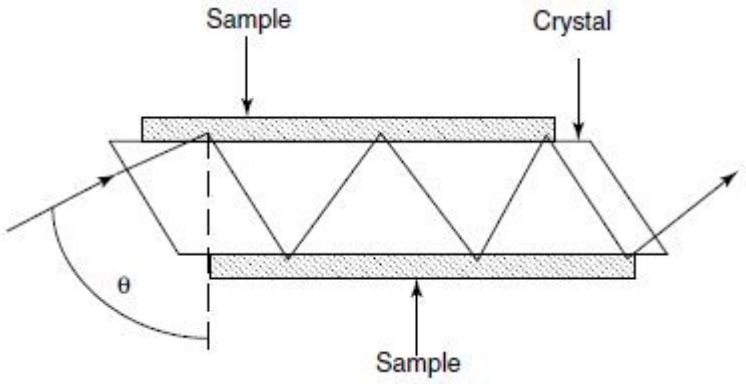

Figure II.15 - Schematic of a typical ATR cell

The sample is normally placed in close contact with a more-dense high-refractive-index crystal such as zinc selenide, thallium bromide-thallium iodide of germanium. As shown in Figure II.15, the infrared beam is directed onto the blunt edge of the ATR crystal and internally reflected through the crystal with a single or multiple reflections. The number of reflections and penetration depth decreases with increasing angle of incidence. The higher lenght-to-thickness ratio of the ATR crystal gives higher numbers of reflections for a given angle. Different designs of ATR cells allow both liquid and solid samples to be examined. A flow-through ATR cell is also possible to be realized, so a continuous flow of solution can be monitored in time.

II.6 Instrumentation

II.6.1.Spin Coater

Spin coating is a procedure used to apply uniform thin films to substrates by rotation at high speed (in rpm). An excess amount of solution is deposed in the center of a substrate and then the substrate is rotated at high speed in order to spread the fluid by centrifugal force. Centrifugal acceleration will cause the solution to spread to, and eventually off, the edge of the substrate leaving a thin film of compound on the surface. Final film thickness and other properties will depend on the nature of the solution (viscosity, drying rate, percent solids, surface tension) and the parameters chosen for the spin process. Factors such as final rotational speed and acceleration contribute to how the properties of the coated films are defined.

A typical spin process consists of the deposition of the solution onto the substrate and then the rotation process. In the deposition part, an amount of solution is deposited. Depending on the viscosity of the fluid and the size of the substrate to be coated, different amounts of solution are required. Higher viscosity and larger substrates require a larger amount of the solution to ensure full coverage of the substrate during the high speed spin step.

After the deposition of the solution it is common to accelerate to a relatively high speed to thin the fluid close to its desired final thickness. In general higher spin speeds and longer spin times create thinner films.

A separate drying step is sometimes added after the high speed step to further dry the sample without substantially thinning it. Generally speed and duration of the rotation are adjusted in order to obtain the desired thickness of the film and complete evaporation of the solvent.

To obtain certain film properties, known the concentration, viscosity, surface tension of the solution, the spin coating instrument allows to vary three parameters: spin speed, spin acceleration and fume exhaust. Spin coaters set several steps. In each step the three spin coating parameters can be set independently of eachother.

II.6.1.1.Spin Speed

The spin speed of the substrate (rpm) affects the degree of centrifugal force applied to the solution as well as the velocity and characteristic turbulence of the air immediately above it. In particular, the high spin speed step generally defines the final film thickness. Film thickness is a balance between the force applied to shear the liquid towards the edge of the substrate and the drying rate which affects the viscosity of the solution. As the liquid dries, the viscosity increases until the radial force of the spin process can no longer appreciably move the compound over the surface. At this point, the film thickness will not decrease significantly with increased spin time.

II.6.1.2.Acceleration

The acceleration of the substrate towards the final spin speed can also affect the coated film properties. Since the solution begins to dry during the first part of the spin cycle, it is important to accurately control acceleration. Typically, 50% of the solvents will be lost to evaporation in the first few seconds of the process. Acceleration also plays a large role in the coat properties of patterned substrates. The acceleration provides a twisting force to the solution.

II.6.1.3.Fume Exhaust

The drying rate of the solution during the spin process is defined by the nature of the fluid itself (volatility of the solvent systems used) as well as by the air surrounding the substrate during the spin process. The solution dries also depending on the ambient conditions around it. It is well known that factors such as air temperature and humidity play an important

role in determining coated film properties. It is also very important that the airflow and associated turbulence above the substrate itself be minimized, or at least held constant, during the spin process. Spin coaters generally employ an exhaust lid in order to limit unwanted random turbulence and and minimize susceptibility to ambient humidity variations.

II.6.2.Solar Simulator

A Solar Simulation system also known as sun simulator reproduces the full spectrum of light (shown in Figure II.16) equal to natural sunlight. The ground level spectrum of natural sunlight is different for various locations on Earth. The constituents of the atmosphere affect both absorption and scattering. Elevation is another factor that affects the ground level spectrum, since the elevation determines how far the sun's radiation must pass through the atmosphere. For any given location the distance the sun's radiation must travel through the atmosphere changes as the day progresses, due to the changing angle of the sun. With the sun directly overhead the direct radiation that passes through travels the shortest distance through Earth's atmosphere to reach the Earth. The spectrum of this radiation is referred to as "Air Mass 1 Direct" (AM1D). For standardization purposes sea level is used as a standard reference site. The global radiation with the sun overhead is referred to as "Air Mass 1 Global" (AM1G). The spectrum of sun's radiation in space does not pass through any air mass hence it is referred to as "Air Mass 0" (AM0).

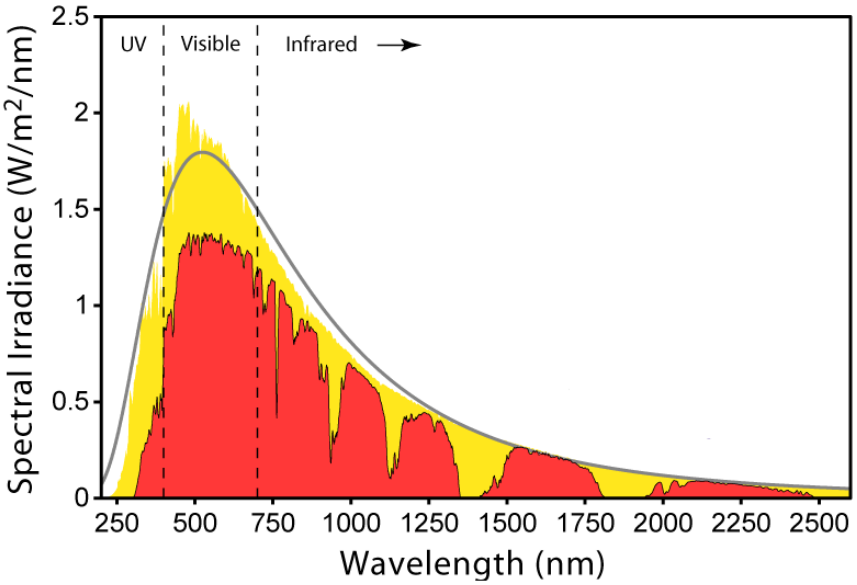

Figure II.16 - Solar Spectrum

Since solar radiation reaching the Earth's surface varies significantly with atmospheric condition, location, time of the day, Earth/sun distance, and solar activity, standard spectra have been developed to provide a basis for standardization of theoretical evaluation of the effects of solar radiation. The most widely used standard spectra are those published by The Committee Internationale d'Eclaraige (CIE), the world authority on radiometric and photometric nomenclature and standards.

The American Society of Testing and Materials (ASTM) has published three spectra, AM0, AM1.5 Direct and AM 1.5 Global for a 37° tilted surface. The conditions for the AM 1.5 spectra were chosen by ASTM because they are representative of average conditions in the 48 contiguous states of the United States. In addition to the standards for different air masses, standards for Non-Uniformity, Temporal Instability of Irradiance, Total Irradiance within 300 Field of View, and how closely the system's radiation spectral distribution matches the sun's radiation have been established by various organizations. In the USA, ASTM has established such standards for Solar Simulators.

The most important part of the device is the light source system. The light source has an ellipsoidal reflector that surrounds a xenon lamp and collects most of the lamp output. The radiation from the lamp is focused onto an optical integrator that helps produce an uniform diverging beam. The beam is diverted by a mirror onto a collimating lens. Special filters are placed between the mirror and the collimating lens to shape the radiation spectra to match various air masses. The output is a uniform beam that closely matches the sun's radiation spectrum for a given air mass.

Solar simulators generally have a shutter that can be operated manually, while the light intensity can be adjusted by varying the intensity of the supply current of the lamp.

II.6.3.UV Lamp

UV lamps emit ultraviolet light from 253.7 nm due to the peak emission of the mercury within the bulb. With the addition of a suitable phosphorescent coating, they can be modified to produce a UVA, UVB, or visible light spectrum (all fluorescent tubes used for domestic and commercial lighting are mercury (Hg) UV emission bulbs at heart).

In this work a 500 W UV lamp was used to irradiate the samples and, therefore, perform the accelerated degradation of the materials under study. The aging of the materials was then analyzed by spectroscopy. The device used is composed of two parts: the lamp reflector, made by a double metal body with insulated handle and built with a particular chemical treatment which allows high UV radiation ratio and low temperature transmittance, and a quartz UV mercury vapour lamp which emits from 180 nm to visible range and offers a strong UV emittance from 254 nm.

II.6.4.Digital multimeter

A multimeter is an electronic measuring instrument that combines several measurement functions. Typically multimeters measure voltage, current, resistance.

Multimeters may use analog or digital circuits, and are then divided into analog

multimeters and digital multimeters. Modern multimeters are often digital due to better accuracy and durability.

The signal analyzed by digital multimeters is converted to a voltage and an amplifier with electronically controlled gain modulates the signal.

An embedded computer is often used, especially to collect different data sets in a single analysis.

In order to carry out accurate measurements, resolution and accuracy of the multimeter have to be considered. Resolution and accuracy in a multimeter are not equal. The resolution of a multimeter is the smallest part of the scale which can be shown. The resolution is scale dependent and in high end digital multimeters it can be configured, with higher resolution measurements taking longer to complete. Absolute accuracy is the error of the measurement compared to a perfect measurement. Relative accuracy is the error of the measurement compared to the device used to calibrate the multimeter. Most multimeter datasheets provide relative accuracy. In order to compute the absolute accuracy from the relative accuracy of a multimeter the absolute accuracy of the device used to calibrate the multimeter has to be added to the relative accuracy of the multimeter.

Digital multimeters generally take measurements with accuracy superior to their analog counterparts. Standard analog multimeters measure with typically 3% accuracy. Standard portable digital multimeters are specified to have an accuracy of typically 0,5%, while mainstream bench-top multimeters are available with specified accuracy of better than 0,01%. Laboratory grade instruments can have accuracies even of a few parts per million.

II.7.Experimental procedures

The samples studied in this work were obtained by depositing on different substrates three different solutions: dye-only, PMMA-only and dye-doped PMMA dissolved in chloroform.

Dye-only solutions were obtained by dissolving in chloroform 1% of Lumogen F Red 305 by weight of $CHCl_3$. Samples were kept under magnetic stirring for at least 3 hours. While in stirring, the solutions were kept into flasks sealed using Parafilm provided by Pechiney.

PMMA-only and dye-doped PMMA solutions were obtained by dissolving in chloroform 10% of PMMA by weight of $CHCl_3$. In addition, in dye-doped PMMA solutions, 6% by weight of Lumogen F Red 305 was dissolved. The latter were named PL6, as P stands for PMMA, L for Lumogen and 6 is the dye percentage.

Thin films were spincoated by a LAURELL WS-400 BZ-6NPP-LITE spincoater. Spin speed was set at 1200 rpm, and acceleration was set at 1272 rpm/s. In order to permit the almost complete evaporation of the solvent, the depositions were carried out for 40 seconds.

Solutions and depositttion settings described above were then adopted in all spectroscopic analyses. Different sample holders were adopted depending on the performed analysis.

FTIR spectra were collected by Thermo Nicolet FT-IR Nexus spectrometer and the substrates used were KBr and NaCl pellets provided by Sigma-Aldrich.

UV-vis spectroscopy was carried out by Jasco-V570 instrument and sample holders were quartz substrates provided by Hellma. UV-vis spectra were also collected for dye-only chloroform solution, composed of dye at 0.1‰ concentration by weight of chloroform.

Fluorescence spectroscopy was carried out by Jasco FP-6600 spectrofluorometer and and the samples were deposited on Thermo Scientific microscope glass slides.

The samples obtained by spincoating were then exposed to UV light at increasing exposure times. The source of UV radiation used in the present work has been a 500W lamp by Helios Italquartz ® (GR.E. 500W model).

The luminescent solar concentrators (OLSC) developed in this work, were fabricated by depositing through spincoating a Lumogen-doped PMMA chloroform solution on glass substrates (22x55x1 mm^3 Thermo Scientific microscope slides) to form thin films. The luminescent solar concentrator realized in this way was then coupled to a Si solar cell (model SLSD-71N4, commercially available from Silonex). The OLSC devices were tested under simulated solar radiation generated by an Abet technologies Sun 2000 solar simulator (100 mW/cm^2), and system efficiencies were calculated by measuring the electrical parameters of the PV cell by means of a Keithley 2612 digital multimeter before and after bonding the OLSC thin film to the solar cell.

Each test was performed by applying a voltage from -0.2V to 0.6V in a 75-points scan. As a result, the multimeter sent back the relative current responses and the V_{oc} and I_{sc} values.

Bibliographic References

1. James W. Robinson, Eileen M. Skelly, George M. Frame “Spectral Interpretation and Applications” in “Undergraduate Instrumental Analysis”, Marcel Dekker, (2005)
2. G. Gauglitz and Tuan Vo-Dinh “Methods 1: Optical Spectroscopy” in “Handbook of Spectroscopy”, Wiley-VCH (2003)
3. G. Gauglitz, T. Vo-Dinh“Handbook of Spectroscopy”, Wiley-VCH, (2003)
4. James W. Robinson, Eileen M. Skelly, George M. Frame “Visible and Ultraviolet Molecular Spectroscopy“ in “Undergraduate Instrumental Analysis”, Marcel Dekker (2005)
5. G. W. Ewing, “Ultraviolet Visible NearInfrared Spectrophotometers” in “Analytical Instrumentation Handbook”, Marcel Dekker (1997)
6. Bernard Valeur, “Absorption of UVvisible light” in “Molecular Fluorescence: principles and applications”, Wiley-VCH, (2002)
7. Satinder Ahuja, Neil D.Jespersen “General principles of spectroscopy and spectroscopic analysis” in “Modern instrumental analysis”, Wilson & Wilson's (2006)
8. James W. Robinson, Eileen M. Skelly, George M. Frame “Infrared Spectroscopy” in “Undergraduate Instrumental Analysis”, Marcel Dekker, (2005)
9. C.-P. Sherman Hsu, F. Settle “Infrared Spectroscopy” in “Handbook of Instrumental Techniques for Analytical Chemistry”, Prentice Hall PTR (1997)
10. G. W. Ewing, “Vibrational Spectroscopy: Instrumentation for Infrared and Raman Spectroscopy” in “Analytical Instrumentation Handbook”, Marcel Dekker (1997)
11. B. Stuart “Infrared Spectroscopy: Fundamentals and applications”, Wiley (2005)
12. N. J. Everall, J. M. Chalmers, P. R. Griffiths “Vibrational Spectroscopy of Polymers: Principles and Practice”, Wiley (2007)
13. G. W. Ewing “Molecular Fluorescence and Phosphorescence” in “Analytical Instrumentation Handbook” - – Marcel Dekker (1997)
14. Bernard Valeur “Characteristics of fluorescence emission” in “Molecular Fluorescence: principles and applications”, Wiley-VCH, (2002)
15. Bernard Valeur “Effects of intermolecular photophysical processes on fluorescence “ in “Molecular Fluorescence: principles and applications”, Wiley-VCH, (2002)

16. Joseph R. Lakowicz “Principles of fluorescence spectroscopy, Volume 1”, Springer (2006)

17. Satinder Ahuja, Neil D.Jespersen “Emission methods” in “Modern instrumental analysis”, Wilson & Wilson's (2006)

Chapter III
Results and Discussion

This chapter presents the results of the research performed during this thesis. The results have been devided into three main sections, namely the study of material degradation and stability following exposure to UV light, the study of possible stabilization techniques, and the study of photovoltaic properties of OLSC devices. The degradation behaviour was monitored through fluorescence spectroscopy, UV-vis spectroscopy and FTIR spectroscopy, while the study on device operation was carried out by means of electrical characterization of illuminated working OLSC coupled with standard silicon solar cells.

III.1.Study of degradation mechanisms in OLSC materials

The materials before and after UV exposure have been studied by means of spectroscopic techniques in order to evaluate their photostability. The carrier matrix and the organic dye were first studied individually and then mixed together in a thin film, the latter representing the active material of the luminescent solar concentrator.

III.1.1.Carrier Matrix

The material constituting the carrier matrix in an OLSC should exhibit high transparency, high refractive index, good chemical resistance and good photostability. Another important requirement is cost effectiveness. The matrix should not absorb photons that can be converted by the dye, so UV-vis bands of the matrix and the dye should not be overlapping. In order to meet these requirements, poly(methyl methacrylate) (PMMA) has been chosen in this work as the material for the carrier matrix. PMMA has refractive index of about 1.5, it is a transparent polymer, a low-cost material, and it has good chemical resistance and presents better light exposure resistance compared to other polymeric binders.

The optical and chemical properties of the chosen matrix were studied before and after degradation by UV exposure. Optical properties were examined by UV-vis spectroscopy while molecular properties were investigated by FTIR spectroscopy.

III.1.1.1.UV-vis

Optical transparency was verified by UV-vis spectroscopy. In the visible region PMMA has a very low absorption intensity. It presents a high absorption peak at about 200 nm as shown in FigureIII. 1.

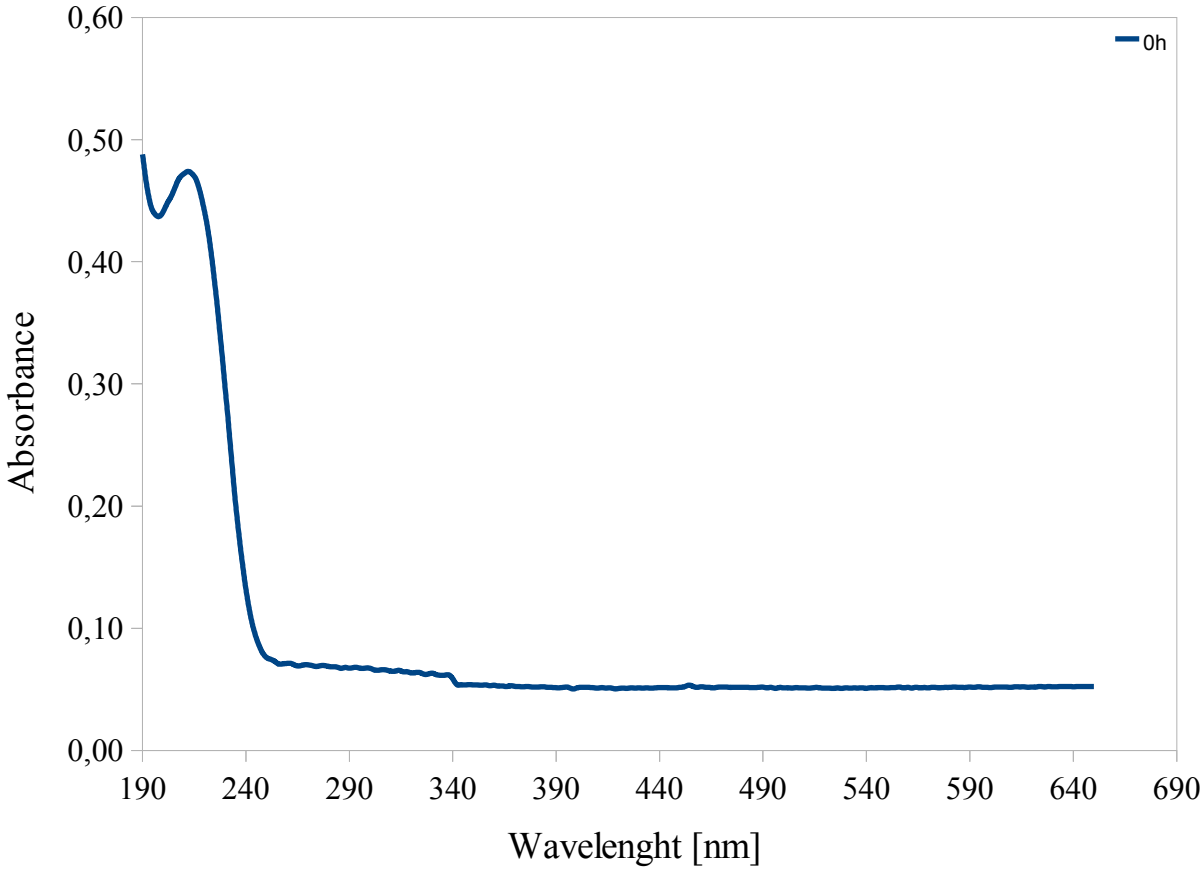

FigureIII. 1 - UV visible absorption spectra of Poly(methyl methacrylate)

The UV lamp emits UV radiation with an emission peak centered at 254 nm, which is therefore partially absorbed by PMMA. The emitted radiation can thus produce a significant degradation of the material.

Changes in the UV and the visible absorption regions of the absorption spectrum were analyzed during the aging process. UV-vis spectra were collected every hour up to a maximum exposure time of 10h. This work only presents spectra of the degraded material up to 5h of exposure as they are sufficient to give an estimate of the degradation kinetics.

The UV-vis spectra of PMMA films at increasing UV-exposure time are shown in FigureIII. 2.

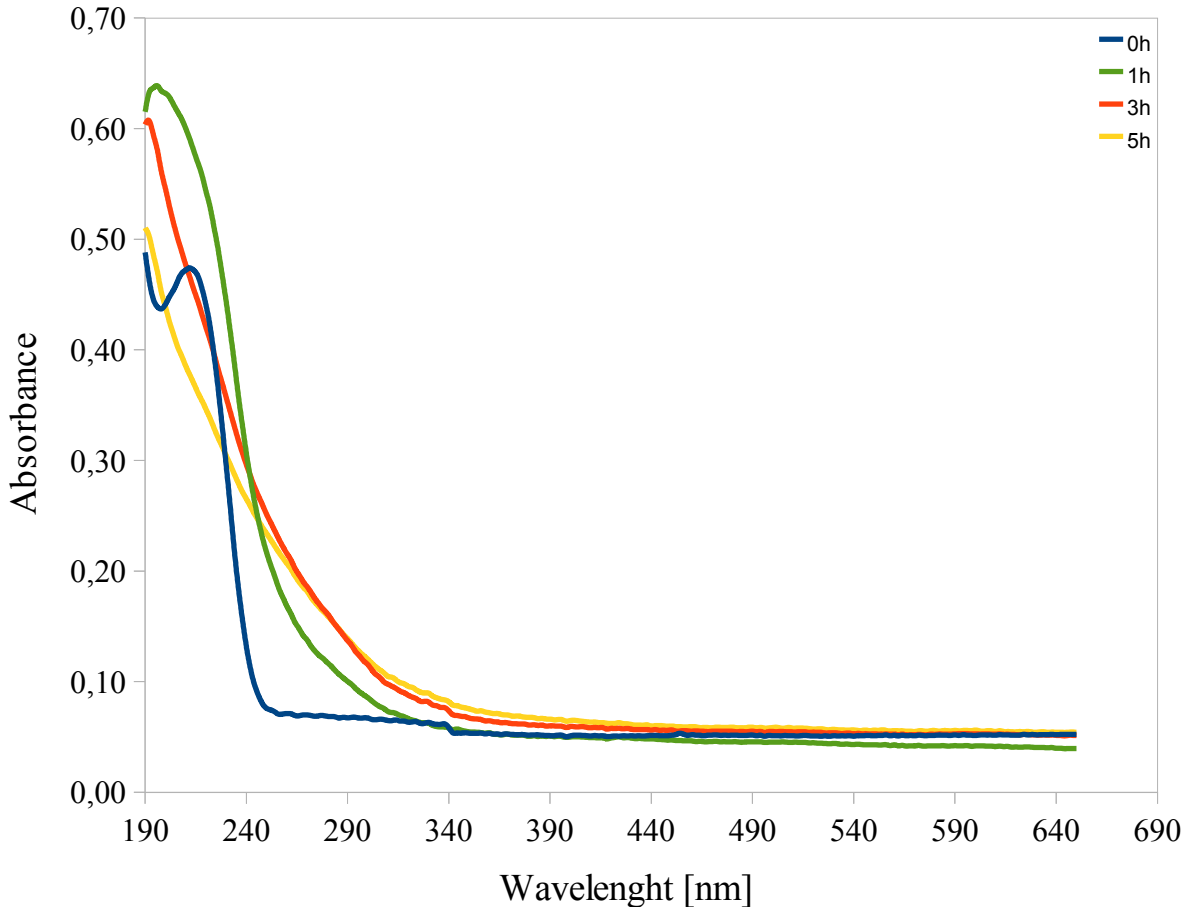

FigureIII. 2 - UV visible absorption spectra of PMMA exposed to UV light after 0h, 1h, 3h, 5h

UV-irradiation of PMMA films causes an increase of absorbance at 250-350 nm range. Around 275 nm a new absorption band is formed after 1 hour. Absorbance at 275 nm increases in PMMA, already after 1h of irradiation but for longer exposure times no significant changes are observed. The increase of absorption in 250-350 nm region can be explained by the formation of an unsaturated group in combination with carbonyl groups resulting from the interaction of PMMA film with high energy light. These results are accordance with previous reports [5-8].

The peak centered at about 230 nm in the spectrum of pristine PMMA exhibits a blue shift of about 15 nm after 1h of irradiation. The rapid increase in intensity may be attributed to changes in optical properties of the thin film (e.g. refractive index) due to modification of chemical structure following the degradation properties. Conversely, the decrease in absorbance over exposure times longer than 1 h may be due to partial loss of material during irradiation.

III.2.1.2.FTIR

FigureIII. 3 shows the FTIR spectrum of pristine PMMA.

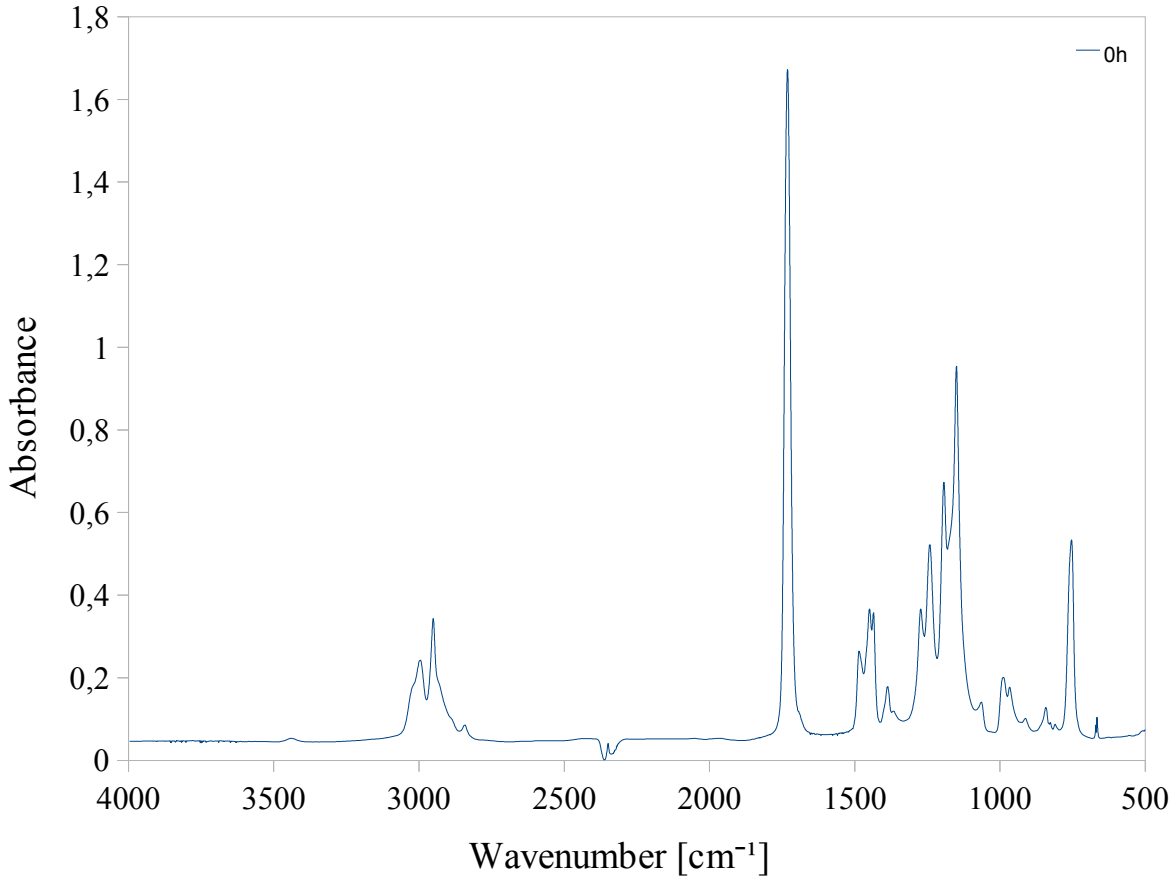

FigureIII. 3- FTIR spectrum of PMMA

The main absorption bands associated to vibrations of chemical groups are listed below:

- the region 3100-2800 cm^{-1} is characteristic for the stretching of C-H bonds; both the symmetric and asymmetric stretching peaks can be detected, being the symmetric at lower energies than the asymmetric;
- the peak at about 1731 cm^{-1} was assigned to the stretching of the carbonyl group C=O;
- the peak at about 1485 cm^{-1} was assigned to the CH_2 bending;
- the region 1200-1100 cm^{-1} is characteristic for the C-O-C stretching region;
- the region 1500-1300 cm^{-1} is characteristic for the C-C stretching region, CH_2, CH_3 bend and wag.

The identification of the peaks in the pristine polymer represents the first step for the examination of the degradation process of the material. The decreasing intensity of a peak can be related to the breaking of the relative molecular group. The appearance of new peaks

corresponds to the formation of new molecular groups.

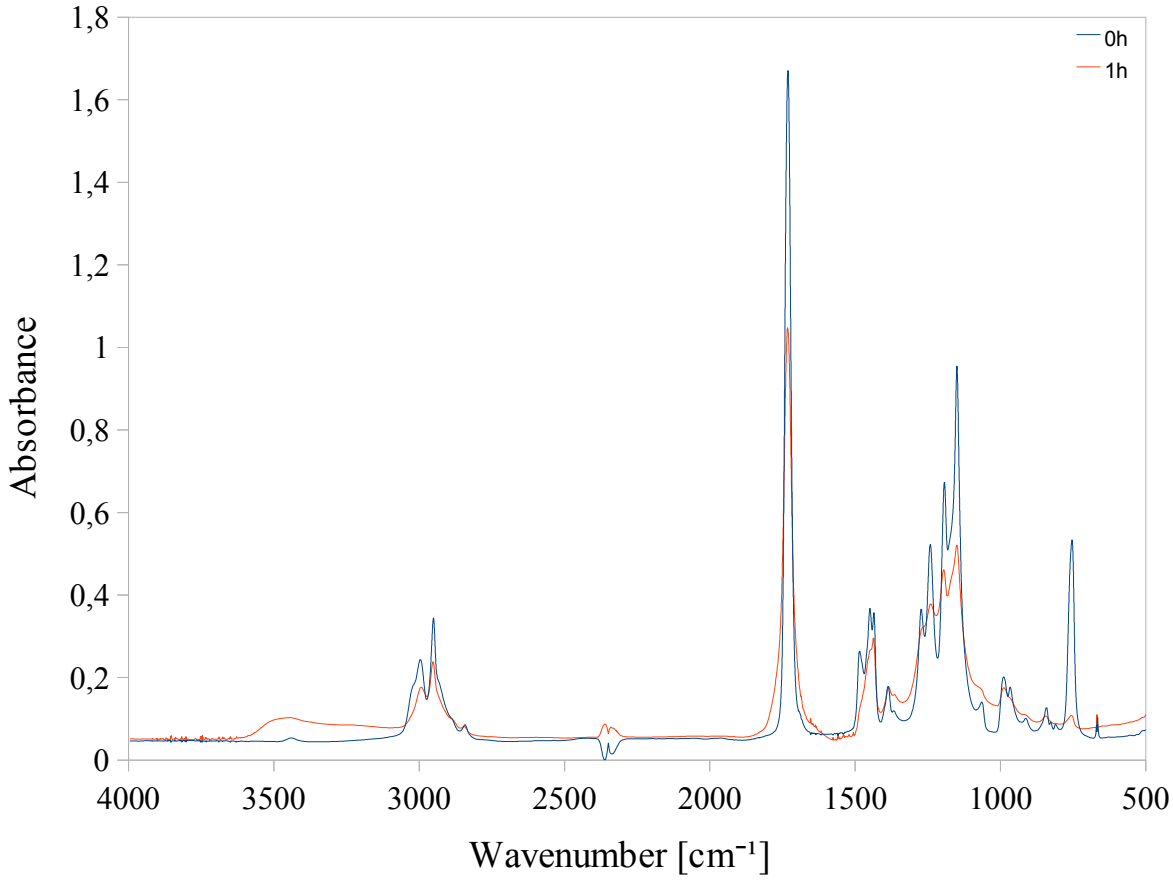

FigureIII. 4 - FTIR spectra of pristine PMMA and after 1 hour of UV irradiation

The first step of the degradation process is shown in FigureIII. 4, where the FTIR spectra of pristine PMMA and PMMA irradiated by UV light for 1 h are shown.

Several changes in the FTIR spectra may be observed already after 1h of UV light exposure. The formation of new species can be observed at about 3500 cm^{-1} and from the broadening of carbonyl region (1900-1600 cm^{-1}) adjacent to the main peak centered at 1731 cm^{-1}. Overall, a general reduction of all peak intensities is found in the whole spectrum. As known from the literature [5,9] the main products of the photodegradation of PMMA in vacuum are methyl formate, methanol, methyl methacrylate. On the other hand, methane, hydrogen, carbon monoxide and carbon dioxide are formed when the polymer is exposed to light in air [5-9]. All these products are derived from the decomposition of ester groups.

FigureIII. 5 shows FTIR spectra of PMMA thin films before UV irradiation and after one, three and five hours of exposure to UV light.

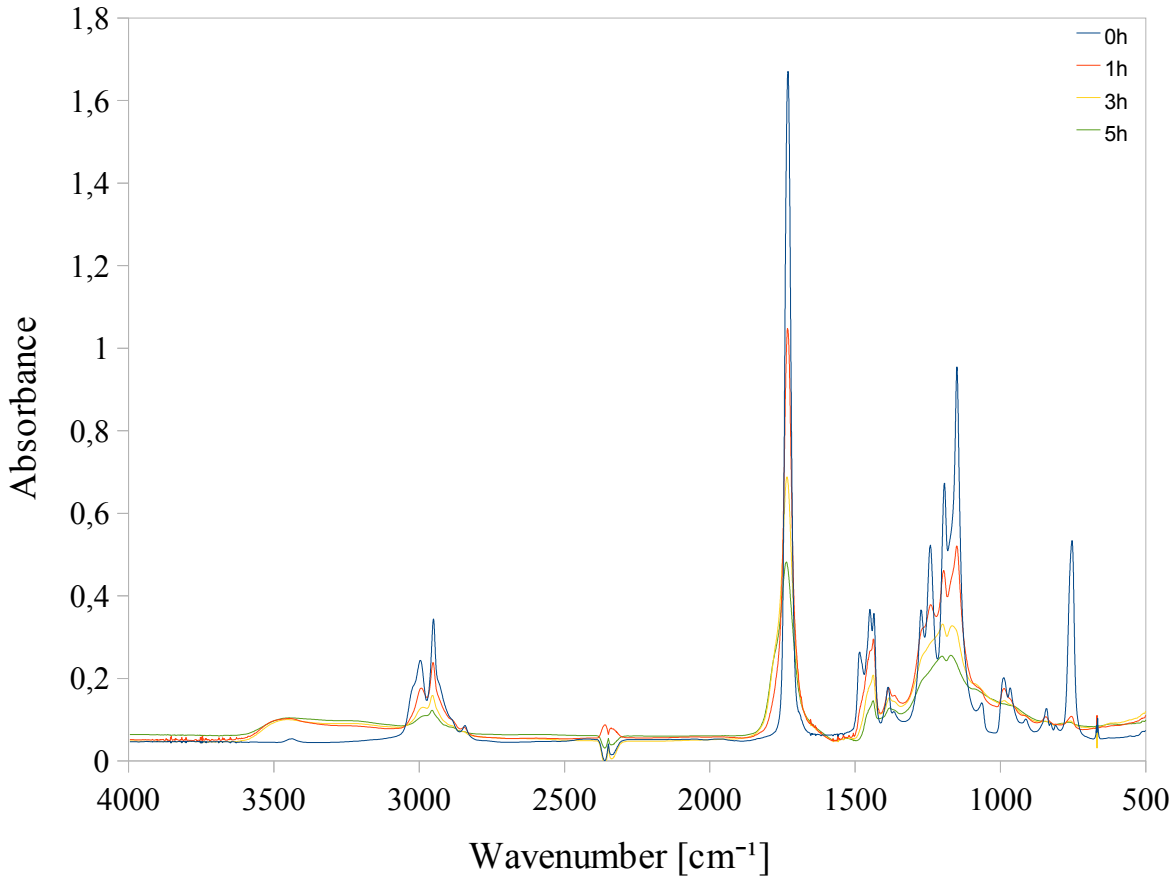

FigureIII. 5 – FTIR spectra of pristine PMMA (blue) and PMMA degraded after 1hour (red), 3 hours (yellow), 5 hours (green) of UV irradiation

The same behaviour is observed for PMMA films exposed to UV light for longer than 1h (yellow and green lines in FigureIII. 5). In particular, the degradation of the PMMA films leads to an increase of the signals in the 3500 cm^{-1} region accompanied by the appearance of two bands in the carbonyl region adjacent to the main peak (1731 cm^{-1}).

After 5h of UV irradiation a large and complex absorption band is formed between 1500 and 500 cm^{-1}resulting from the formation of new species.

In order to better clarify the changes in the FTIR spectra of degraded samples, a more detailed analysis of the spectra is needed, primarily focusing on FTIR regions characteristic of the PMMA. In particular, the CH stretching region, the region around the carbonyl peak and the C-C and C-O-C stretching region will be considered. FigureIII. 6 shows FTIR spectra of PMMA films in the C-H stretching region (3700-2500 cm^{-1}). In the spectrum of pristine PMMA three main peaks can be distinguished, centered at 2995 cm^{-1}, 2950 cm^{-1} and 2840 cm^{-1}. In degraded PMMA films these peaks can still be observed, although they are characterized by low intensity and are shifted in wavelength. The peak at 2950 cm^{-1} undergoes a shift of 5 cm^{-1} so after 5h of UV exposure it is at 2955 cm-1 while the peak centered at 2995 cm^{-1} in the pristine PMMA FTIR spectrum after 5h of UV exposure is observed at 2980 cm^{-1}.

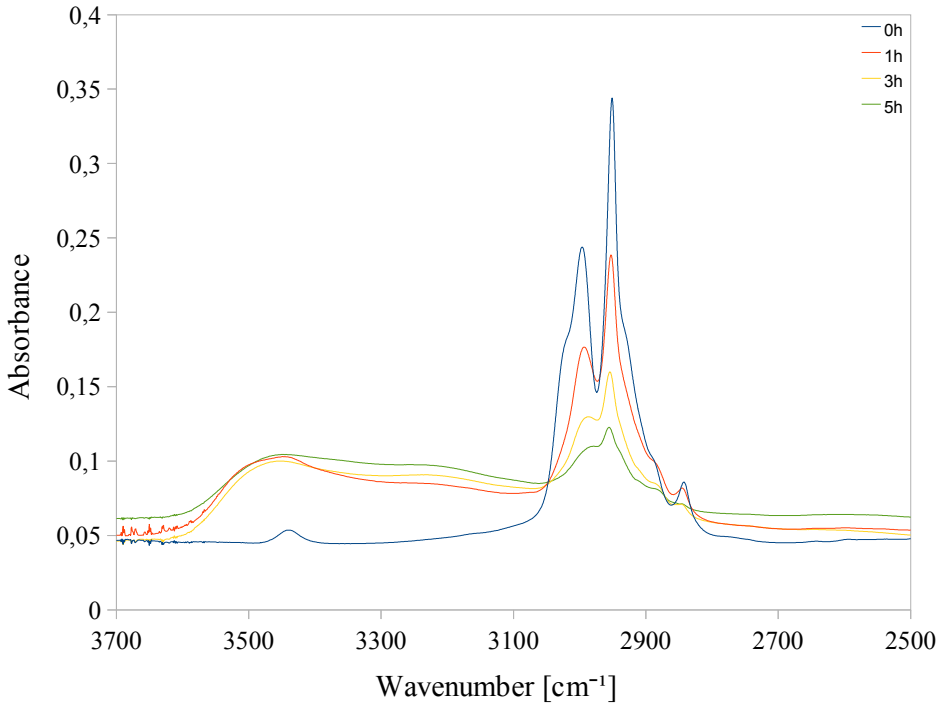

FigureIII. 6 - C-H stretching region of pristine and degraded PMMA

The decrease in intensity may be attributed to gradual disappearance of C-H bonds, although loss of material during the degradation process may also give a significant contribution to this decrease. However the decrease of FTIR absorption intensity of methyl/methylene groups can be due not only to degradation resulting from side groups abstraction, but also to oxidation [6]. In particular, oxidation products formed during exposure of the polymer films to UV light may undergo further photolysis and volatile low molecular weight products can be evolved [5,6].

The new broad band appearing at about 3500 cm^{-1} is typical for free (non-associated) and hydrogen-bonded hydroxyl/hydroperoxide groups, as also reported in the literature [6,9].

The FTIR spectra of PMMA films in the carbonyl region at different UV-light exposure times are shown in FigureIII. 7.

By observing the behaviour of the carbonyl region during the degradation process, a significant modification of the main peak at 1731 cm^{-1} is clearly visible. The absorbance of the main carbonyl peak centered at 1731 cm^{-1}, attributed to the stretching of C=O bond in the ester group, decreases continuously during irradiation but simultaneously the development of carbonyl shoulder at 1754-1760 cm^{-1} takes place. The first absorption band can be attributed to aliphatic ketones, while the second one to peracid and perester groups [6]. The total amount of carbonyl groups changes irregularly during UV-irradiation because of competitive reactions: decay of ester groups and oxidation with formation of new carbonyls [6].

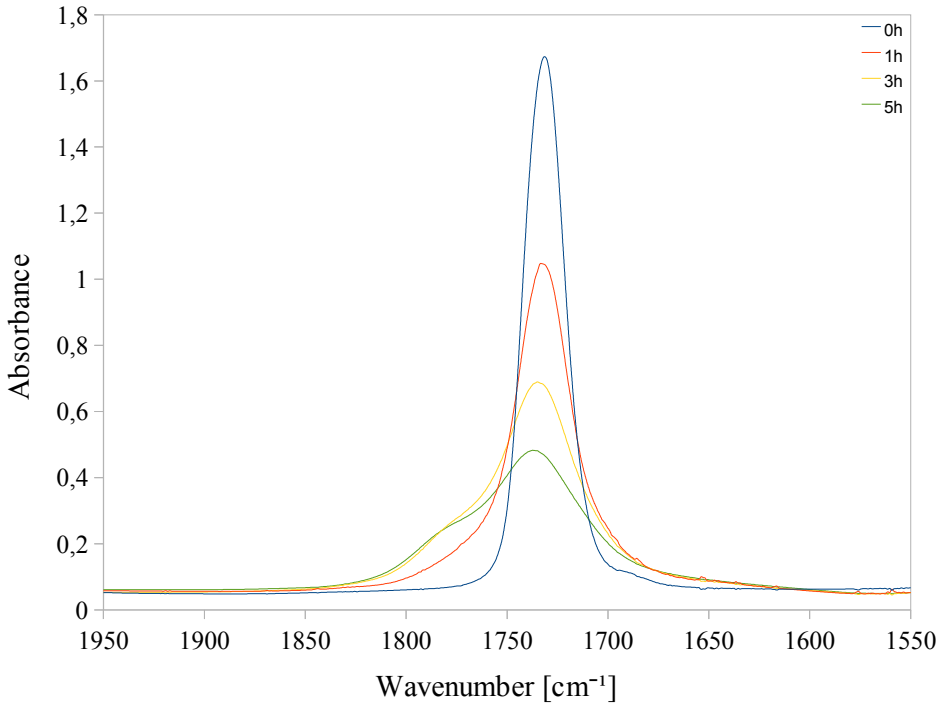

FigureIII. 7 - PMMA degradation in carbonilic region

The modifications occurring in the 1300-1000 cm^{-1} region characteristic of the stretching vibrations of C-O-C bonds can be also used to monitor the degradation process of PMMA. In particular, a change in the amount of these groups should be clearly noticeable in FTIR spectra of degraded samples.

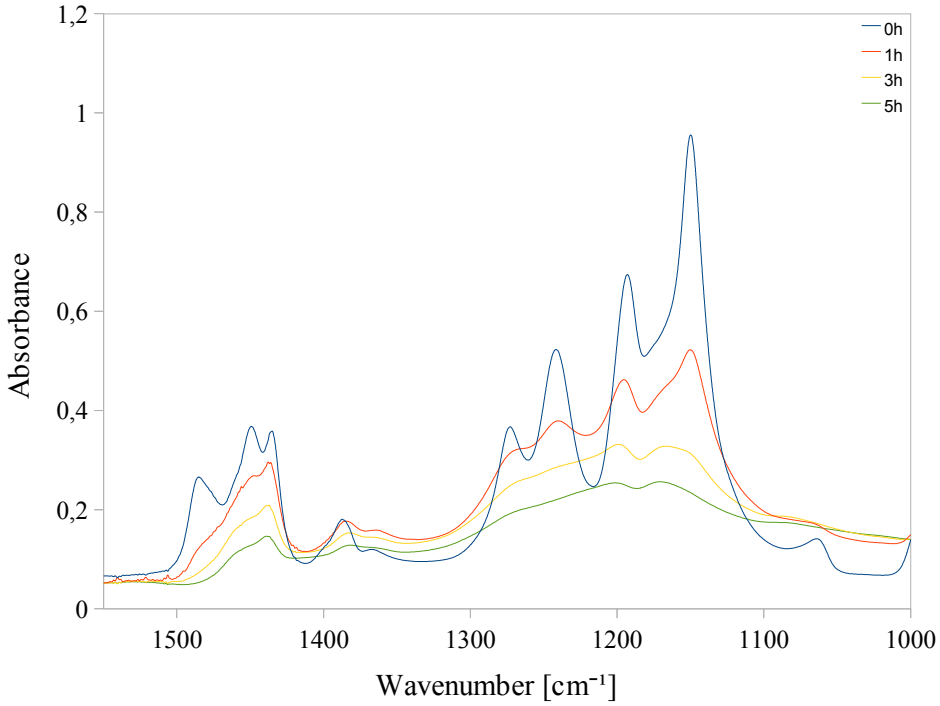

FigureIII. 8- C-C and C-O-C stretching regions of PMMA exposed to UV light after 0h, 1h, 3h, 5h

FigureIII. 7 shows an overall decrease during UV irradiation accompanied by a broadening of the peaks and by the development of more complex features in the 1300-1100

cm^{-1}. These modifications to the signals attributed to the asymmetric stretching vibration of C-O-C bonds may be ascribed to destructive reactions occurring to side groups during UV exposure [3,4,6].

III.2.2.Organic dye

Luminescent species mixed in the carrier matrix absorb incident light and isotropically emit it at a red-shifted wavelength. Total internal reflection in the device ensures collection of part of the emitted light in the solar cells at the sides of the device. Ideally the energy of the emitted photons is slightly higher than the band gap of the attached solar cells, to ensure near-unity conversion efficiency. Organic dyes suitable for LSC technology, therefore, should exhibit high luminescence quantum efficiency (LQE) and good solubility in the organic matrix and in organic solvents. To avoid self-absorption of emitted photons the Stokes shift of the organic dye should be as high as possible, where the Stokes shift is defined as the difference in wavelength between absorption and emission peak maxima. To verify Lumogen F Red 305 Stokes shift, fluorescence and UV visible spectra were collected, as shown in

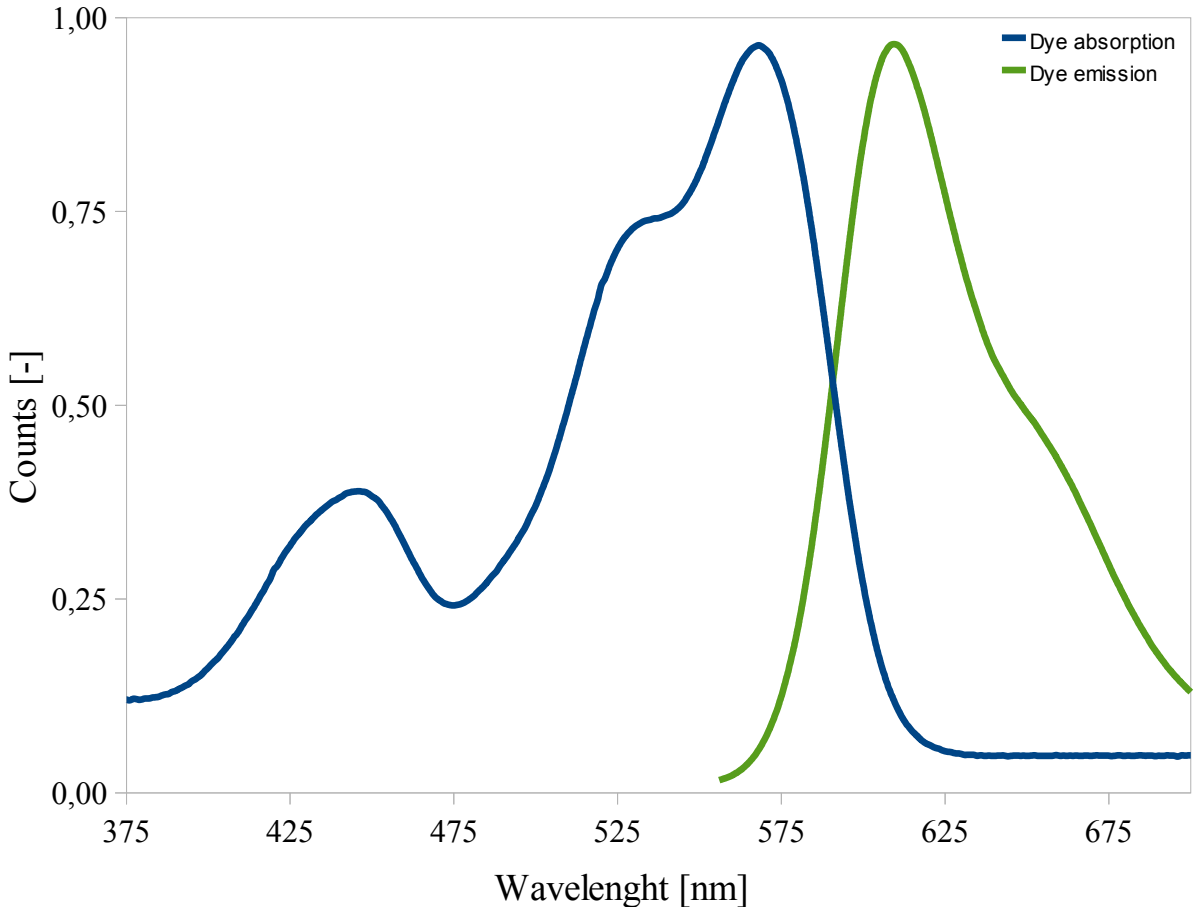

FigureIII. 9- Absorption and emission spectra of Lumogen Red 305

FigureIII. 9. The organic dye presents a Stoke shift of 41 nm when it is deposited

alone, and a Stoke Shift of 36 nm when the dye is dispersed in the carrier matrix.

As performed on PMMA, degradation studies of Lumogen F Red 305 were done by irradiating the samples under UV light and collecting fluorescence, UV visible and FTIR spectra of the material at increasing exposure times.

III.2.2.1.UV-vis

FigureIII. 10 shows UV-vis spectrum of a Lumogen F Red 305 thin film.

Four different peaks can be identified in the dye UV-vis spectrum. Two peaks are found in the UV region (from 190 nm to 350 nm) at 194 nm and 283 nm, and two peaks are found in the visible region (from 350 nm to 700 nm) at 445 nm and 540 nm.

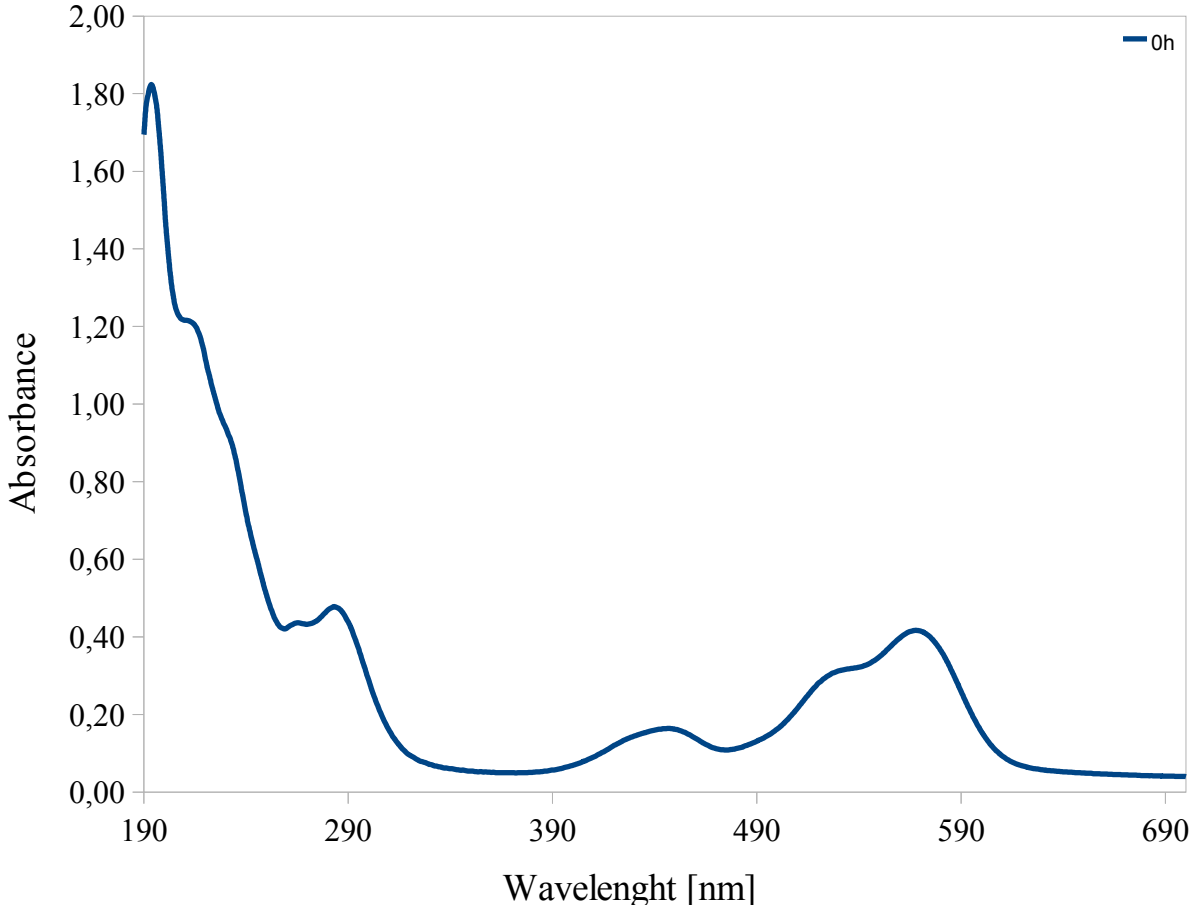

FigureIII. 10- UV-vis spectrum (190-700 nm) of Lumogen F Red 305 thin film

The peaks in the UV region are very high in intensity. The dye, therefore, is expected to behave as UV absorber when combined in the polymeric matrix.

The dye exhibits two peaks in the visible region as already mentioned in III.1.2.1. The peak centered at 445 nm is attributed to the absorption of side groups. The main peak is attributed to the absorption of the perylene core [10]. It is a composite peak, with a maximum at 568 nm if the dye is in solid state and at 578 nm if the dye is in solution. In solution each dye molecule is weakily interacting to other molecules compared to solid state and in UV-vis

this is translated in a red shift. FigureIII. 11 shows the UV-vis spectrum of a dye thin film deposited by spincoating (blue line) and the spectrum of the dye in $CHCl_3$ solution (red line).

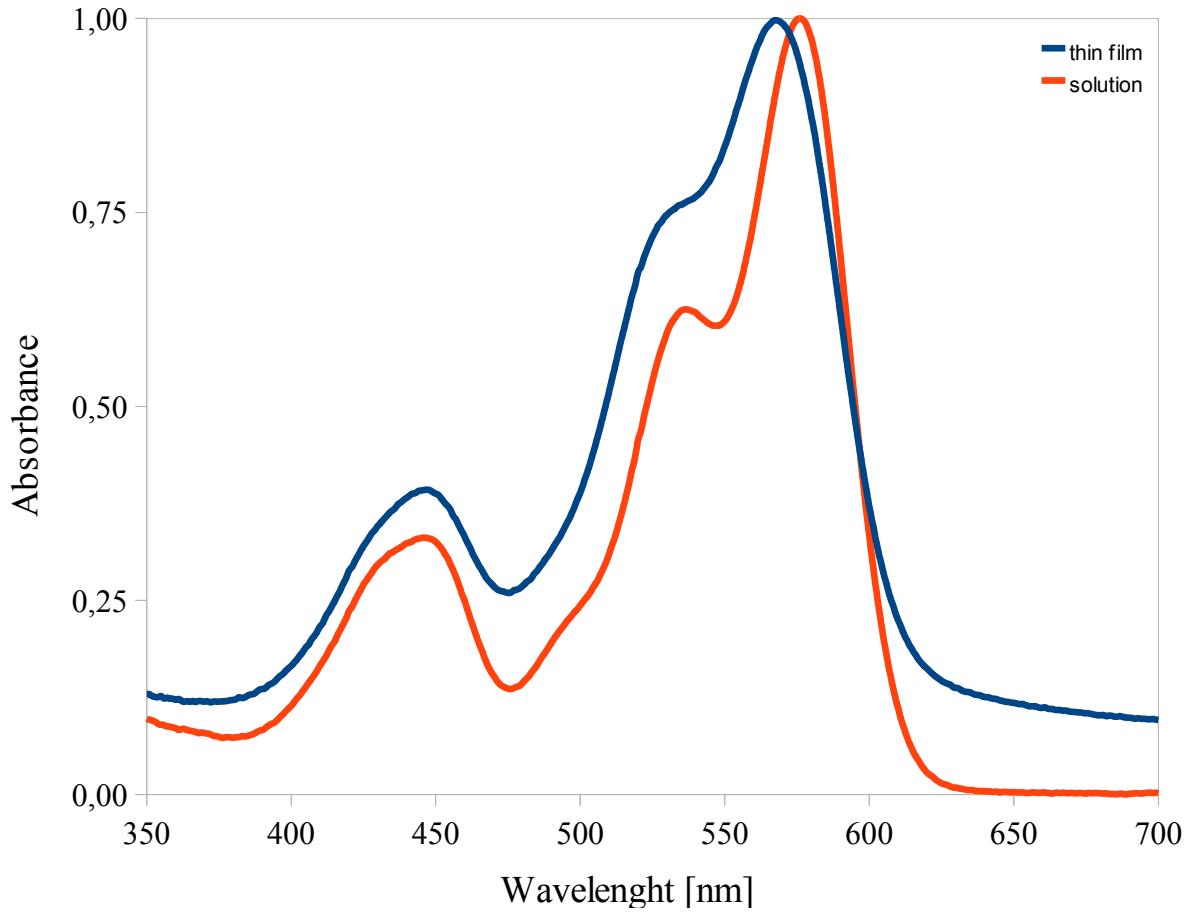

FigureIII. 11- UV-vis spectra of dye thin film (blue line) and dye in CHCl3 solution (red line). In order to highlight the red shift, absorption intensities are normalized

The absorption peak centered at 445 nm was assigned to lateral chromophore substituents after comparing Lumogen UV-vis spectrum with the UV-vis spectrum of Perylene diimide (PDI). PDI is an organic dye that shows a similar structure to Lumogen, but it does not possess lateral substituents (see FigureIII. 12).

As shown in FigureIII. 13 the UV-vis spectrum of PDI film in the visible region shows only one absorption band. It is a single composite peak and it could be attributed to a single absorbing species. Conversely, in the visible region, Lumogen F Red 305 exhibits two distinctly separated peaks. These peaks can therefore be attributed to two different absorbing groups. The composite peak may be assigned to the perylene core as a similar composite peak is also found in the UV-vis spectrum of PDI. On the other hand, the peak centered at 445 nm may be attributed to the lateral chromophore groups.

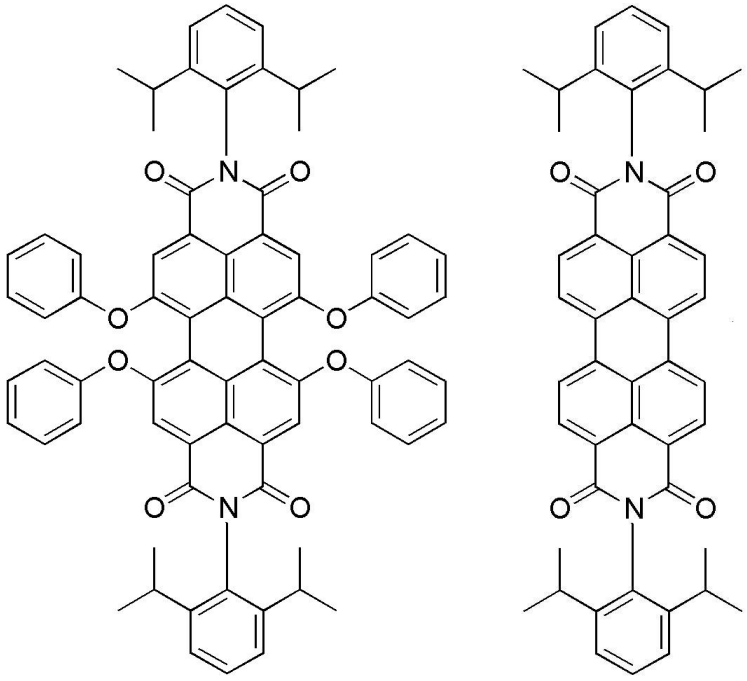

FigureIII. 12- Molecular structures of Lumogen F Red 305 (left) and Perylen Diimide (right)

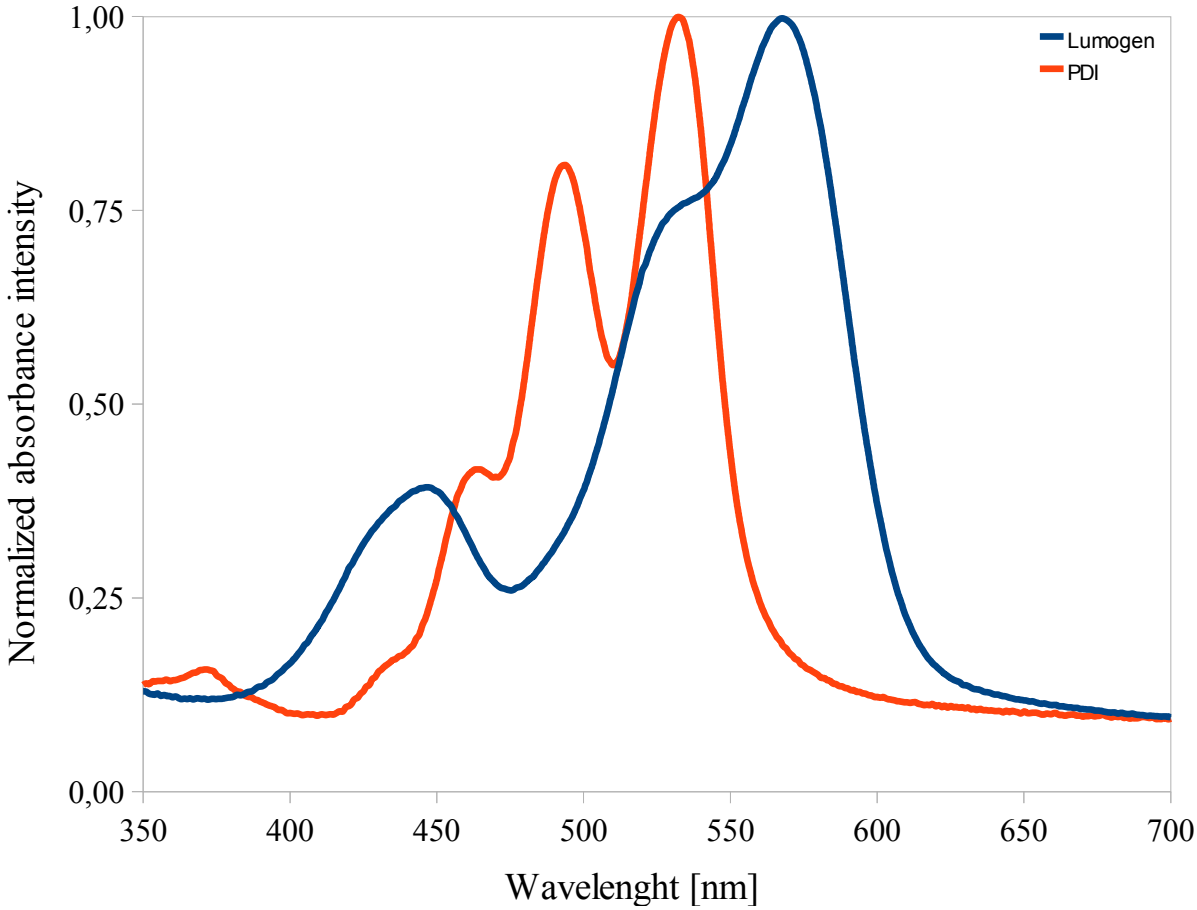

FigureIII. 13- UV-vis spectra of Lumogen F Red 305 film (blue line) and PDI film (red line). In order to better compare the spectra, absorption intensities are normalized

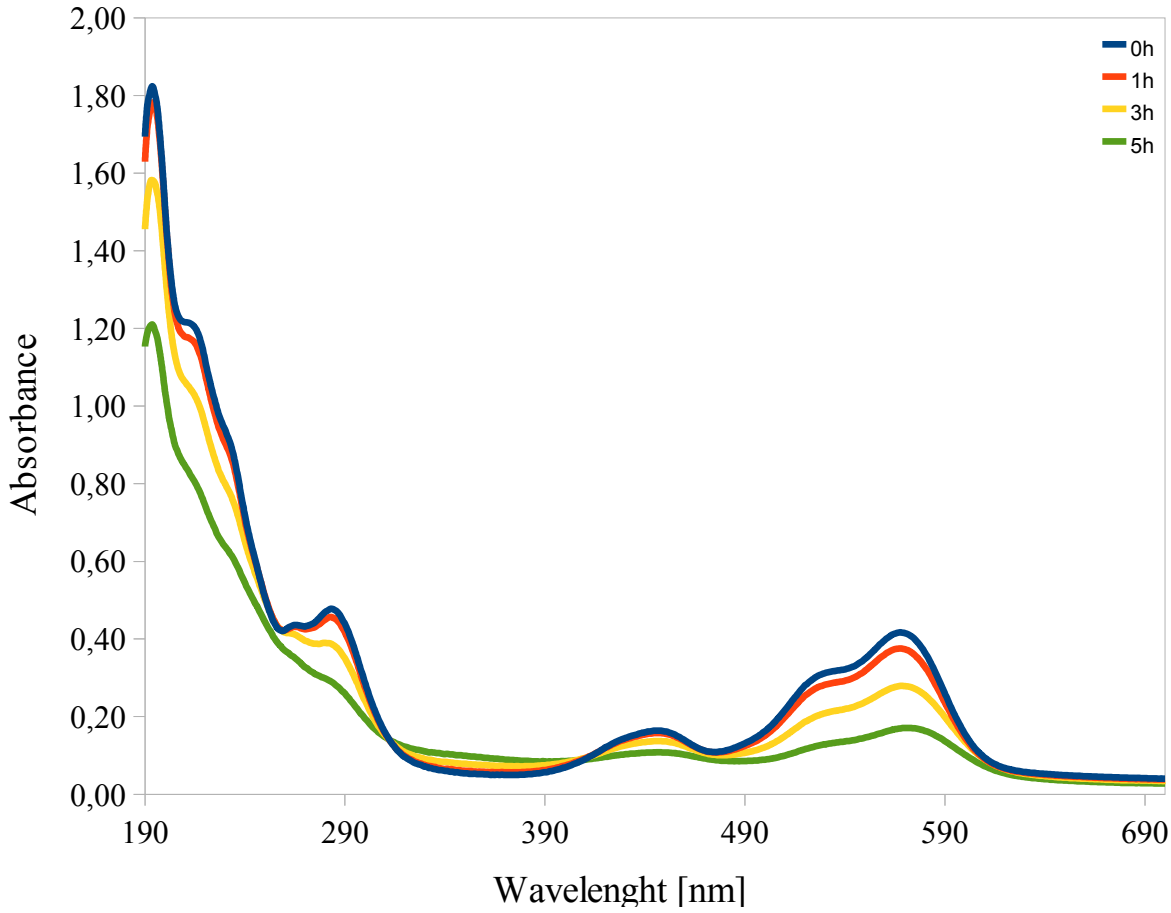

FigureIII. 14- UV-vis absorption spectra of Lumogen F Red 305 degraded dye after 0h, 1h, 3h, 5h of UV exposure

The degradation process of Lumogen F Red 305 was investigated by monitoring the modification occurring to the UV-vis spectra at increasing UV-irradiation times. FigureIII. 14 shows the UV-vis spectra of the pristine dye and the spectra of the dye after 1h, 3h, 5h of UV exposure.

FigureIII. 15 shows a close-up on the visible region of the Lumogen UV-vis spectra at increasing irradiation times.

A decrease of intensity for both absorption peaks can be observed. In addition, a 5 nm red shift is found for the main absorption peak from 568 nm to 573 nm.

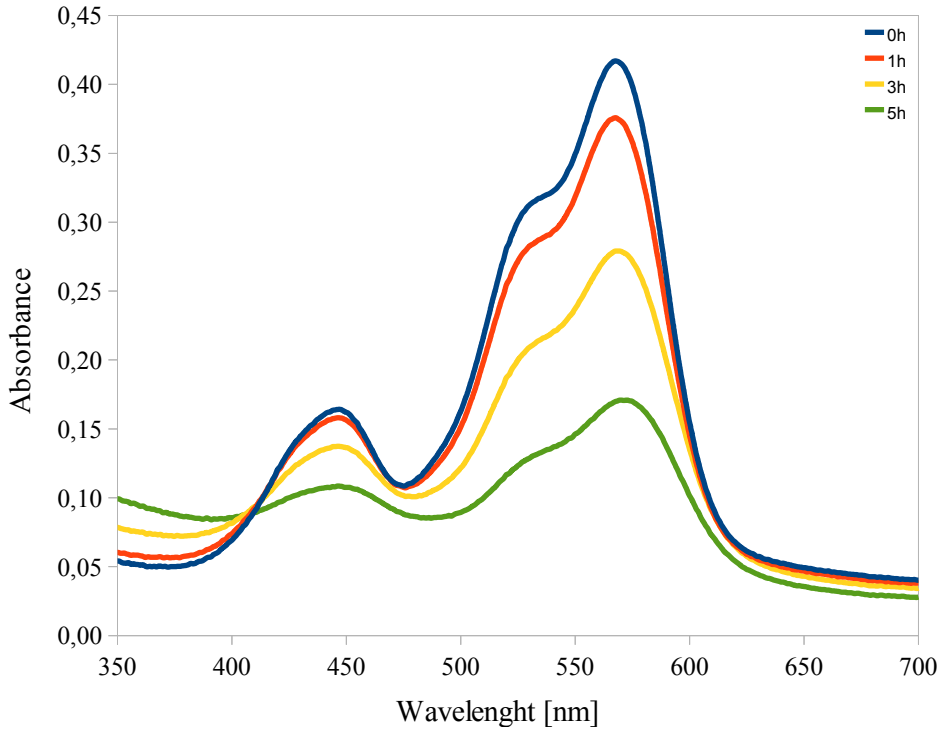

FigureIII. 15- UV-vis spectra focused on 350-700 nm region of pristine Lumogen F Red 305 film and degraded after 1h, 3h, 5h of UV exposure

Similarly to what performed on fluorescence spectra, ratios between lower wavelength and higher wavelength absorption peak were calculated to investigate how the degradation process evolves. The results are shown in FigureIII. 16.

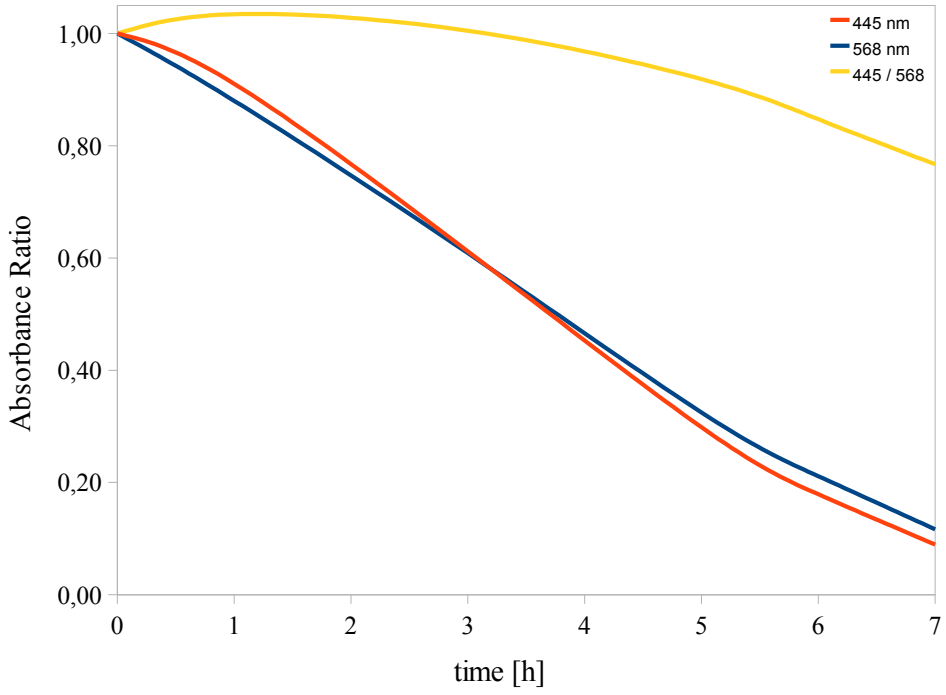

FigureIII. 16- Trends of degradation process by UV-vis spectroscopy. Red and blue lines are the ratios of the intensities of degraded material to the intensity of the pristine material

The yellow line, representing the ratio between higher and lower energy absorption peaks, mantains a constant value equal to 1 up to 5h UV-exposure times.

However, if longer exposure times are considered, a different behaviour is found. In particular, after about 6h exposure time, the high energy peak shows a faster decrease in absorption intensity with respect to the lower energy peak. This may indicate faster disappearance of chromophore species compared with perylene core during the degradation process.

III.2.2.2.Fluorescence

Emission spectra of Lumogen F Red 305 thin films, deposited by spin coating onto quartz substrates, were investigated by fluorescence spectroscopy. According to the product datasheet, the chosen dye should have an emission peak centered at 613 nm.

As shown in previous section, the dye presents two main absorption peaks in UV-vis spectrum. The peak with a maximum at 445 nm is attributed to lateral chromophore absorption and the wide composite peak with a maximum at about 568 nm is attributed to the perylene core absorption. In order to understand the emission phenomenon, fluorescence spectra were collected. Theoretically, the excitation wavelenght employed in fluorescence emission studies should be the same as the absorption peak wavelength (445 nm and 568 nm) in order to maximize the emission process. However, during fluorescence emission measurements, part of the monochromatic light used to excite the fluorescent molecule is reflected by the sample and is recovered by the detector, thus appearing in the emission spectrum as a false emission peak. Therefore, in order to prevent the presence of a peak centered at 568 nm in the emission spectrum generated by reflected light from the sample, the dye molecule was excited in the region of perylene core absorption at a wavelength of 540 nm. In addition, excitation at 445 nm was also performed, to take into account the contribution to light absorption given by the lateral chromophores. FigureIII. 17 shows the fluorescence spectrum of the dye excited by a 445 nm light source and the spectrum of the dye excited by a 540 nm light source.

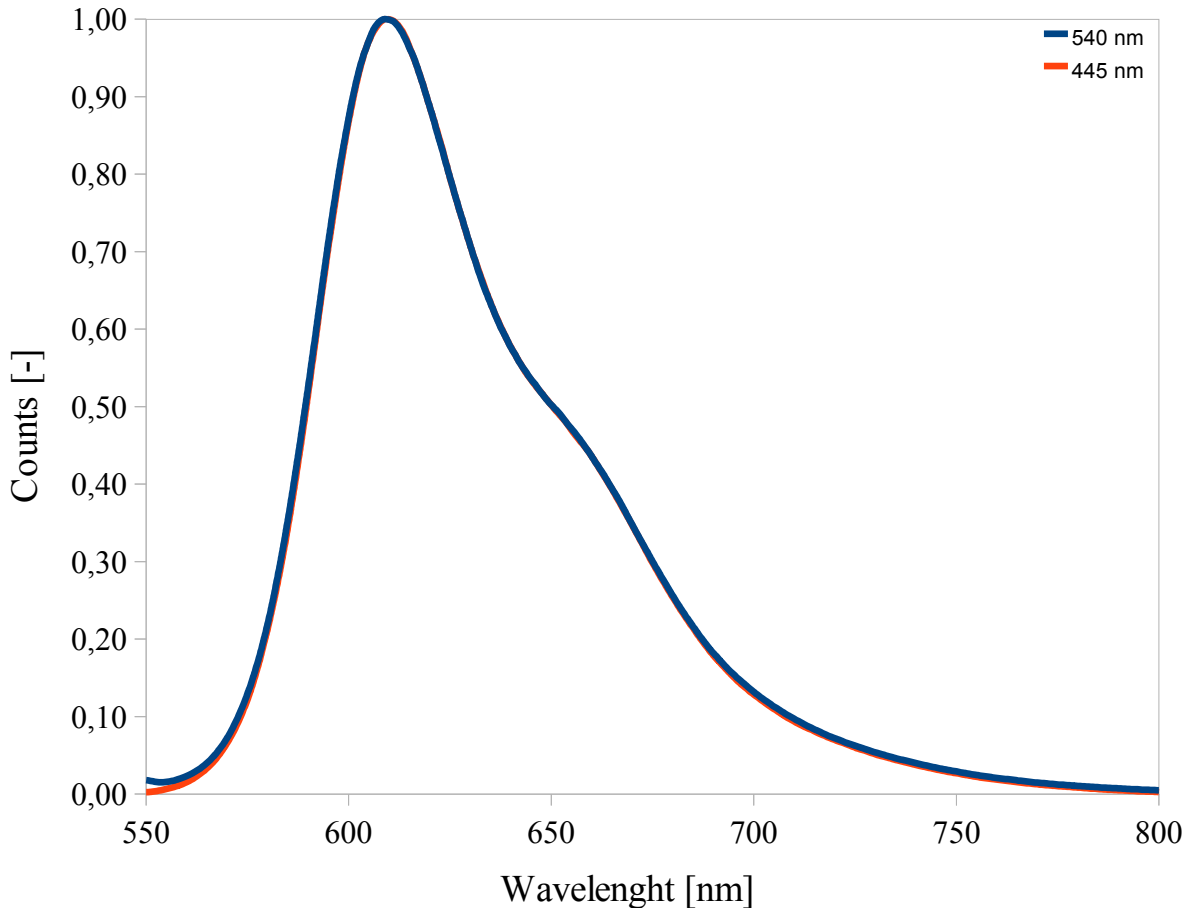

FigureIII. 17- Emission spectra of Lumogen F Red 305 thin film excitated by 540 nm light and by 445 nm light

The spectra shown in FigureIII. 17 present the same structure. The emission phenomenon is therefore the same. There are no competing mechanisms occurring during fluorescence emission. During experimental analyses the intensity of the emission spectrum of the dye excited at 445 nm was found to be lower than that obtained by 540 nm light excitation. This may be attributed by the difference in relative absorption intensity between the two main absorption peaks in the UV-vis absorption spectra.

Once the equivalence between the emission spectra was verified, degradation studies were carried out through fluorescence spectroscopy. Changes in fluorescence spectra were analyzed during the aging process.

For every step of the aging process, two fluorescence spectra were collected from the same sample by illuminating it at 445 nm and 540 nm.

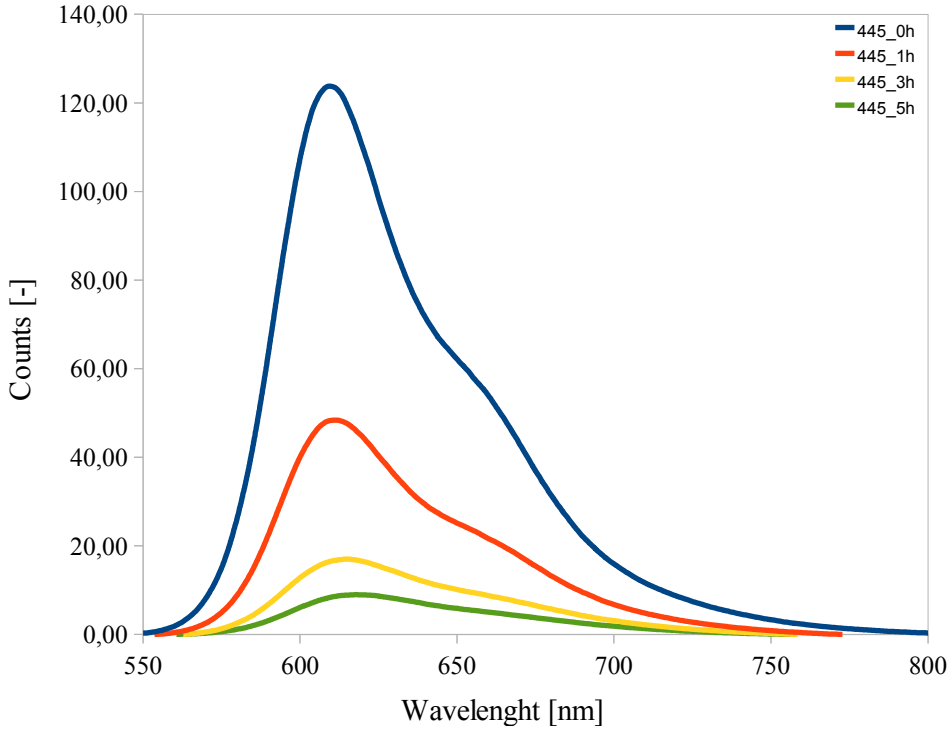

FigureIII. 18- Fluorescence spectra of a Lumogen F Red 305 thin film degraded till 5h collected by illuminating the sample at the chromophores absorption region (445 nm).

FigureIII. 18 and FigureIII. 19 show the fluorescence spectra of the dye in solid state collected at increasing UV-exposure time. The former shows the fluorescence spectra of the sample illuminated at 445 nm, the latter shows the fluorescence spectra of the same sample illuminated at 540 nm.

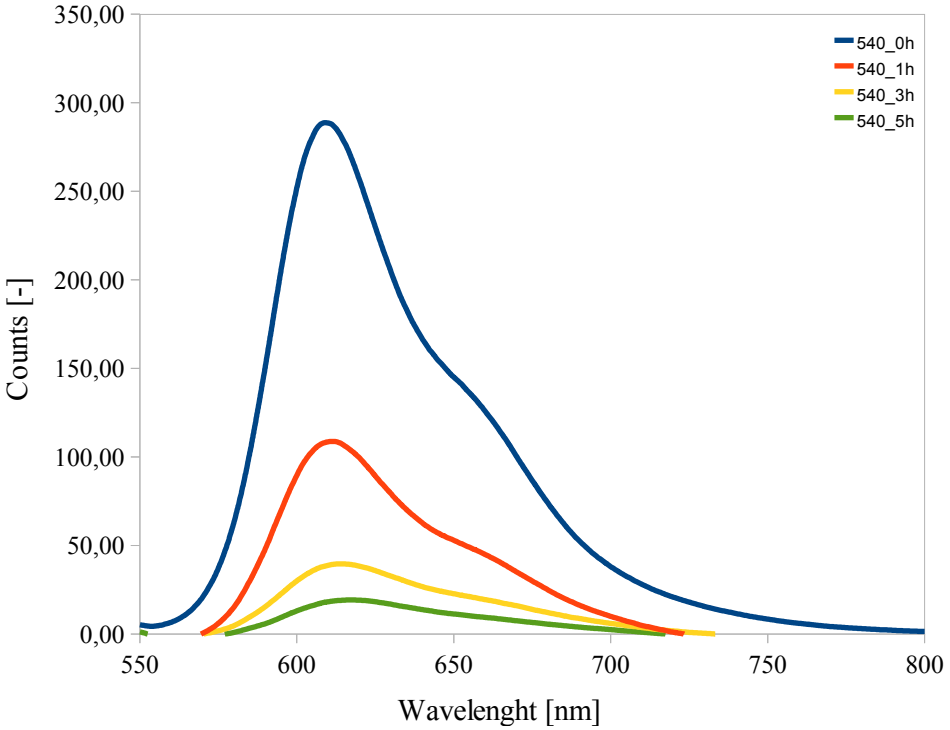

FigureIII. 19- Fluorescence spectra of a Lumogen F Red 305 thin film degraded till 5h collected by illuminating the sample at the perylene core absorption region (540 nm).

The blue line is the fluorescence spectrum of the pristine dye thin film, the red, yellow and green lines are the spectra of the film degraded after 1h, 3h and 5h, respectively.

In both cases, a decrease in intensity is observed by increasing UV-exposure time. In addition, a 10 nm red shift of the emission peak is found after 5h of UV irradiation.

In order to compare the modifications occurring to the emission spectra shown in FigureIII. 18 and FigureIII. 19, the intensities of the emission peaks were calculated at varying UV-exposure time.

FigureIII. 20 shows the variation of emission intensity with UV-exposure time as a function of excitation wavelength. In addition, the ratio between the emission peaks obtained by excitation at 445 and 540 nm is also shown. The yellow line in FigureIII. 20 shows that no significant difference can be found in the two trends, confirming that the emission phenomenon is only related to the same molecular group (the perylene core) regardless the excitation wavelength.

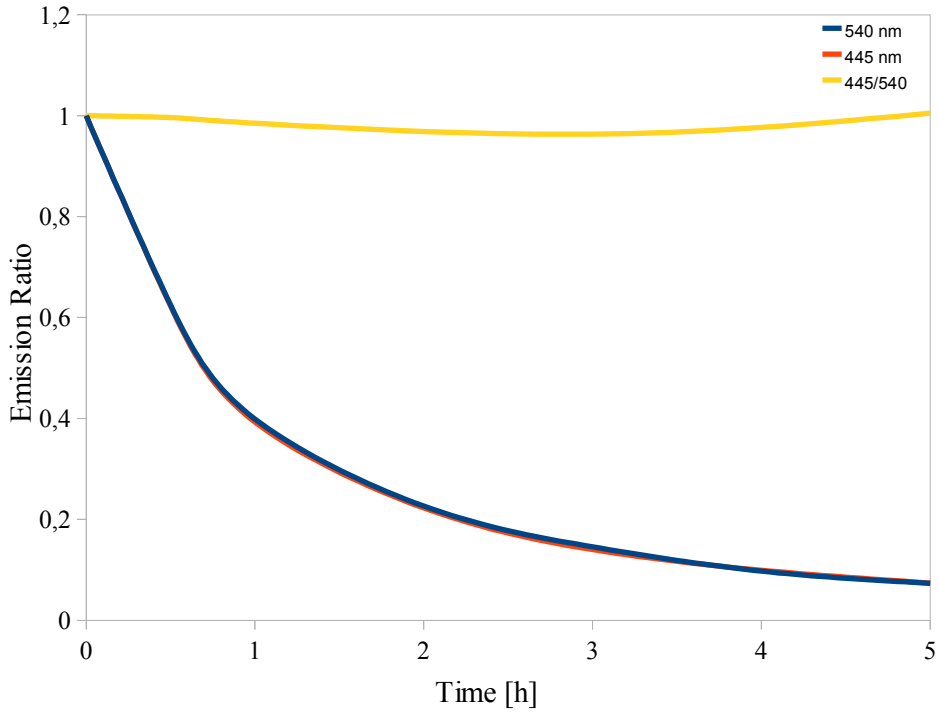

FigureIII. 20- Trends of degradation process of the same sample. Red and blue lines are the ratios of the intensities of degraded material to the intensity of the pristine material

Interestingly, a two-step decrease in emission intensity can be observed from FigureIII. 20. In the first 2h a sharp intensity decrease is observed which reaches a plateau for longer UV exposure.

III.2.2.3.FTIR

FTIR spectroscopy was used to monitor the modifications occurring to the dye molecule upon UV-exposure times.

FigureIII. 21 shows the FTIR spectrum of a Lumogen F Red 305 in the solid state.

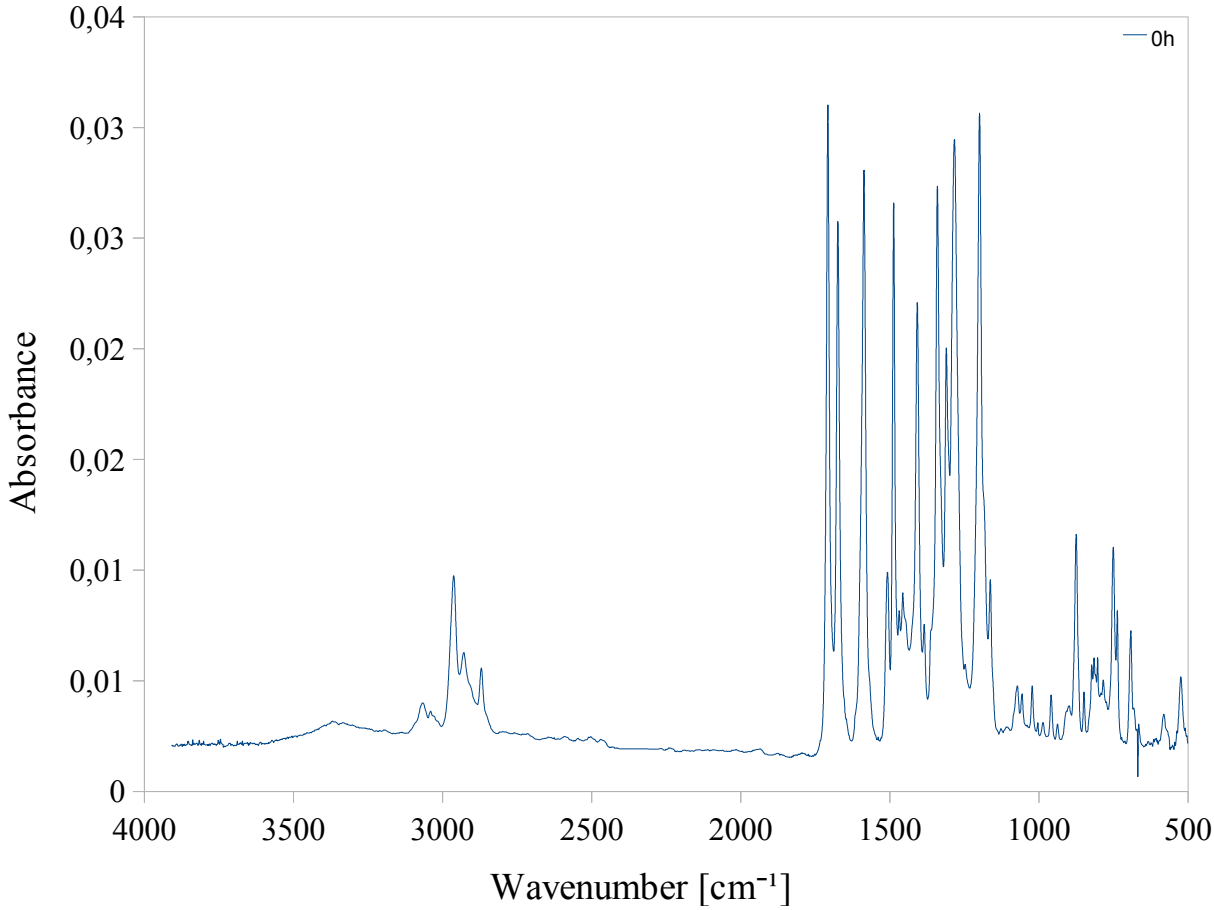

FigureIII. 21- FTIR spectrum of pristine Lumogen F Red 305

The FTIR spectrum of the dye shows a well defined C-H stretching region, where signals associated to C-H aromatic (3200-3000 cm^{-1}) and aliphatic (3000-2800 cm^{-1}) stretching vibrations can be clearly recognized.

The region between 1800 cm^{-1} and 1000 cm^{-1} includes a complex set of peaks related to the stretching vibrations of carbon bonds and CH deformation.

From 1000 cm^{-1} to 650 cm^{-1} the out-of-plane region can be identified.

In order to determine how the degradation process affects the dye and how the UV light alters its molecular structure, comparisons with molecules with known spectra were made. This comparison also helped to identify the characteristic vibrations assigned to the signals visible in the IR spectrum.

The main absorption bands in the FTIR spectrum of the dye, associated to vibrations of chemical groups have been identified by a comparison with the FTIR spectrum of PDI, as also

done in the UV-vis analysis presented previously. FTIR spectra of PDI (red line) and Lumogen F Red 305 are shown together in FigureIII. 22.

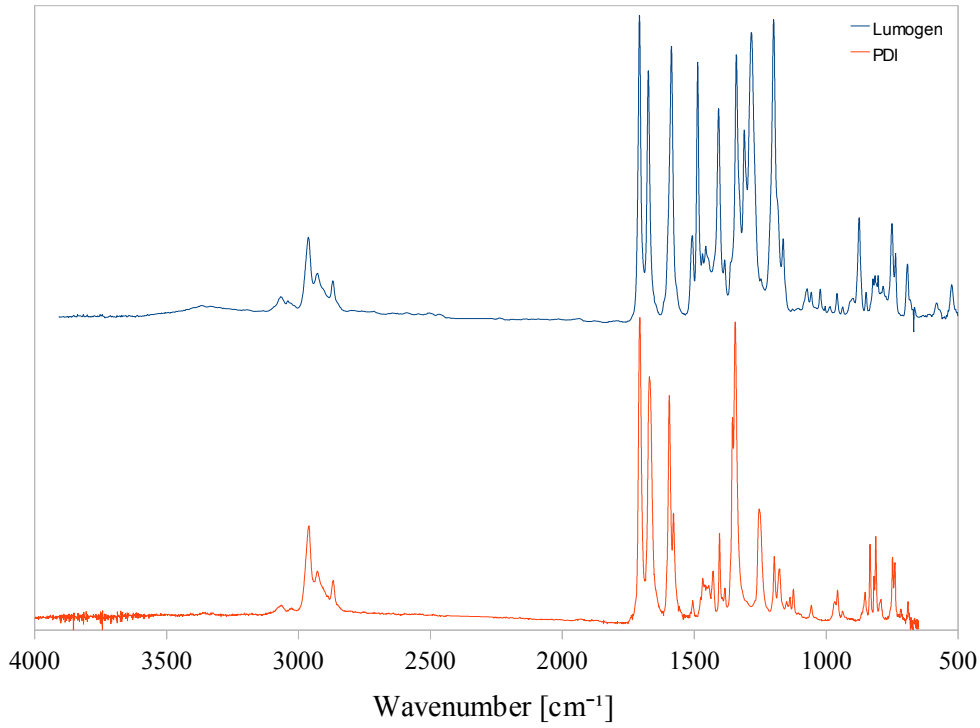

FigureIII. 22- FTIR spectra of PDI and Lumogen F Red 305

In order to assign the main IR peaks of the dye to characteristic bond vibrations, a detailed study on each region of the IR spectrum is presented below.

FigureIII. 23 shows a highlight of the C-H stretching region for both molecules.

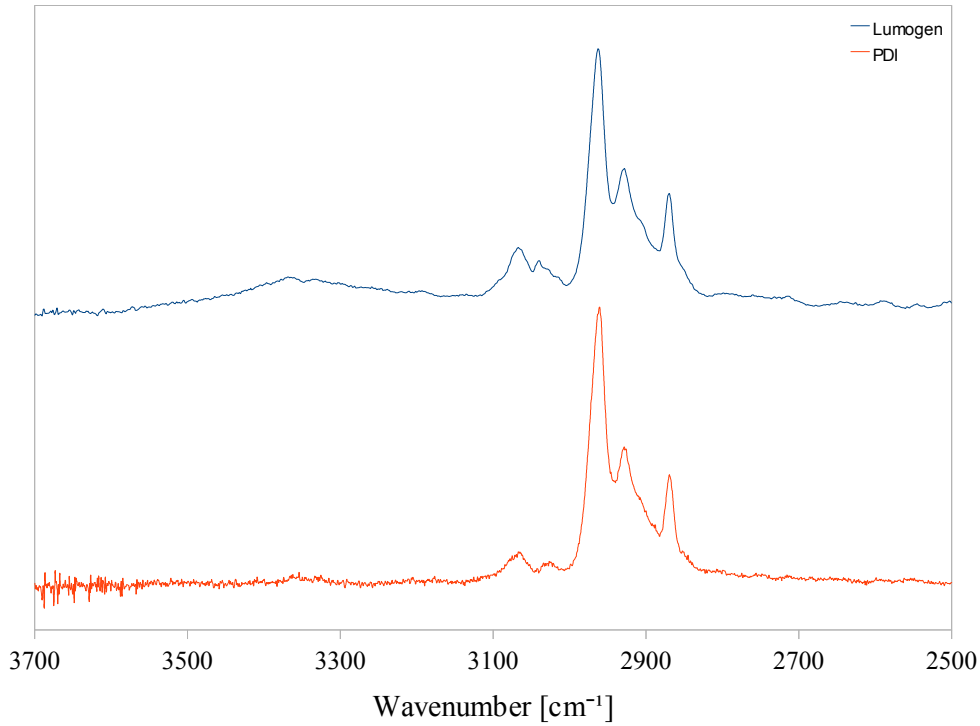

FigureIII. 23- Lumogen F Red 305 and PDI: C-H stretching region

As shown in FigureIII. 23, Lumogen F Red 305 and PDI present the same aliphatic

groups. Therefore in FTIR spectrum, the C-H aliphatic regions (3000-2800 cm^{-1}) of Lumogen F Red 305 and PDI show the same structure with three narrow peaks with equal intensity ratios centered at 2962 cm^{-1}, 2928 cm^{-1}, 2870 cm^{-1}. Conversely, in the aromatic C-H stretching region (3200-3000 cm^{-1}) some differences between the two spectra can be observed. In the FTIR spectrum of the Lumogen dye the aromatic C-H band is more defined in comparison to PDI, and this may be due to a larger amount of aromatic C-H generating that signal. This difference can be explained by the presence of four additional lateral substituents present in the Lumogen F Red 305 molecule, which are indeed four aromatic rings.

Extending the comparison between Lumogen and PDI to the 1800-1000 cm^{-1} region allowed a more detailed analysis of the main absorption peaks of the dye molecule.

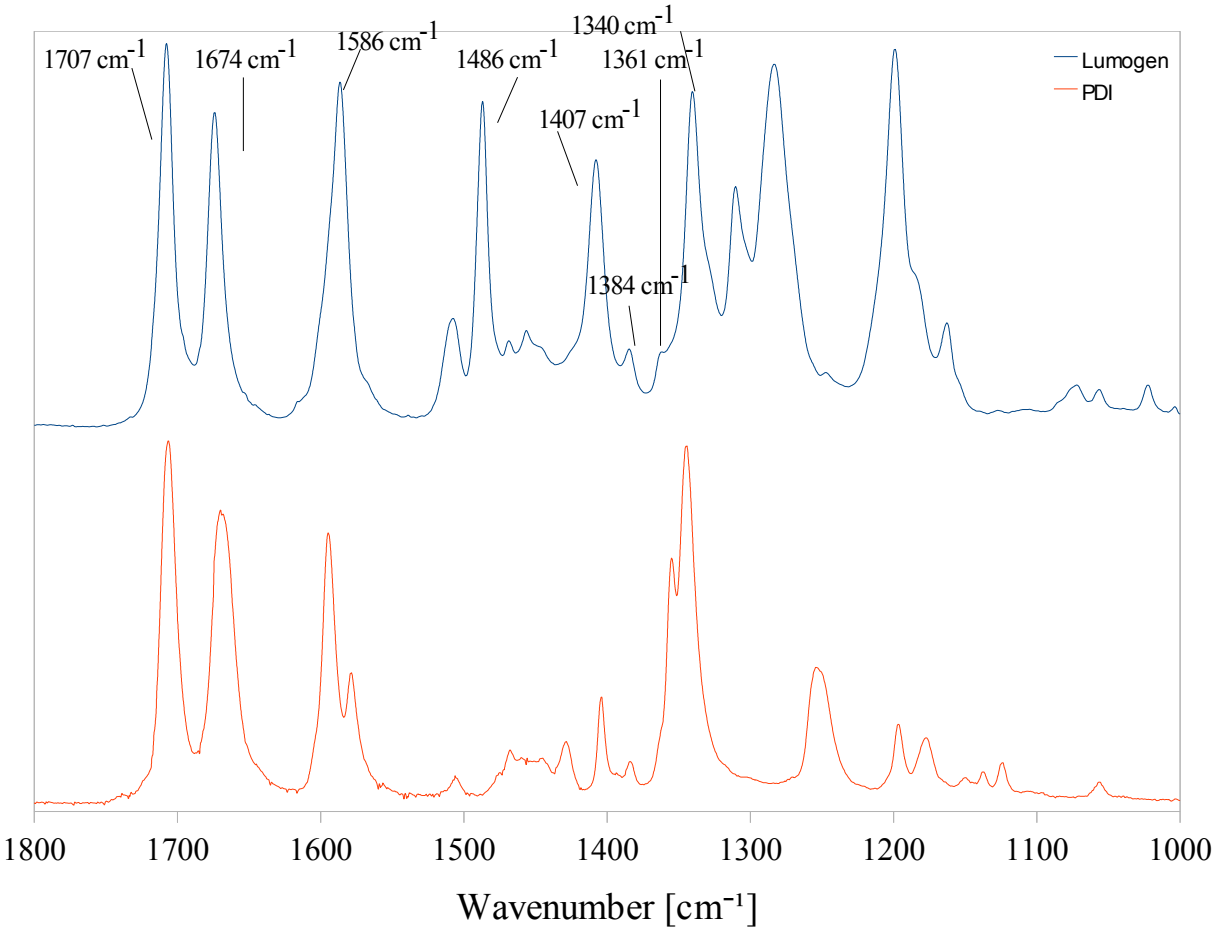

FigureIII. 24– FTIR spectra of Lumogen F Red 305 and PDI focused on double bonds and single bonds stretching regions.

The FTIR spectra of the two molecules in the 1800-1000 cm^{-1} region are shown in FigureIII. 24, where some differences can be clearly observed. The two molecules possess the same perylene core, therefore the main differences between their FTIR spectra should be ascribable to vibrations of the bonds relative to the lateral substituents. An in-depth analysis of the peaks in this region was carried out and presented below.

In the carbonyl region (1800-1650 cm^{-1}), two narrow peaks (1707 cm^{-1} and 1674 cm^{-1}) are observed in both spectra. They can be assigned, therefore, to the in phase and out-of-phase vibrations of C=O bonds, which are present in both molecules.

The peak centered at 1586 cm^{-1} found in the Lumogen spectrum can be assigned to the stretching vibrations of C=C bonds in the perylene core. A similar peak is observed also for PDI molecule, accordingly. The peak centered at 1486 cm^{-1} is observed in the Lumogen F Red 305 spectrum, but not in the spectrum of PDI. Accordingly, it could be related to the stretching vibrations of C=C bonds in the lateral aromatic rings, which are not present in the PDI molecule.

Although with some difference in the relative intensity, the peaks at 1407 cm^{-1}, 1384 cm^{-1}, 1361 cm^{-1} and 1340 cm^{-1} are observed in both spectra. As these peaks are related to single bond stretching vibrations, they could be attributed both to C-C stretching and C-N stretching.

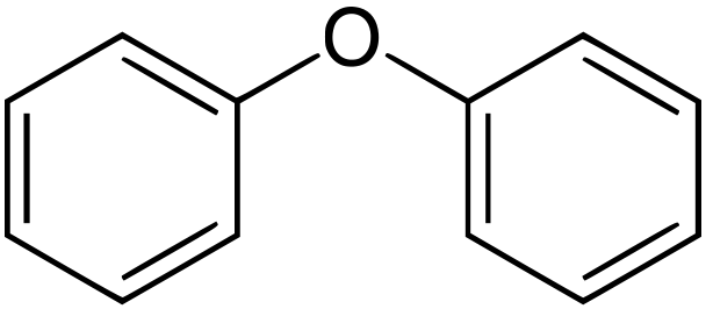

FigureIII. 25- Molecular structure of DPE

It is worth noticing that C=C bonds in the lateral substituents may also give a contribution to the 1586 cm^{-1} FTIR signal, as evident by comparing the FTIR spectrum of Lumogen F Red 305 to the FTIR spectrum of a simpler molecule, Diphenyl ether (FigureIII. 25).

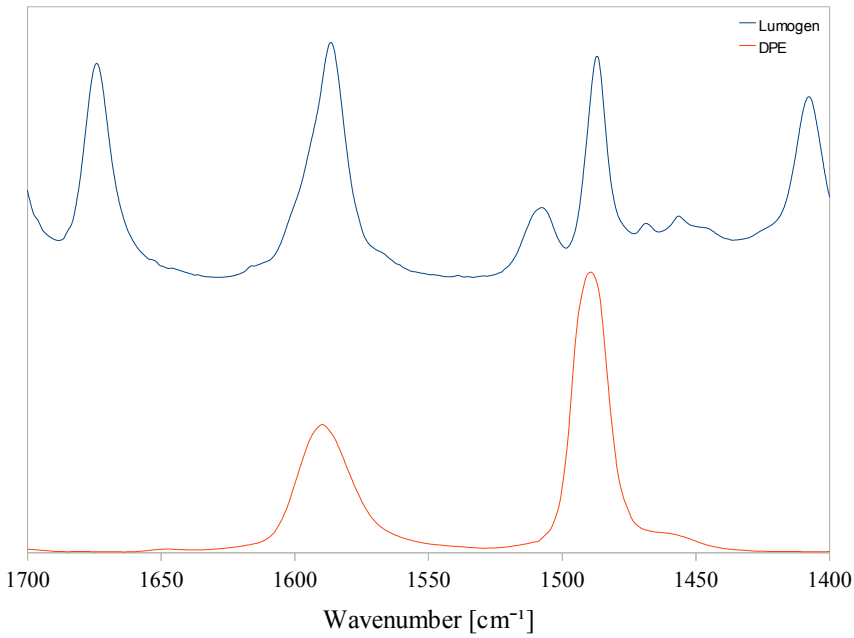

FigureIII. 26- FTIR spectra of Lumogen F Red 305 and DPE focused on C-O-C stretching region

Indeed, a low intensity peak at 1590 cm^{-1} is also present in the DPE FTIR spectrum. FigureIII. 26 shows FTIR spectra of Lumogen and DPE in the 1700-1400 cm^{-1} region.

A comparison of FTIR spectra of Lumogen F 305 Red and PDI in the out-of-plane region (1000-650 cm^{-1}) is shown in FigureIII. 27.

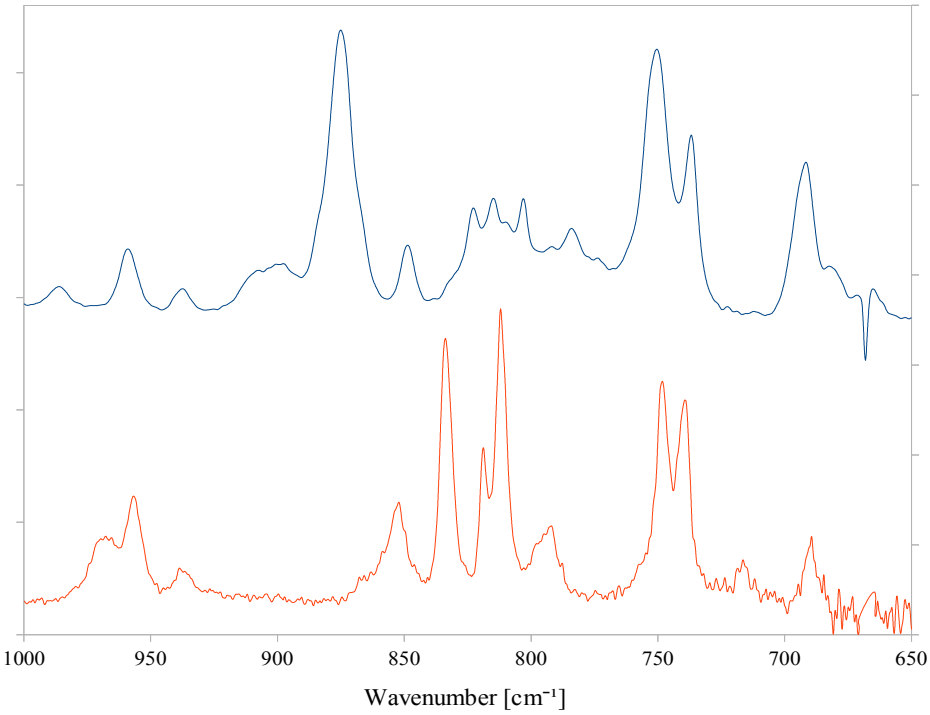

FigureIII. 27- FTIR spectra of Lumogen F Red 305 and PDI, focused on Out-of-Plane region

The most important difference between these spectra in the out-of-plane region is represented by the peak centered at 877 cm^{-1} in the FTIR spectrum of Lumogen. The assignement of this peak was possible on the basis of a further comparison between Lumogen and DPE in the out-of-plane stretching region (as shown in FigureIII. 28).

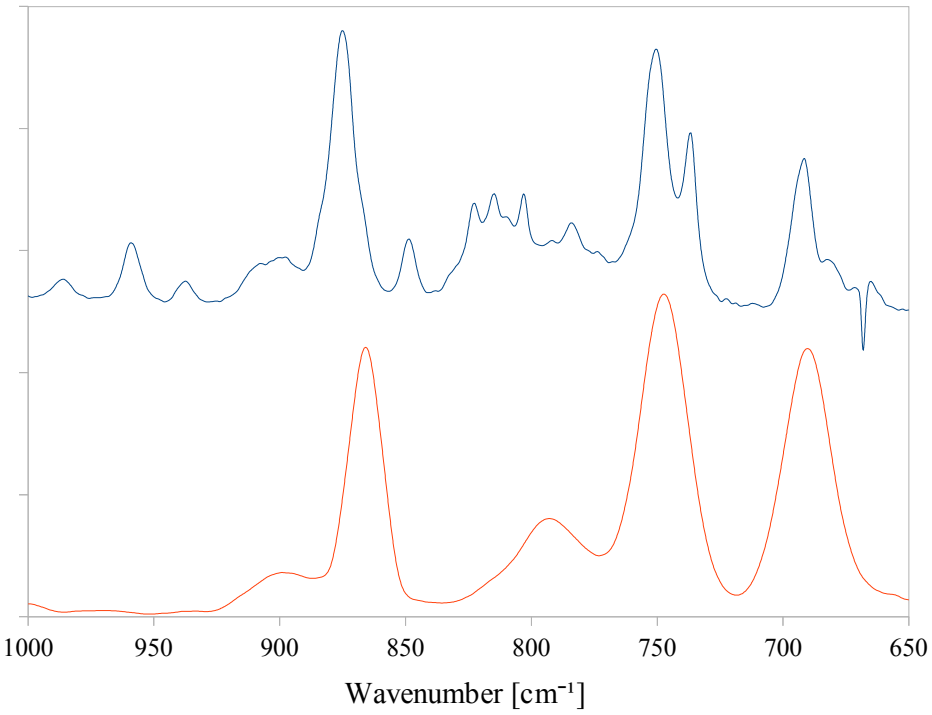

FigureIII. 28- FTIR spectra of Lumogen F Red 305 and DPE focused on out-of-plane stetching region

In particular, both Lumogen and DPE show a single sharp peak around 850-880 cm^{-1}. This peak was assigned in DPE to the benzene ring breathing by means of quantum chemical calculations[11,12]. Accordingly, the peak centered at 877 cm^{-1} found in Lumogen molecule was similarly attributed to the breathing of the benzene ring of the lateral chromophores. The ring breathing is an important indicator of the behaviour of the lateral substituents during the degradation process, therefore it has been monitored during the UV-irradiation studies.

In order to better understand the degradation mechanism of the chosen dye, three main peaks were monitored. The peaks centered at 1586 cm^{-1} and at 1342 cm^{-1} were elected as the markers of the degradation of the perylene core while the peak characteristic of the ring breathing (877 cm^{-1}) was chosen as the indicator of the modification occurring to the lateral substituents.

FigureIII. 29 shows the FTIR spectrum of the dye molecule after 0h,1h, 3h, 5h of UV exposure.

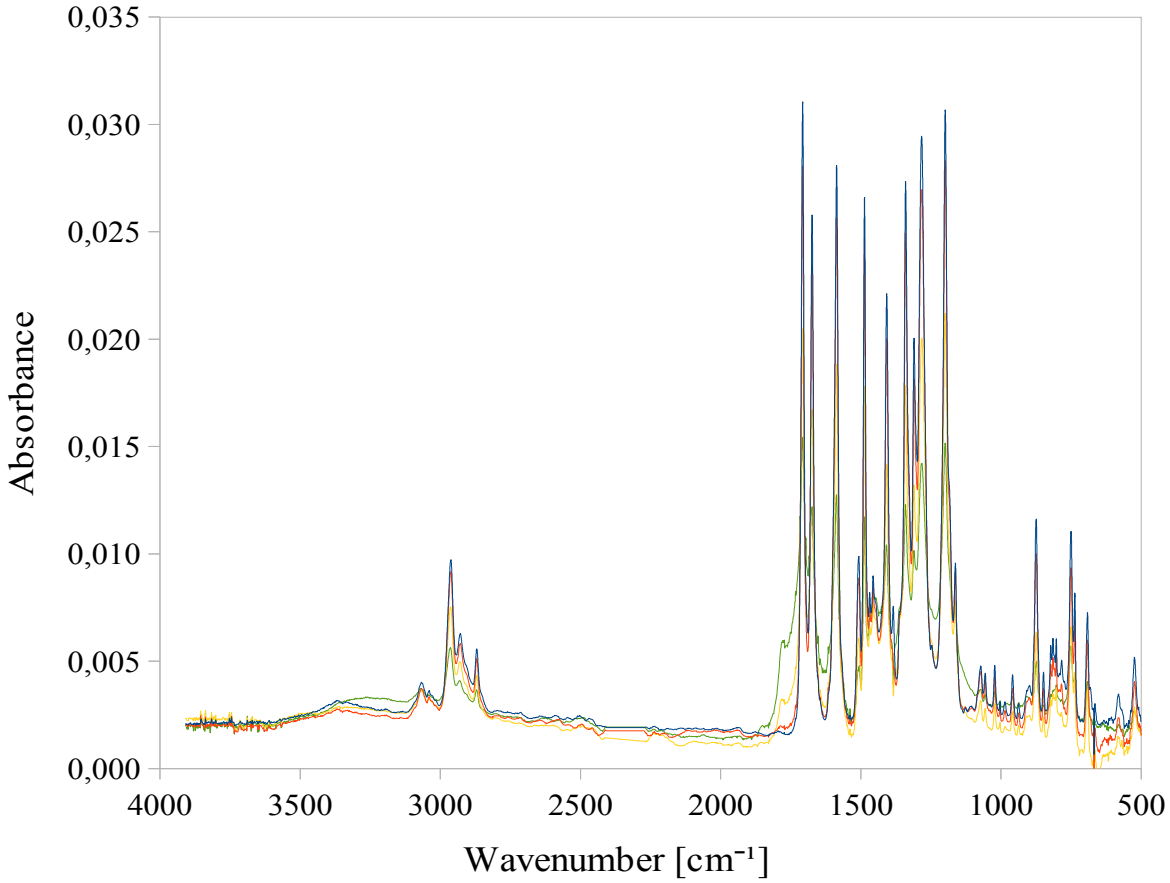

FigureIII. 29- FTIR spectra of pristine dye (blue line) and of the dye degraded after 1h (red line), 3h (yellow line) and 5h (green line)

Focusing on the most important regions of the FTIR spectrum a more accurate analysis can be performed.

The C-H stretching region is shown in FigureIII. 30.

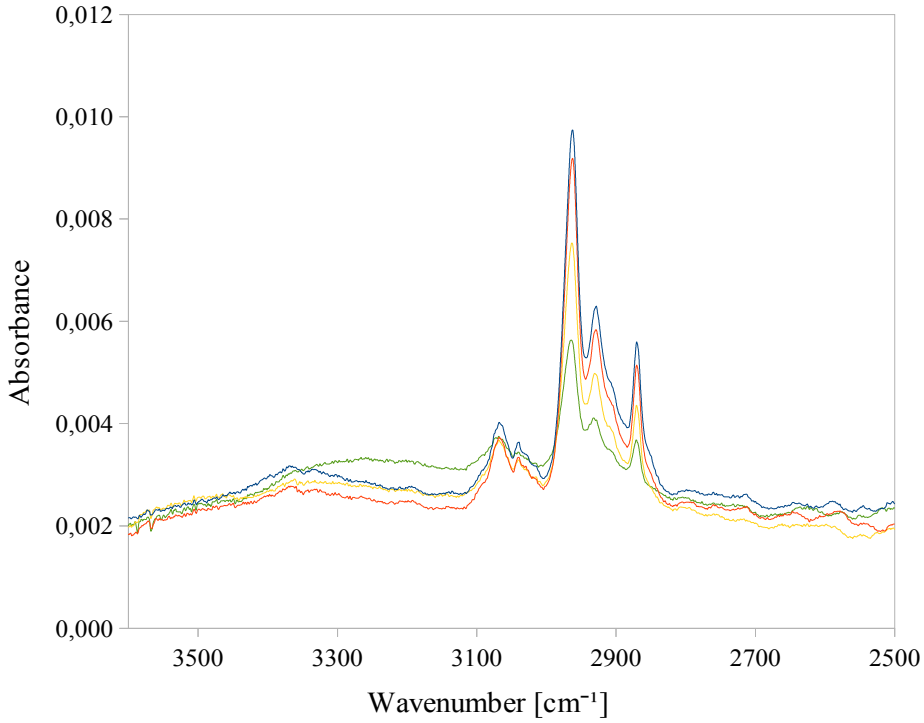

FigureIII. 30- C-H stretching region of FTIR spectra of the degraded dye

The blue spectrum is the spectrum of the pristine dye. The degradation after UV exposure leads to a decrease in intensity of the C-H stretching peaks, both aromatic and aliphatic. A new broad band seems to appear at about 3300 cm^{-1}. This new feature may be due to formation of hydroxyl species occurring during photo-oxidation, although moisture absorption by the dye sample may also have occurred.

In phase and out-of-phase C=O stretching peaks of pristine and degraded dye are shown in FigureIII. 31.

In the carbonyl region a decrease in intensity is observed. The FTIR spectra of degraded dye exhibit a wide band at around 1775 cm^{-1} whose intensity progressively increases upon UV-exposure time. As this band is still in the carbonyl region, it may be assigned to stretching vibrations of C=O bonds of new oxidized species formed during irradiation.

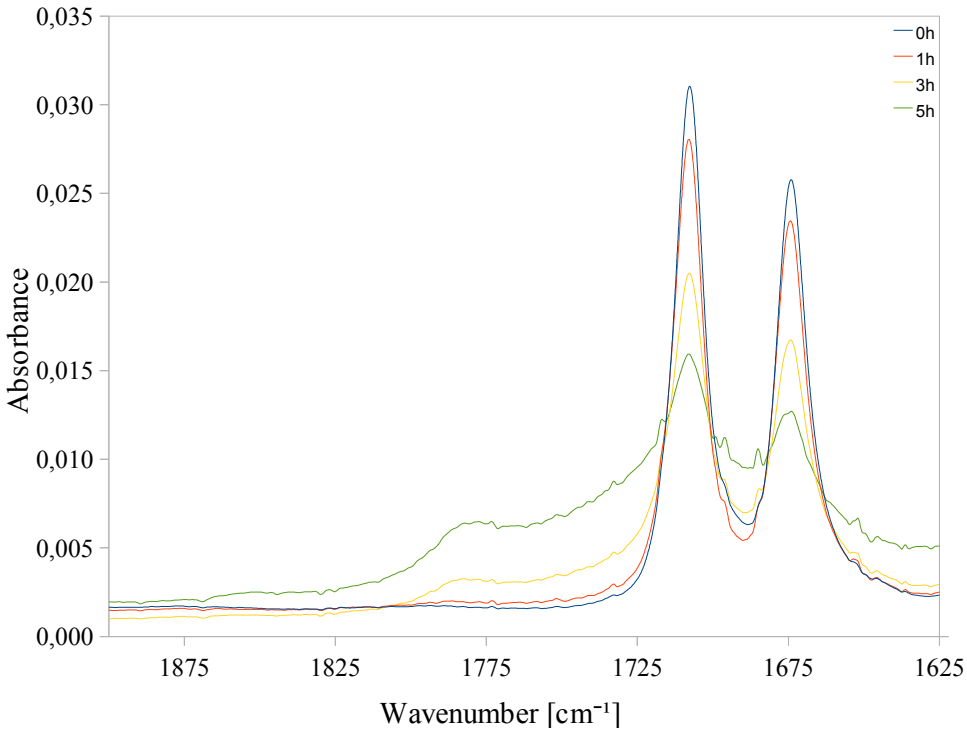

FigureIII. 31- C=O stretching vibrations in FTIR spectra of pristine and degraded dye

The FTIR spectra of pristine and degraded dye molecule focused on the C-C stretching and the single-bond stretching regions are shown in Figure III. 32.

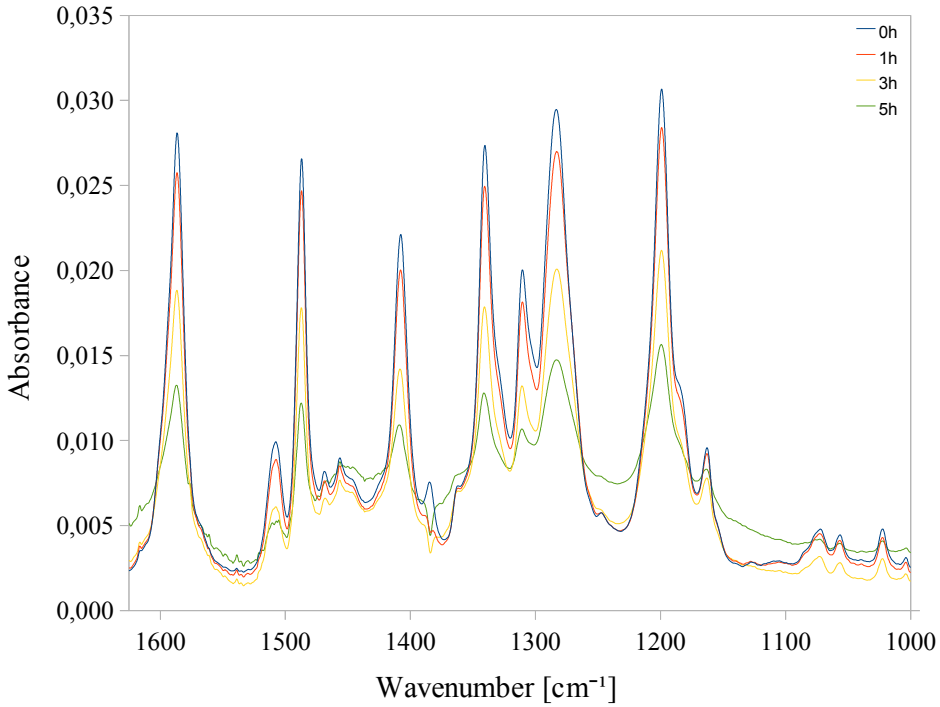

Figure III. 32- C-C and single-bond stretching regions of FTIR spectra of pristine and degraded dye

A generalized decrease in intensity can be observed in this region accompanied by a broadening of the absorption bands that increases with UV-light exposure time.

The appearance of more complex features in this region may be related to the

formation of degraded species upon UV-irradiation that generate additional IR signals compared to the pristine dye molecule.

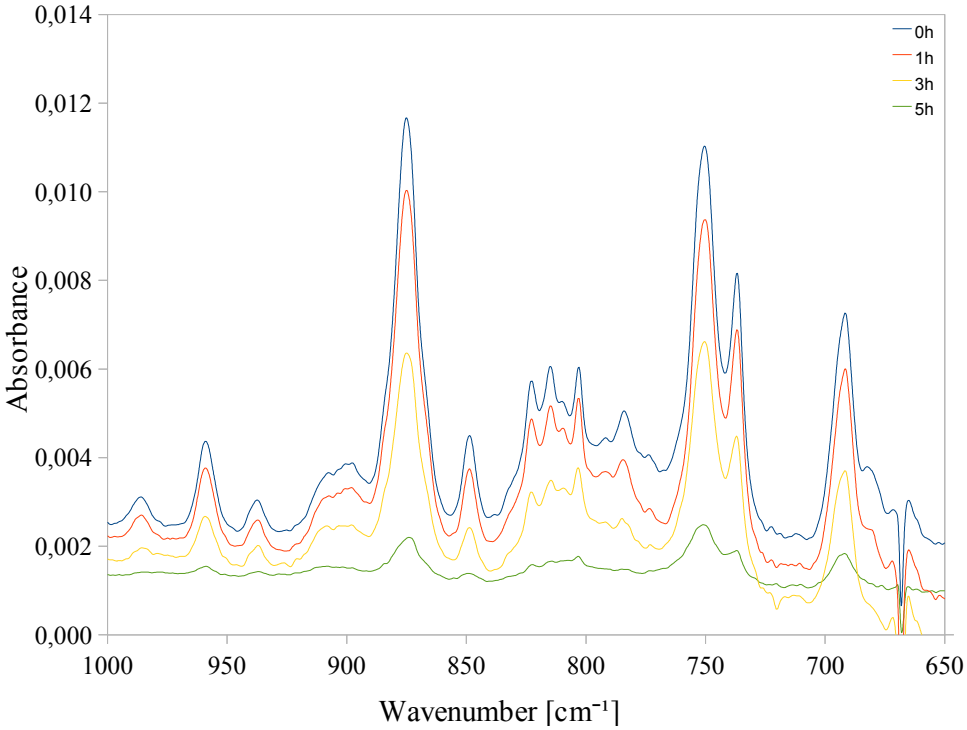

FigureIII. 33– Out of plane region of pristine and degraded dye

FigureIII. 33 shows the out-of-plane region (1000-650 cm^{-1}) of FTIR spectrum.

In the out-of-plane region no peaks appear to form upon UV-exposure. As already seen in the other regions of the spectrum, the degradation of dye samples leads to a decrease in intensity of FTIR bands also in the out-of-plane region.

In order to highlight possible trends occurring during the degradation process, absorption intensities of characteristic peaks of the dye molecule were calculated. In particular, the signal assigned to the aromatic ring breathing was monitored and compared to characteristic signals of the perylene core, namely the peak centered at 1586 cm^{-1} and the peak centered at 1342 cm^{-1}. FigureIII. 34 shows the results of the calculations carried out on the intensities of such peaks.

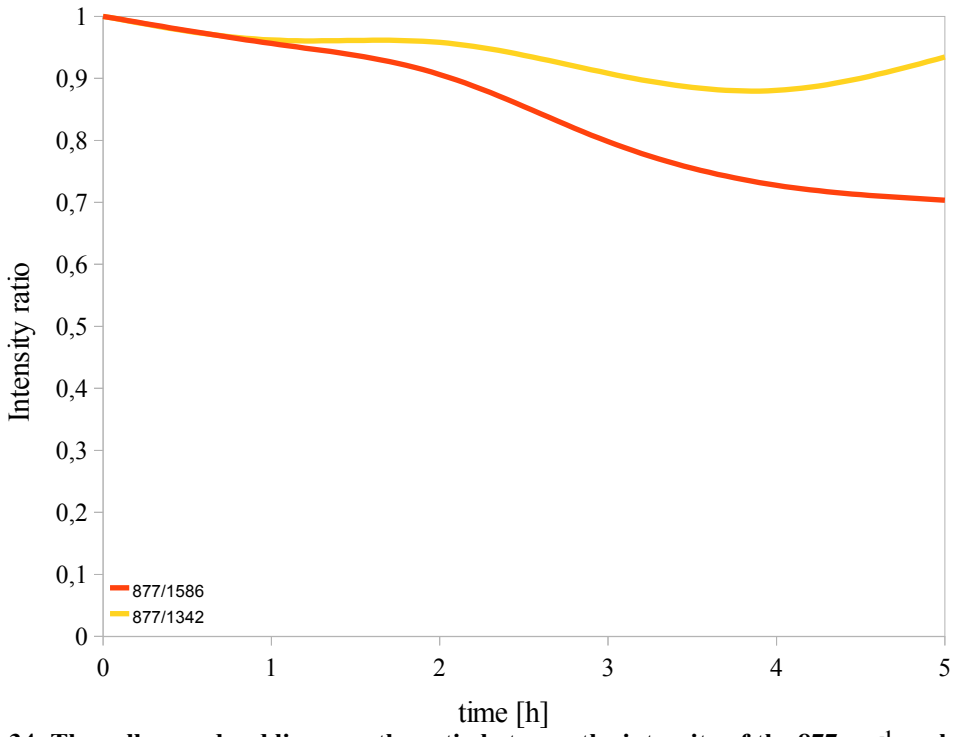

FigureIII. 34- The yellow and red lines are the ratio between the intensity of the 877 cm^{-1} peak and the intensities of the peak at 1586 cm^{-1} (red line) and the peak at 1342 cm^{-1} (yellow line).

Both the yellow and red lines show only a slightly negative trend, meaning that the rate of disappearance of the peak associated to the lateral phenyl ring breathing appears somewhat faster than the signals attributed to the perylene core. This observation may suggest that the degradation process affects more easily the lateral substituents rather than the perylene core structure.

III.2.3.OLSC materials

In order to optimize luminescence properties of Lumogen F Red 305, the dye has to be mixed in relatively low concentration in a transparent matrix (the carrier matrix). When this solution is deposited as thin film, dye particles are uniformly distributed as small clusters in the free volume of the polymeric binder. Self-absorption is therefore significantly reduced, as generated photons have a lower probability to hit an adjacent absorbing species. The solution used in this work was obtained by mixing PMMA and Lumogen F Red 305 in $CHCl_3$ as solvent. PMMA concentration was set to 10% by weight of chloroform. According to previous work on the same system, the dye concentration was set at 6% by weight of PMMA. The solution so obtained has been called PL6, being 6 the dye percentage.

PL6 films were deposited by spincoating, at 1200 rpm for 40 seconds.

Spectroscopic studies were carried out by means of fluorescence, UV-vis and FTIR spectroscopies. The results obtained from these analyses were then compared to those obtained from the study on the organic dye.

III.2.3.1.Fluorescence

The absorbing peaks of PL6 sample are individuaed in the UV-vis spectrum of the PL6 film, shown in FigureIII. 35.

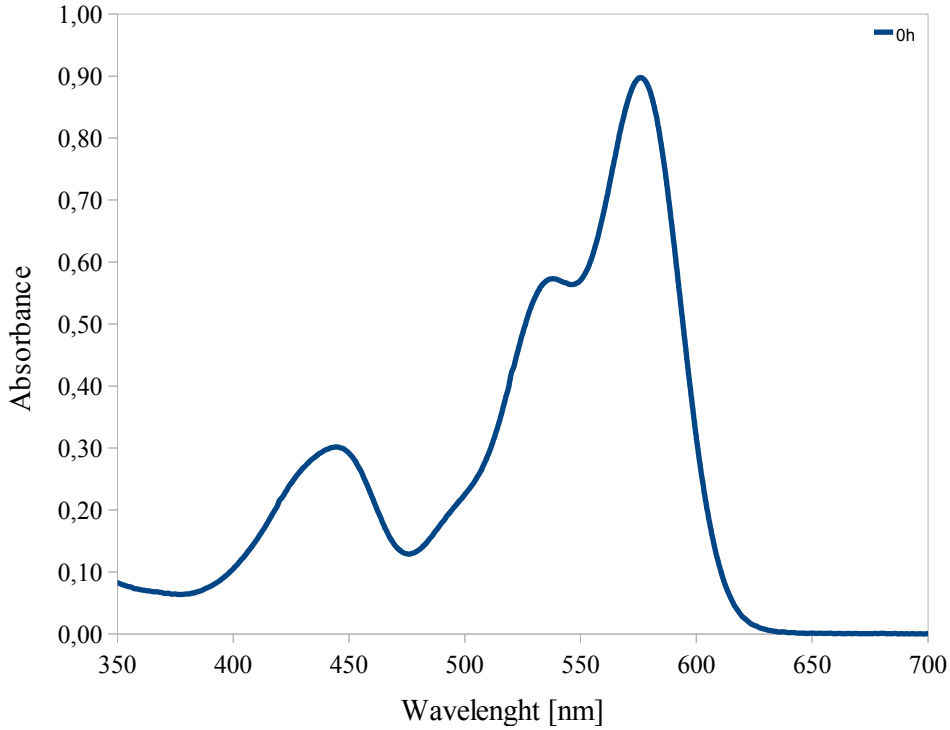

FigureIII. 35- UV-vis spectrum of PL6 thin film

Similarly to what discussed in section III.1.2.1, the fluorescence spectra were collected by irradiating the sample at 445 nm and 540 nm.

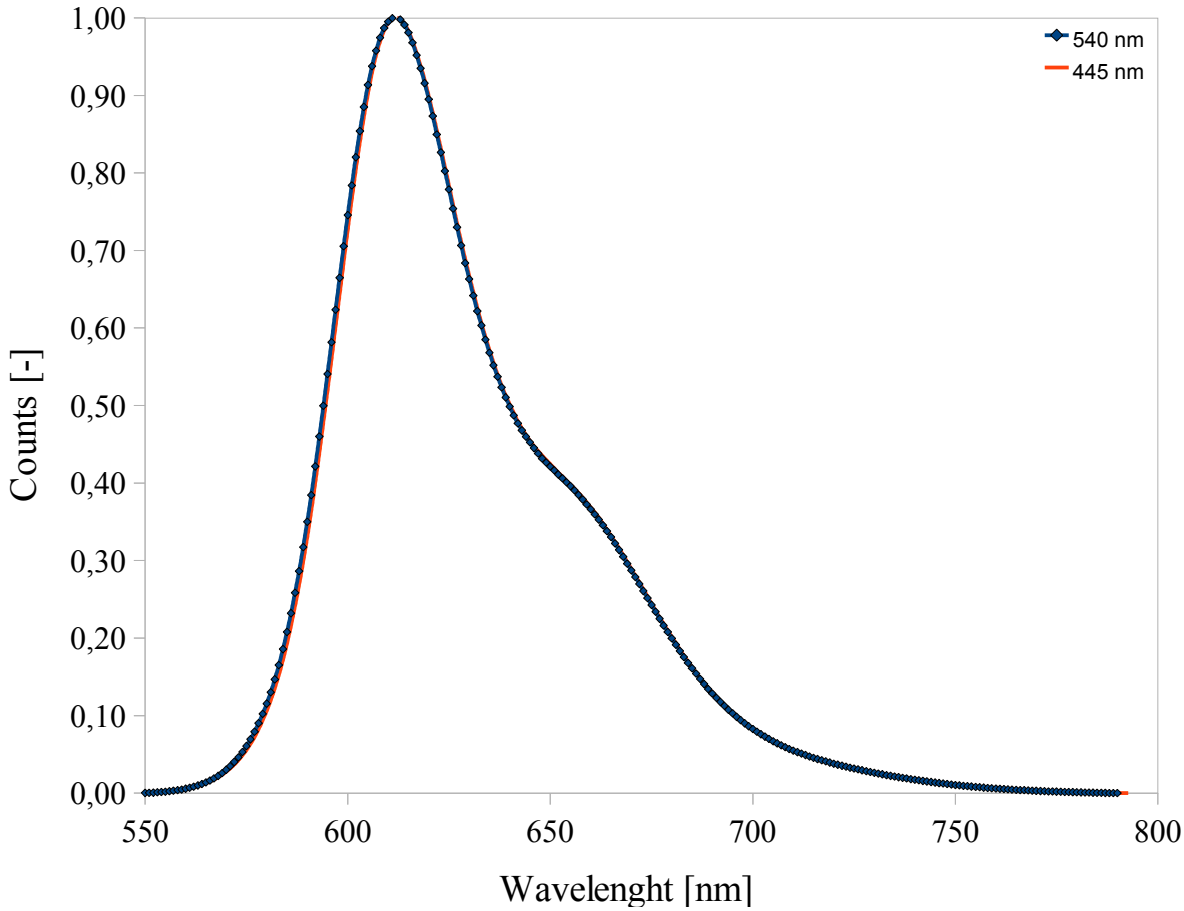

FigureIII. 36- Fluoresce spectra of PL6 illuminated at 445 nm absorption peak (red line) and at 540 nm (blue line). Spectra are normalized to 1

As found in the case of dye-only samples, the same structure of the emission spectrum is found for both excitation wavelengths (445, 540). There is no evidence of emission mechanisms in conflict, suggesting that the emission may still be carried out by a single group within the dye molecule (see FigureIII. 36).

Fluorescence spectra of degraded PL6 samples were collected so as to monitor the evolution of the emission phenomena with increasing UV-exposure time. Analyses were carried out in the same experimental conditions as for the dye molecule alone, in order to be able to perform comparisons and highlight differences in the degradation behaviour.

FigureIII. 37 and FigureIII. 38 show the spectra of pristine and degraded PL6 samples, exposed to a 445 nm light and to 540 nm light, respectively.

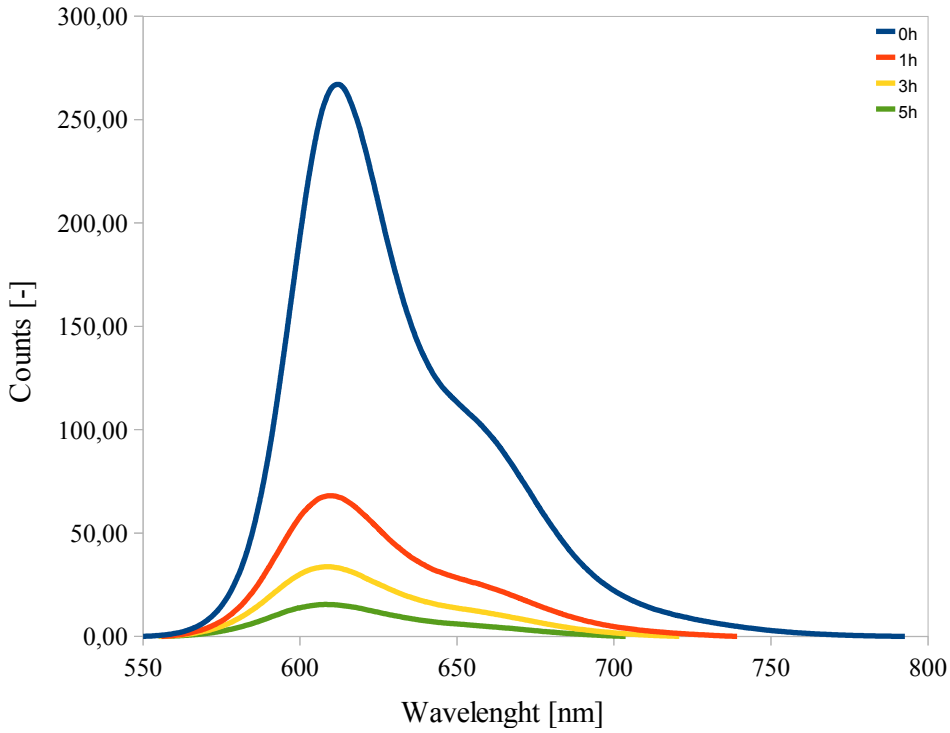

FigureIII. 37- Fluorescence spectra of a PL6 thin film degraded till 5h collected by illuminating the sample at the chromophores absorption peak (445 nm)

The blue line represents the fluorescence spectra of pristine PL6 thin film, the red, yellow and green lines represent the spectra of the film exposed for 1h, 3h, 5h to UV-light.

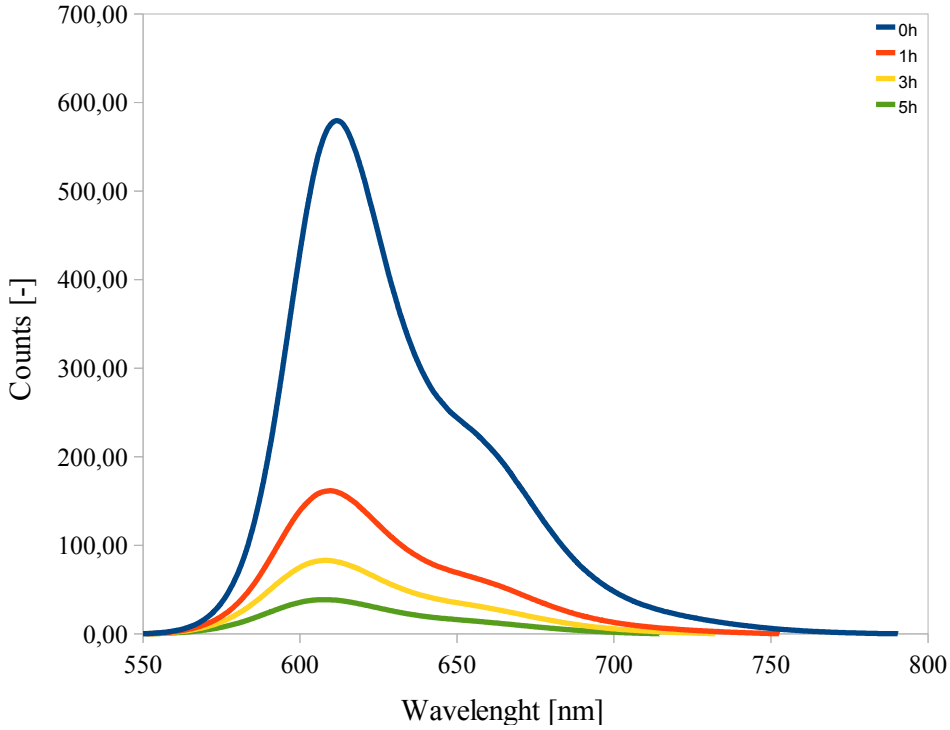

FigureIII. 38- Fluorescence spectra of a PL6 thin film degraded till 5h collected by illuminating the sample at the perylene core absorption peak (540 nm)

The emission peak intensity decreases upon exposure to UV-light. As a result of degradation, a 5 nm blue shift of the main emission peak is also observed after 5h of UV-

irradiation.

In order to better understand the effects of the degradation on the emission peak intensity, intensity ratios were calculated. Relative emission intensities were calculated for spectra excited with 445 and 540 nm light source and are shown in FigureIII. 39.

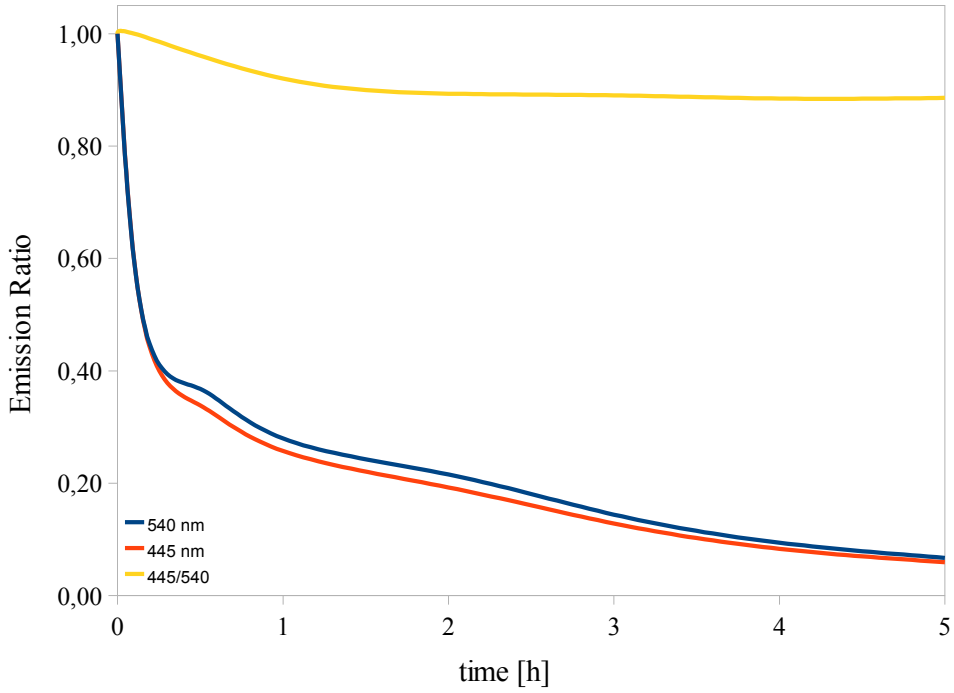

FigureIII. 39- Trends of degradation process of a PL6 sample by fluorescence spectroscopy. Red and blue lines are the ratios of the intensities of degraded material to the intensity of the pristine material

A similar decay rate is observed for both spectra. In addition, a two-step decrease rate is observed, as also found in the UV-vis analysis. Primarily the intensity of the emission peak decreases very fast (from 0 to 30 minutes), and then tends to a plateau.

III.2.3.2.UV-vis

FigureIII. 40 shows the UV-vis spectrum of a PL6 sample deposited on a glass transparent substrate by spincoating.

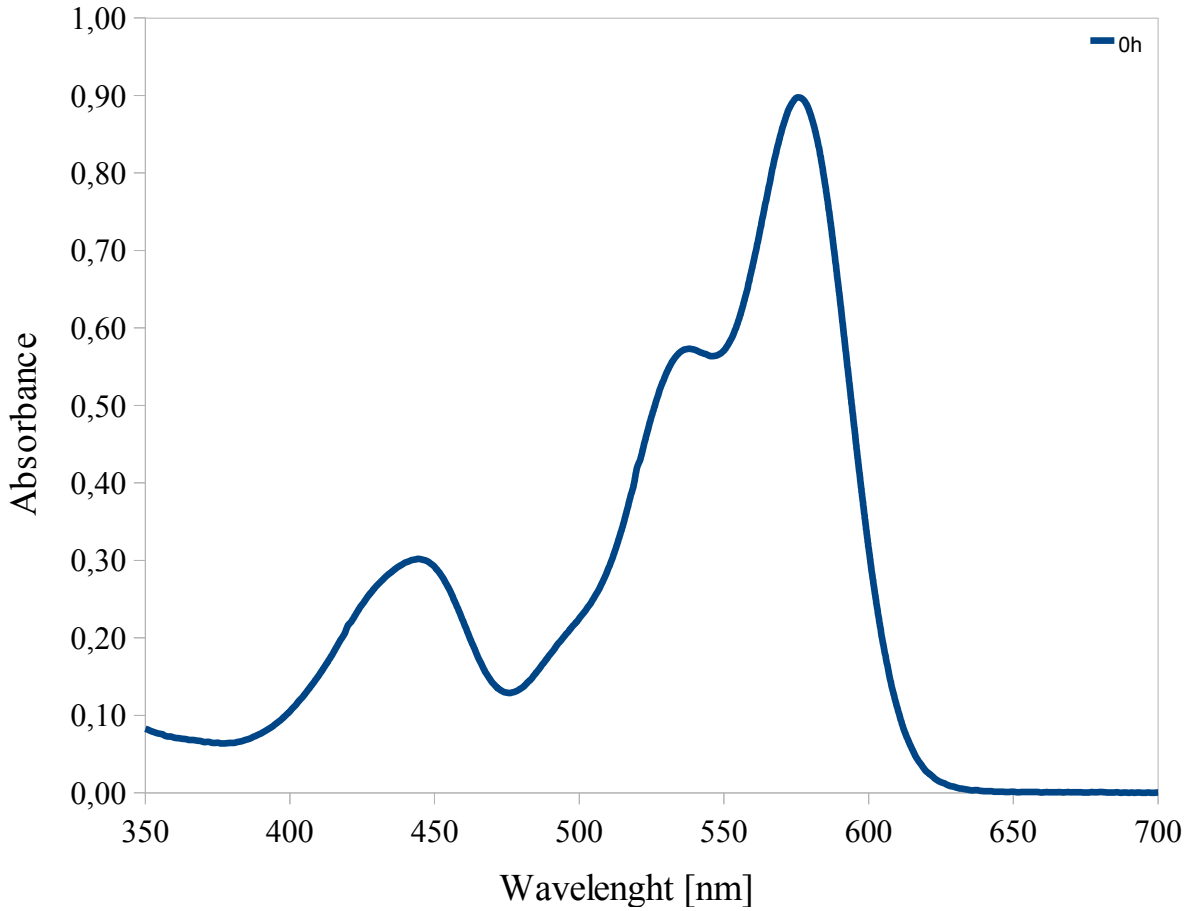

FigureIII. 40- UV-vis spectrum of a pristine PL6 thin film

The spectrum shown in FigureIII. 40 is similar to UV-vis spectrum characteristic of the dye alone. Two different peaks are observed. The position of the peak at higher energy, which was attributed to the absorption of chromophoric lateral substituents in section III.1.2.2, centered at 445 nm does not change compared with the dye-only spectrum. In addition the same structure is observed. Conversely the peak attributed to the absorption of the perylene core undergoes a 8 nm red shift with respect to the spectrum of dye-only as the maximum in the spectrum of the dye alone is at 568 nm while in PL6 is at 576 nm.

FigureIII. 41 shows the spectra of PL6 after 0h, 1h, 2h, 3h, 4h of exposure to UV light.

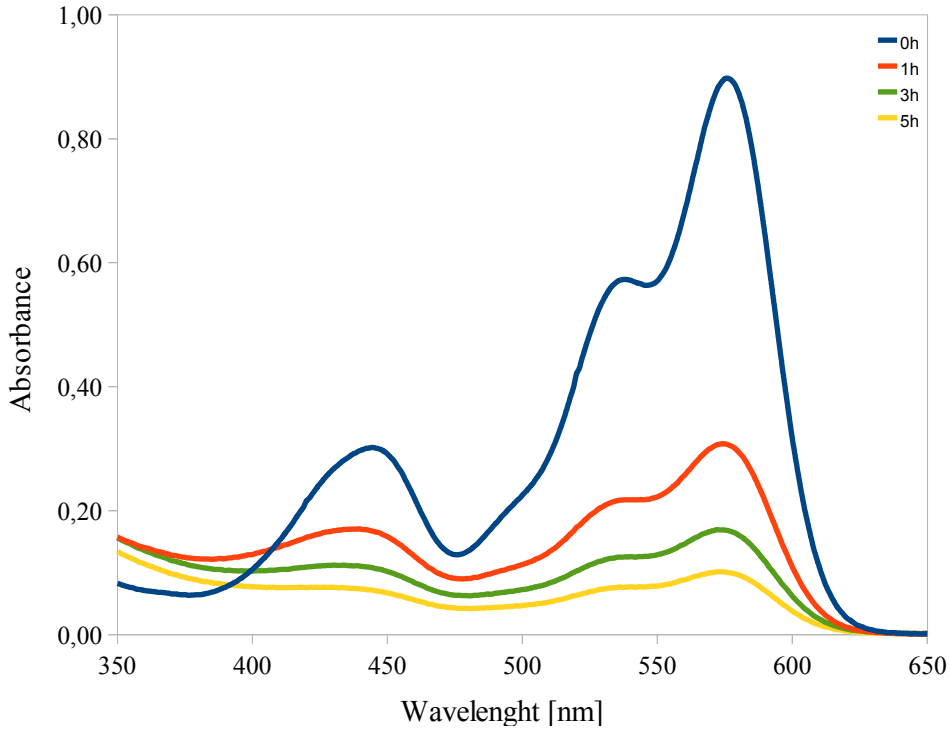

FigureIII. 41- UV-vis spectra of pristine PL6 film and PL6 film degraded after 1h, 3h, and 5h of exposure time to UV light

Absorption intensities in UV-vis spectra decrease with increasing time of exposure as also reported on the dye-only system.

Intensity ratios were calculated in order to highlight differences between the degradation process of the two main peaks characteristic of the two absorbing species.

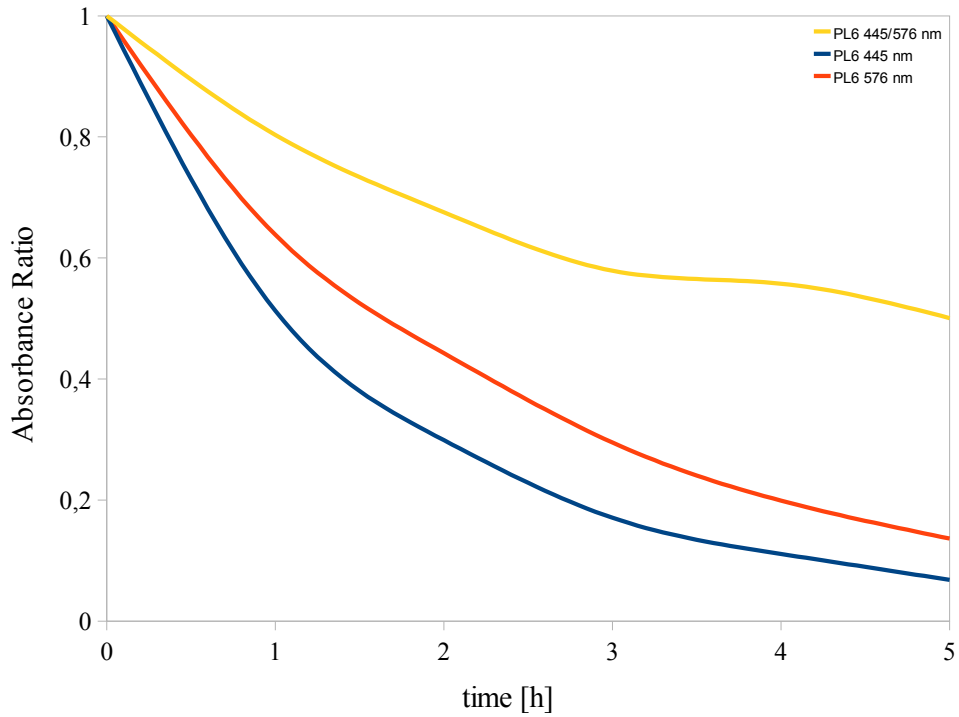

FigureIII. 42- Trends of degradation process by UV-vis spectroscopy. Red and blue lines are the ratios of the intensities of degraded material to the intensity of the pristine material

As shown in FigureIII. 42 the signal attributed to the absorption of the lateral substituents undergoes a faster decrease at increasing exposure times with respect to the decay observed for the absorption peak related to the perylene core. This behaviour is in agreement with the results obtained in the dye-only system.

Additionally, the trends observed in FigureIII. 42 suggest a two-step decay with a faster decrease in the first hour that approaches a plateau for longer UV-exposure times.

III.2.3.3.FTIR

FigureIII. 43 shows the comparison between PMMA FTIR spectrum (red line) and PL6 FTIR spectrum (blue line).

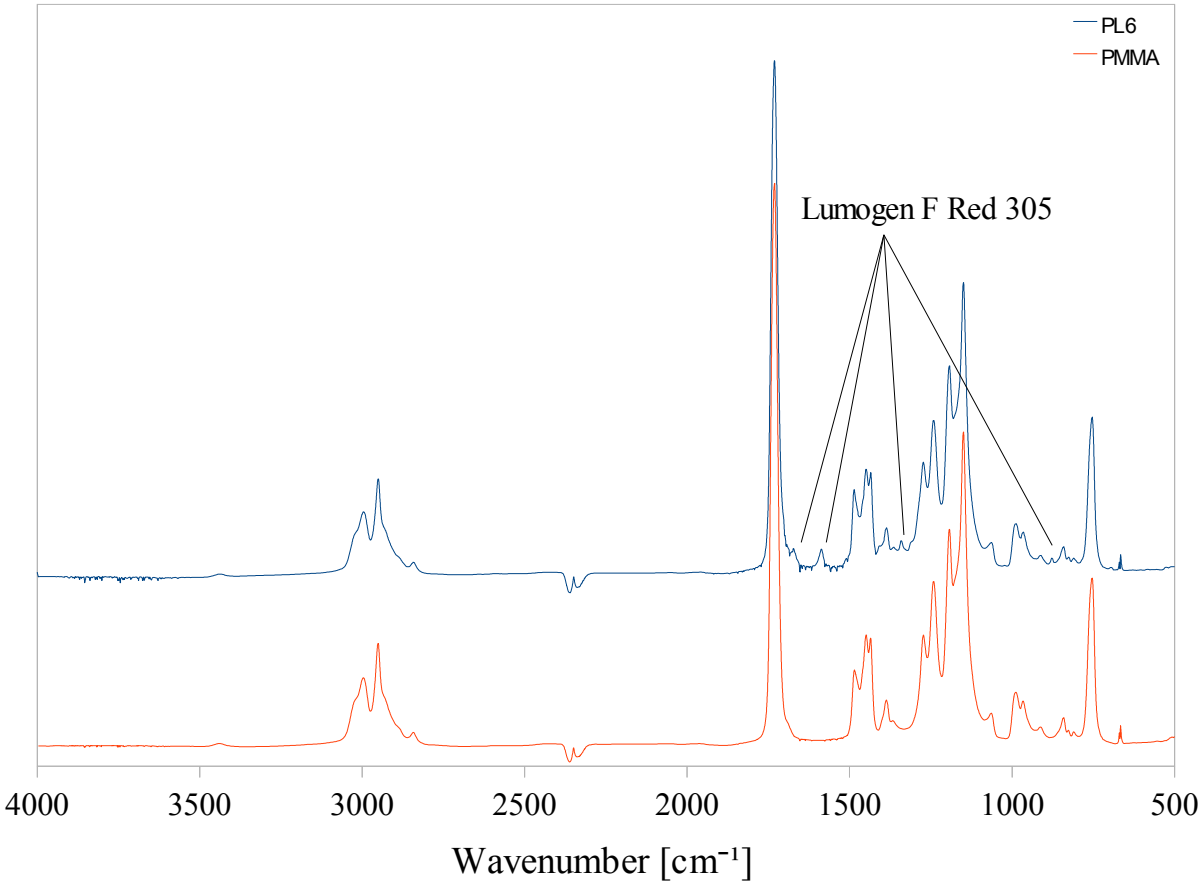

FigureIII. 43- FTIR spectra of PL6 thin film (blue line) and PMMA thin film (red line)

From a comparison between these two spectra, it is possible to identify the absorption peaks ascribable to the Lumogen molecule.

The first peak, attributed to the lower energy C=O stretching vibration of the dye molecule, can be observed at 1672 cm^{-1}. The stretching vibrations of the C=C bonds of the perylene core are responsible for the peak at 1586 cm^{-1}. Stretching vibrations of the dye can be observed also at 1342 cm^{-1}. Finally, the signal atributed to the ring breathing is found at 877 cm^{-1}. These four peaks were monitored over UV-exposure time in order to evaluate the effect

of degradation on the dye molecule when mixed in PMMA matrix (see FigureIII. 44).

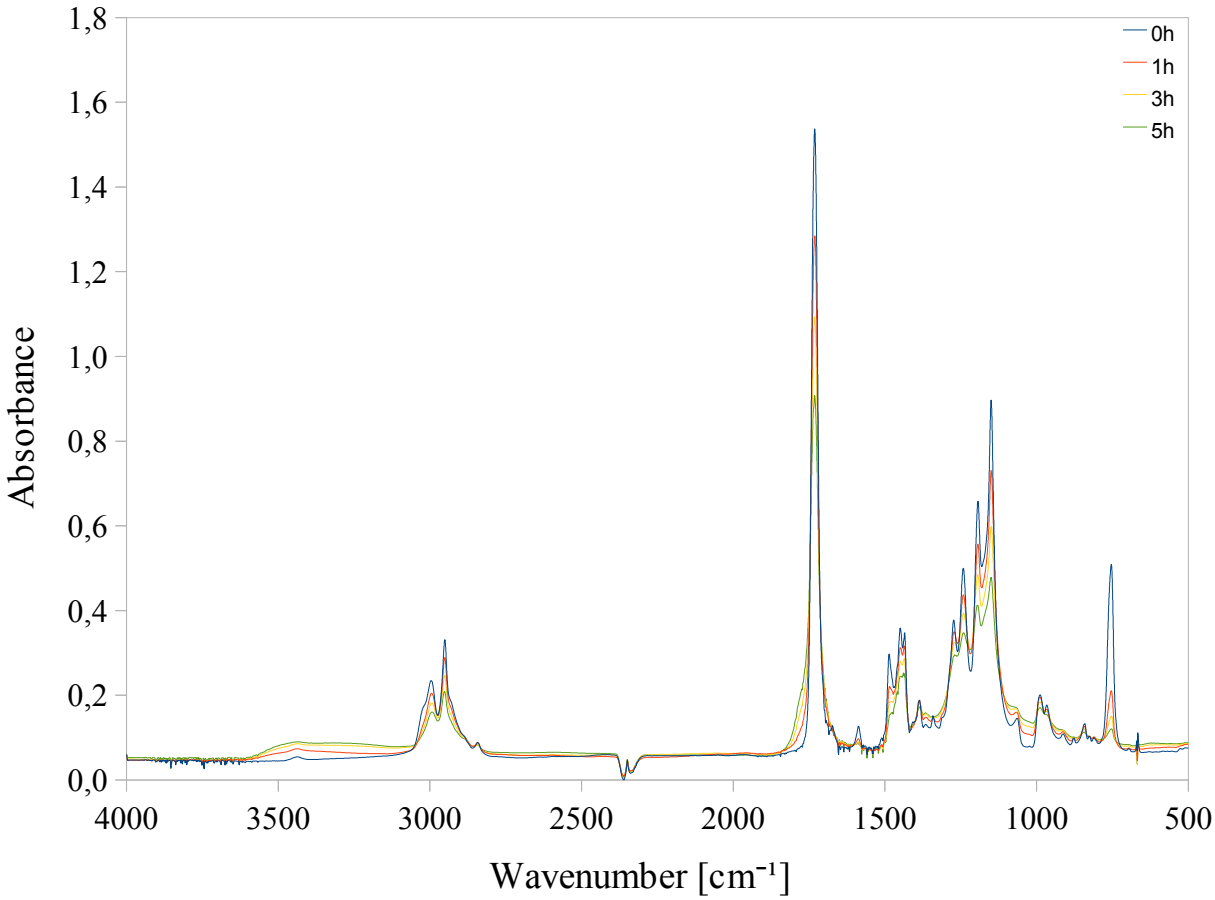

FigureIII. 44- FTIR spectra of PL6 thin film at increasing UV-exposure times.

The degradation of the PL6 films leads to an increase of the signals in the 3500 cm^{-1} region accompanied by the appearance of two bands in the carbonyl region adjacent to the main peak (1731 cm^{-1}), as also found in the degradation of PMMA.

In addition, a general decrease of the peaks associated to band vibrations in the PMMA molecule is observed. The peaks attributed to vibrations in the dye molecule exhibit a progressive decrease of intensity at increasing exposure to UV-light, as also reported for the dye-only films. However, different rate of intensity decay are observed, as discussed more in detail in the next chapter. A similar trend is also found for PMMA, which appears to undergo a slower degradation process when mixed with Lumogen.

III.2.4. Comparisons between spectroscopic results

In the previous section PMMA, dye and PL6 thin films were analyzed by fluorescence, UV-vis and FTIR spectroscopies. In order to understand differences in degradation process, the results of these studies have to be compared. Two main comparisons were carried out. Firstly the FTIR spectra of degraded PMMA and PL6 were compared, as different degradation

rates for the polymer matrix were observed. Comparisons were then carried out between the spectroscopic results obtained on the organic dye and those obtained on the PL6 compound, in order to evaluate the role of the dye in the degradation process.

III.2.4.1. Lumogen F Red 305 as UV absorber

As shown in FigureIII. 5 and FigureIII. 44, a PMMA thin film degrades faster than a PL6 film, although relative intensities of absorption bands characteristic of PMMA in both spectra are similar. The dye appears to be responsible for this difference in degradation rate, as both PMMA and PL6 film were deposited in the same conditions and present comparable thicknesses as absorption intensities of FTIR spectra are comparable, and the presence of Lumogen F Red 305 in PL6 compound is the only difference between PMMA and PL6 compounds.

FigureIII. 45 compare the FTIR spectra of PMMA and PL6 films both after 5h exposure to UV-light.

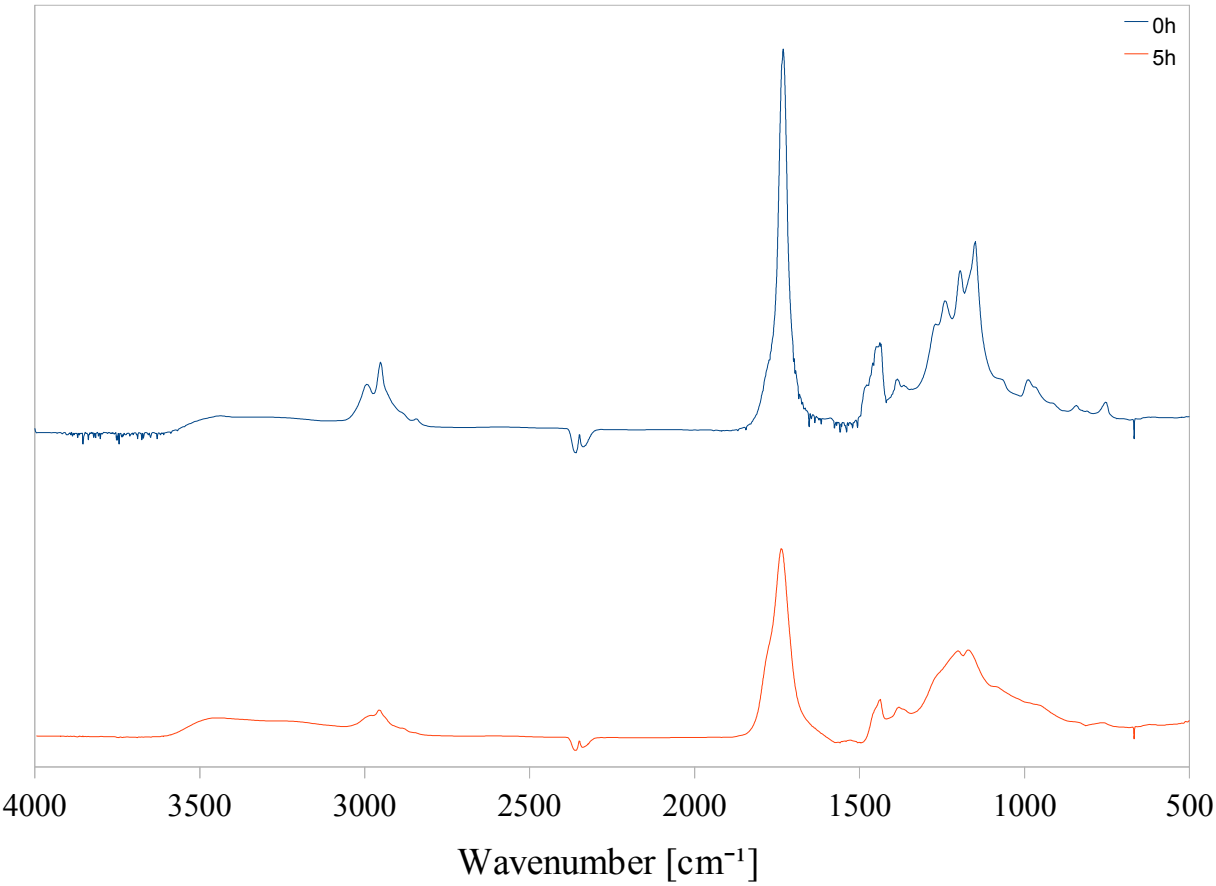

FigureIII. 45- FTIR spectra of PL6 sample and PMMA, both after 5h of UV exposure

In both FTIR spectra, the formation of similar signals attributed to degraded species appearing during UV-exposure is observed. This observation suggest that the organic dye does not participate in chemical reactions that lead to the degradation of the polymeric binder. On

the other hand the relative intensity of characeristic bands differs significantly between PMMA and PL6 thin films.

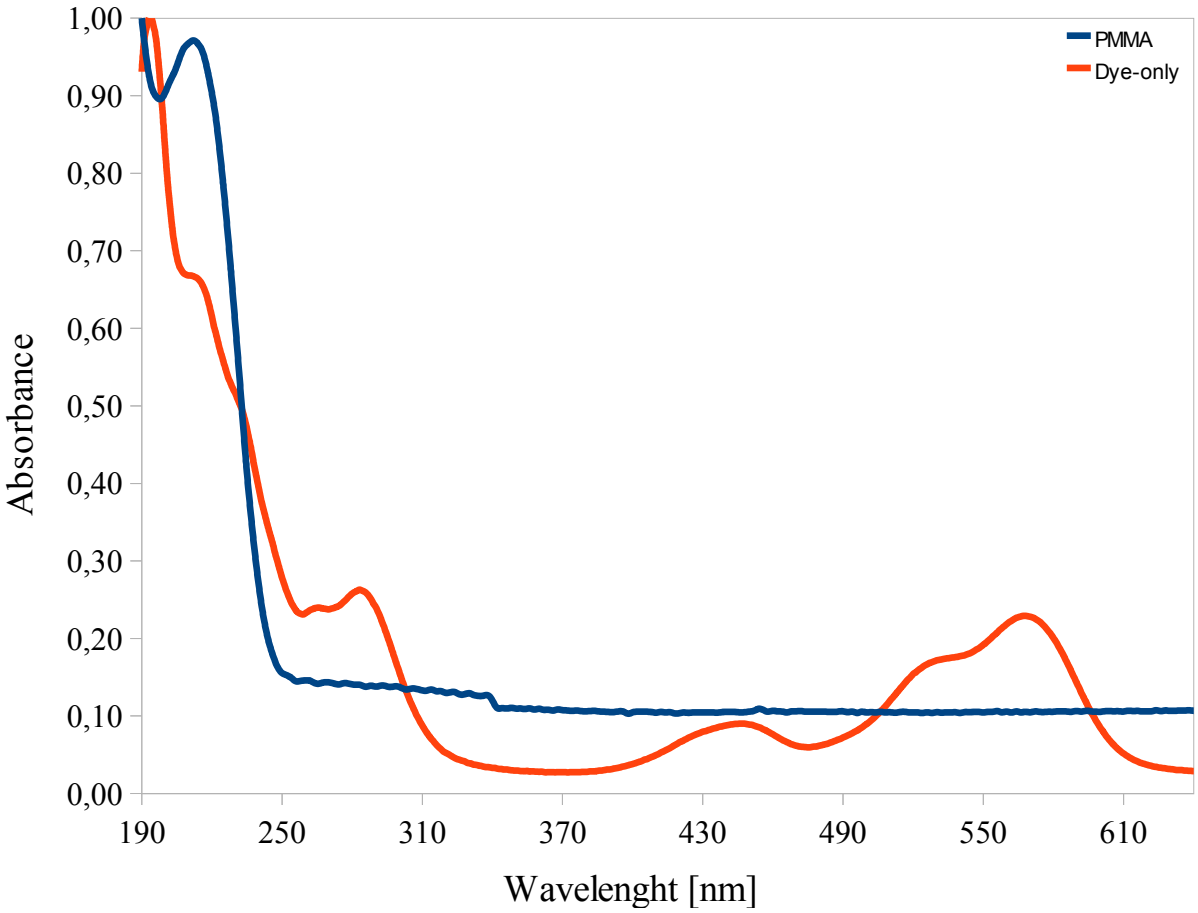

FigureIII. 46- Normalized UV-vis spectra of Lumogen F Red 305 (red line) and PMMA (blue line) thin films

As shown in FigureIII. 46 , the dye presents a strong photon absorption in the UV lamp emission region (emission peak centered at 254 nm). The high-energy photons absorbed by the dye molecule can be converted by the dye into lower energy photons or may lead to a non-radiatvie electronic relaxation. These processes may prevent these high-energy photons from interacting with the polymeric matrix. The amount of high-energy photons that can be absorbed by the matrix is therefore reduced. A lower amount of UV photons absorbed by the matrix may lead to a lower rate of the degradation process.

FigureIII. 47 shows the trend of the reduction in intensity of the FTIR peaks characteristic of CH stretching (2950 cm^{-1}), of C=O stretching (1730 cm^{-1}) and of C-O-C stretching vibration (1150 cm^{-1}) of PMMA.

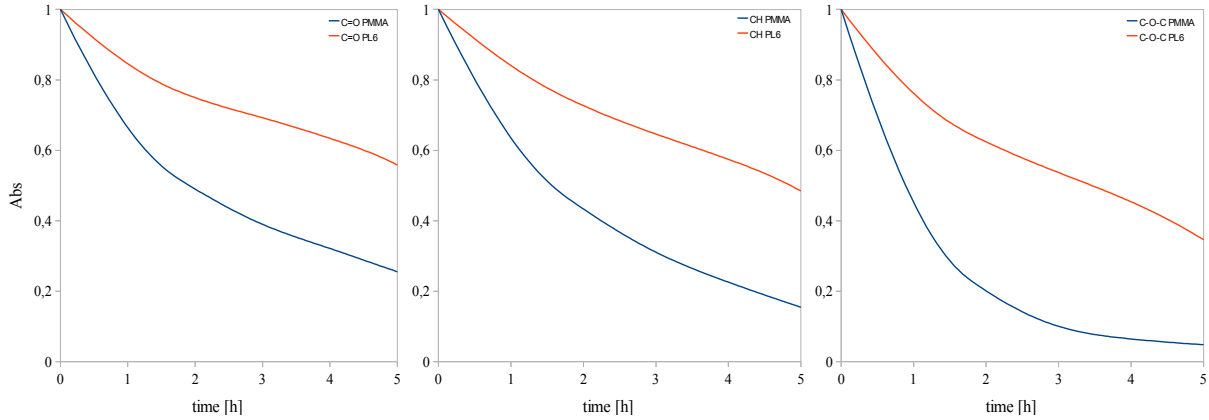

FigureIII. 47- Trends of the decrease in intensity of three main peaks of PMMA and PL6 samples after UV exposure

As shown in the plots, all PMMA characteristic peaks monitored during UV-exposure show a slower decrease in intensity when Lumogen is present in the thin film. This behaviour suggests that the organic dye acts as UV-absorber during the irradiation process of the OLSC thin film, thus protecting the polymer matrix and reducing its degradation rate.

III.2.4.2. Comparison between dye degradation trends

In spectroscopic analyses, degradation processes can be monitored by examining the ratios between characteristic vibrations. The results presented in the previous chapters on the organic dye have suggested a different rate of degradation of the lateral substituents compared to the perylene core. In particular, a faster decay was observed for the signals attributed to the lateral substituents with respect to the perylene core. In addition, different degradation rates were found for the dye molecule in dye-only films and in PL6 films. In particular, abrupt changes in the spectroscopic characeristics were observed for the dye dispersed in the polymer matrix. Conversely, a much slower degradation was exhibited in the dye-only films.

The relative decay of characteristic FTIR signals attributed to the dye is reported in FigureIII. 48, where a plot of the intensities of the peak assigned to the lateral substituents (ring breathing at 877 cm^{-1}) divided by the intensities of the peak assigned to the perylene core (stretching vibrations at 1586 cm^{-1}) is presented.

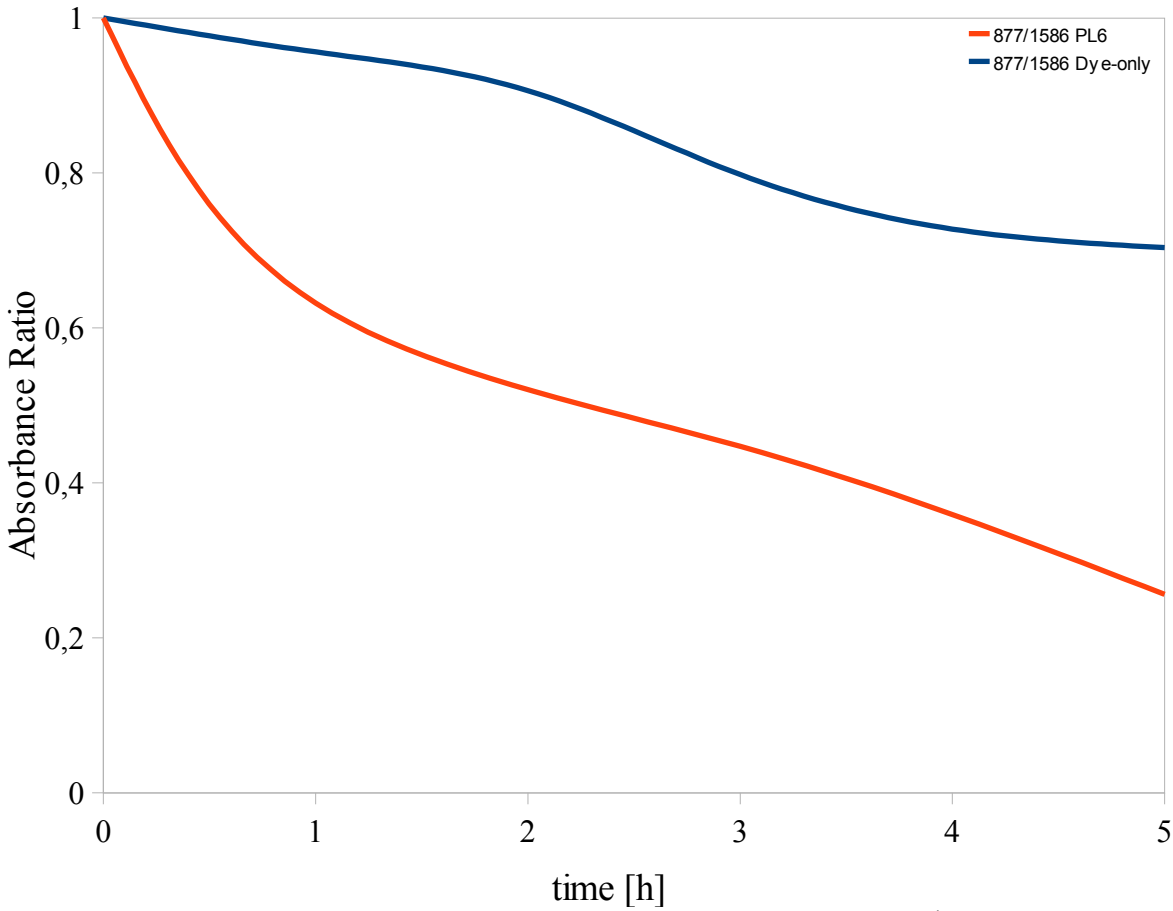

FigureIII. 48- Ratios between FTIR characteristic peaks of ring breating (877 cm^{-1}) and perylene core C=C stretching vibrations (1586 cm^{-1}) in dye-only and PL6 samples

Two different degradation rates are observed, with a faster decay found in PL6 films.

These results suggest that the lateral substituents in the dye molecule undergo a much faster degradation process compared to the perylene core when dye molecule is dispersed into a polymeric carrier. Indeed, after 5h UV-exposure the intensity of the signal attributed to the ring breathing (877 cm^{-1}) exhibits a 70% decrease compared to the perylene core (1586 cm^{-1}) in PL6 thin films. Conversely, in dye-only films, only a 25% decrease is observed.

An even sharper difference between dye-only and PL6 thin films is observed in UV-vis spectra, reported in FigureIII. 49.

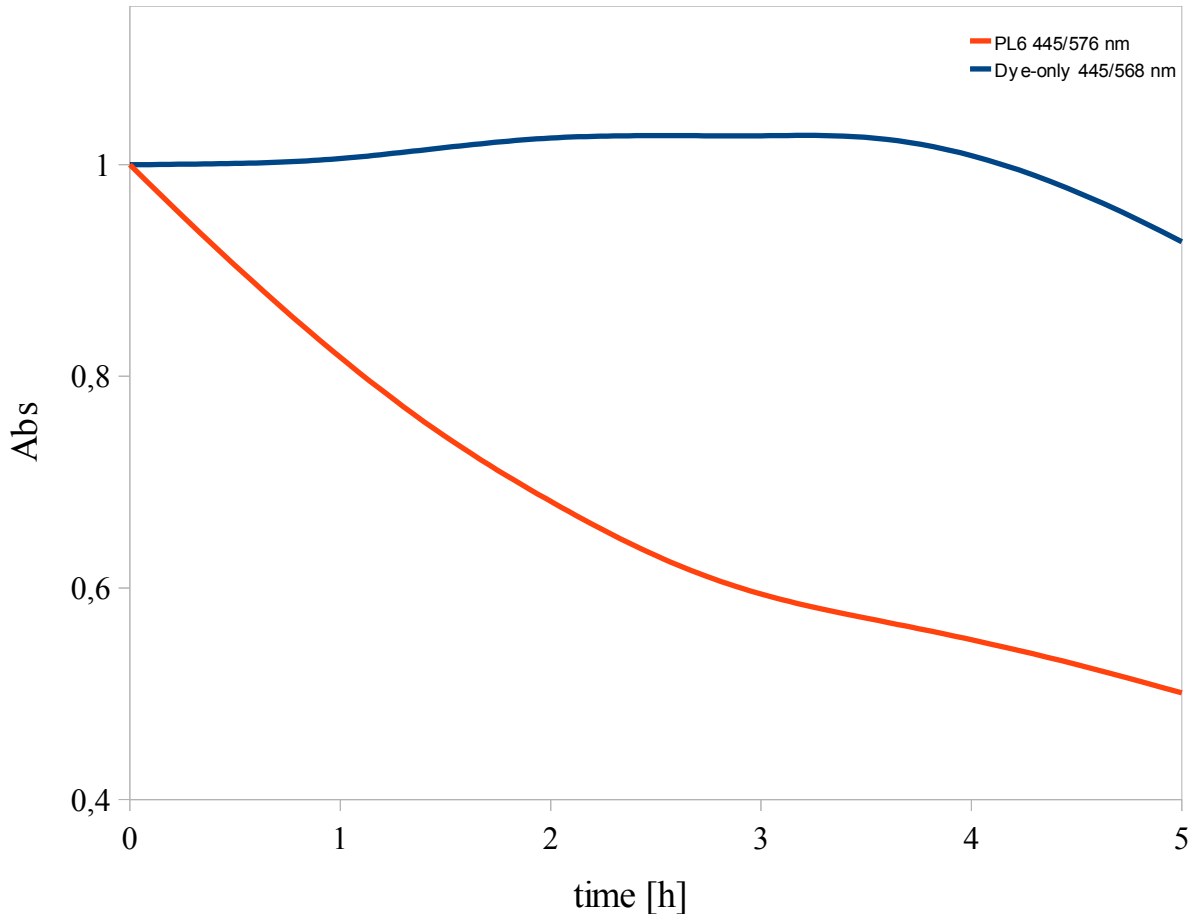

FigureIII. 49- Ratios between UV-vis characteristic peaks of the lateral substituents (445 nm) and of the perylene core (576 in PL6 samples and 568 in dye-only samples)

The blue curve, related to the dye in dye-only samples, shows an almost constant trend with a slope equal to 1. Conversely, the dye in PL6 compounds seems to deteriorate much faster than in dye-only samples. In particular, after 5h of exposure to UV light, PL6 sample shows a 50% decrease in the ratio between UV-vis absorption peak attributed to the lateral substituents and the absorption peak assigned to the perylene core. This observation may indicate that the extinction rate of dye lateral substituents is almost equal to that of the dye perylene core, in the case of dye-only samples. On the other hand, a much faster degradation is observed when Lumogen is dispersed into a polymeric matrix. Lumogen F Red 305 molecule, therefore, seems to be fairly stable to UV exposure in dye-only films.

Additional results by UV-vis spectra that could further confirm the supposed degradation mechanism were obtained by subtracting spectra of the sample degraded at different irradiation times from the pristine spectrum of the dye. This subraction process was performed for both dye-only samples and PL6 samples.

The subtraction spectra normalized to the absorption maximum, shown in FigureIII. 50, were calculated by subtracting the spectra of PL6 film after UV exposure from the pristine spectrum, in order to be able to highlight the absorption spectrum of the degraded species.

Firstly a blue-shift of the degraded species is observed. The peak attributed to the perylene core undergoes a blue shift of about 18 nm and the peak attributed to lateral chromophore subtituents undergoes a blue shift of about 27 nm. These blue-shifts may be due to an increase of the band-gap of the material following decrease in electron delocalization in the dye molecule upon UV-exposure. Therefore the degraded species isolated by subtraction of UV-vis spectra seems to exhibit a larger absorption band gap.

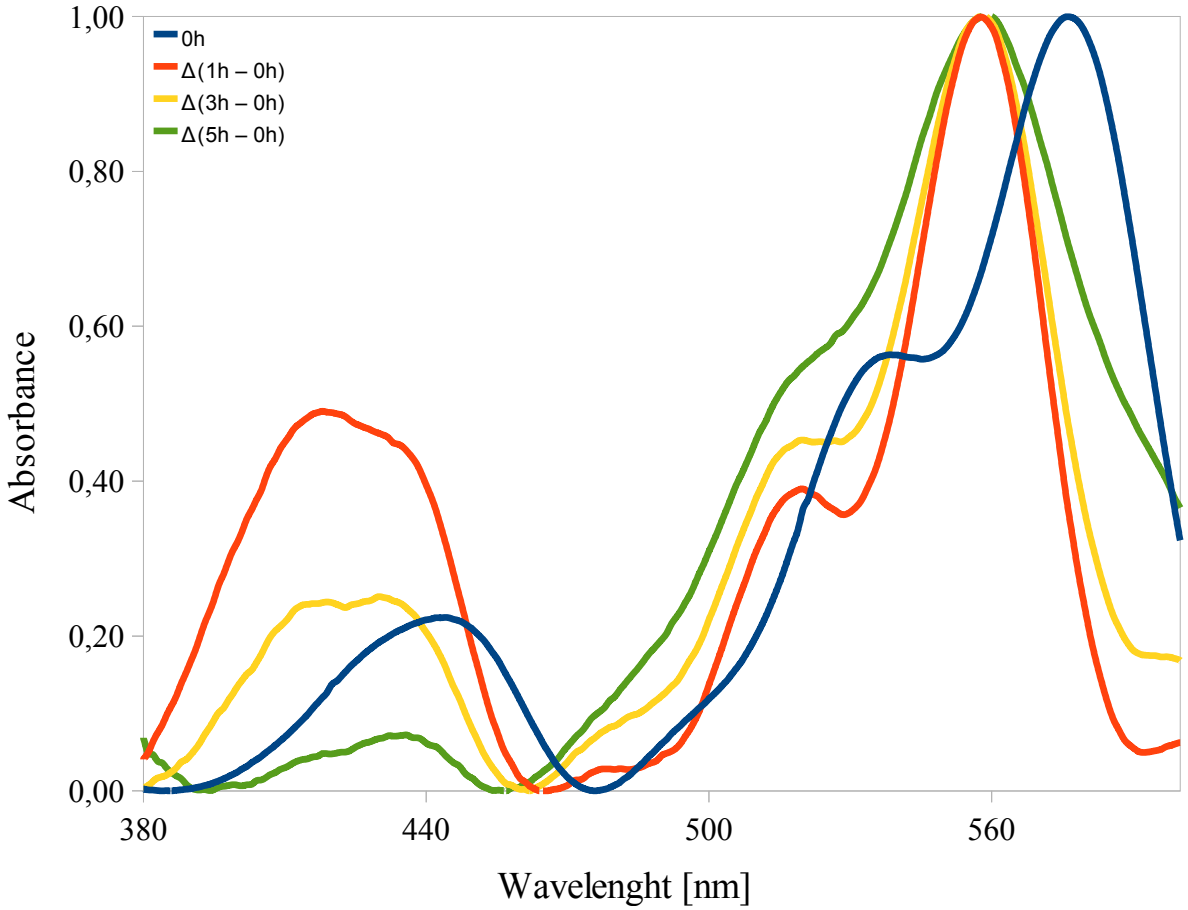

FigureIII. 50- UV-vis subtracted spectra

In addition, a progressive decrease of the 445 nm peak intensity is observed upon UV-exposure. Such a decrease further supports the hypothesis of a degradation mechanism of the dye molecule involving the abstraction of the lateral substituents from the perylene core, as already observed from FTIR analysis results reported earlier.

UV-vis subtraction spectra of dye-only samples were also calculated (data not shown), but no significant modifications were observed, further confirming a lower tendency to photo-degradation of dye-only films comparated to PL6 films.

The spectroscopic analyses performed in this work (fluorescence, UV-vis, FTIR) suggest stability of Lumogen F Red 305 to UV irradiation when exposed as dye-only film and instability of the dye when dispersed in the polymeric matrix. In order to firther clarify the

reasons of dye stability in dye-only films, DSC and 1H-NMR analyses were also carried out.

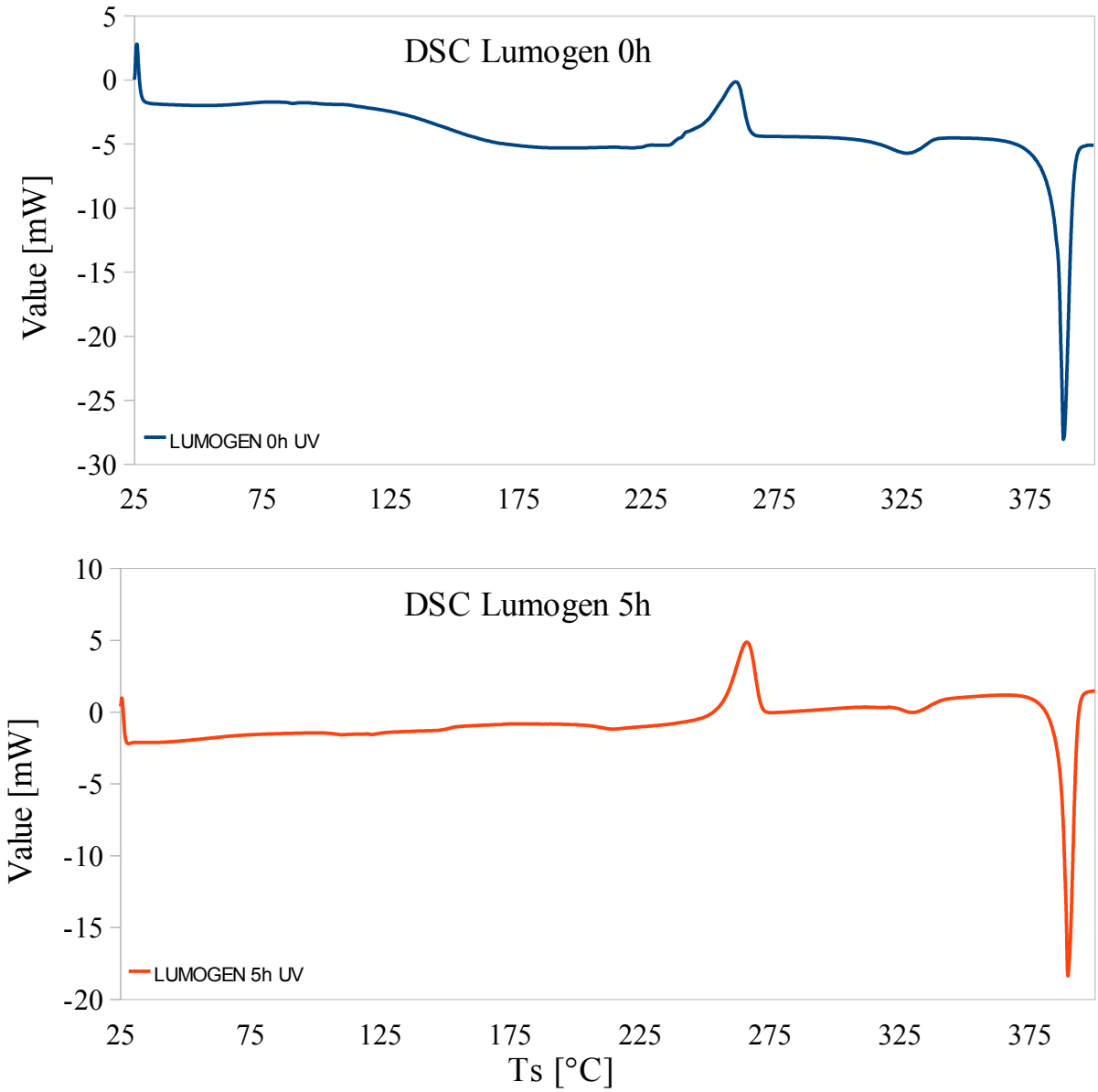

FigureIII. 51- DSC spectra of pristine and degraded dye in dye-only samples

FigureIII. 51 shows the DSC scans obtained from pristine dye-only films and from dye-only films exposed to UV light for 5h.

The DSC trace of pristine Lumogen shows a glass transition at about 150°C, a crystallization peak at about 250 °C and a melting peak centered at about 390°C. The presence of an intense melting point suggests a semi-crystalline structure of the dye with a high content of crystalline phase. The glass transition point suggests the existence of an amorphous portion of the material, which partially crystallizes at about 250°C (exothermic peak).

The semi-crystalline structure of the dye may contribute to the stability of dye-only films to UV light exposure. In order to verify this hypothesis, a DSC scan on dye-only films after 5h UV-exposure was also performed and it is shown in FigureIII. 51 (red line).

The DSC trace of degraded dye-only film shows a crystallization exothermic peak and a melting endothermic peak similarly to what found in pristine dye-only film while the glass transition il less evident and probably shifted to higher temperatures. Accordingly, UV exposure seems to cause some degradation of the material, which appears to affect mainly the amorphous portion of the dye.

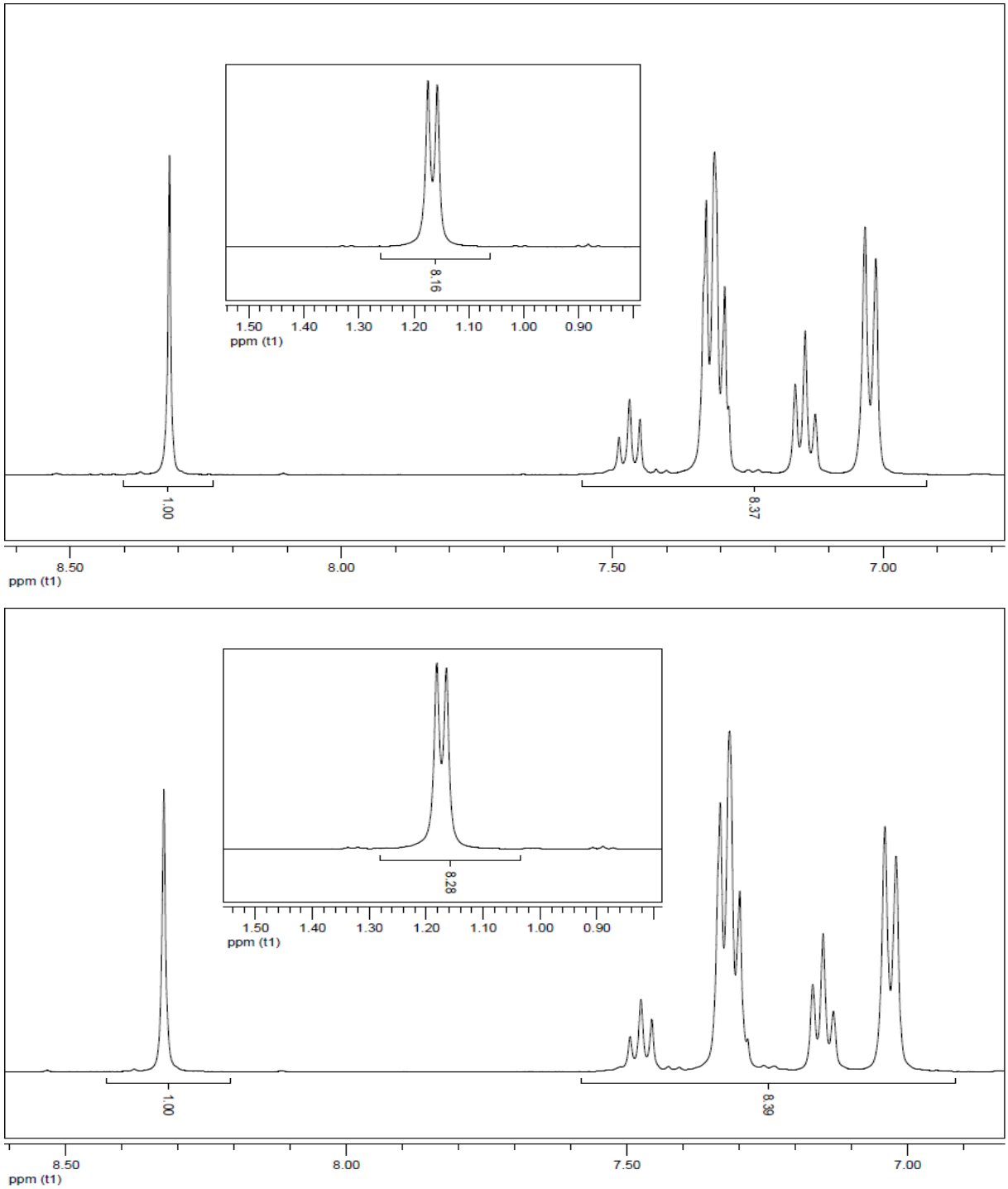

FigureIII. 52- 1H-NMR spectra of dye-only thin film after 0h, 5h of UV-exposure

1H-NMR spectra on the dye-only films were also collected and are shown in FigureIII. 52 where 1H-NMR spectra for both pristine and 5h degraded samples are presented. In accordance with results reported earlier, 1H-NMR spectroscopy futher confirms the hypothesis of a relative stability of the dye-only films, as no significant differences between pristine and degraded 1H-NMR spectra are observed.

In particular, the relative intensities of aromatic (δ=7.00÷7.50) and aliphatic (δ=1.2÷1.1) hydrogens do not change with UV-exposure time.

As a result, a substantial stability of dye-only films to UV-light was observed and confirmed by FTIR, UV-vis, fluorescence, 1H-NMR spectroscopies as well as by calorimetric analysis. Conversely, a significant degradation of the dye was observed in thin films of dye doped polymer matrix. The reason of such instability may be the absence of crystalline order of the dye molecule when mixed in a polymeric matrix. Indeed, the amorphous phase of the dye, present in higher amounts in dye doped polymer films, may undergo a faster degradation process, thus leading to rapid destruction of the dye molecule. Conversely, due to higher crystallinity, dye-only films are able to exhibit relatively high stability to UV-exposure.

III.2.Parametric study of OLSC devices

III.2.1.Thin film OLSC device

The dye used in this work (Lumogen F Red 305), presents two main absorption peaks in the visible region centered at 445 nm and 568 nm, respectively. The longer-wavelength peak undergoes a red shift of about 8 nm when the dye is in solution, and shows a much more noticeable fluorescence phenomenon when it is present in solution.

PMMA was chosen as carrier material because of its high transparency, low cost, and relatively good mechanical and photochemical resistance.

Despite different casting techniques were tested, spincoating deposition technique was definitely chosen, in order to obtain thin films as homogeneous as possible. In addition, spincoating allows obtaining film thicknesses in the order of 100 nm reproducibly. Such a low thickness may contribute to the decrease in the reabsorption effects, as all the absorptions and the emissions are confined within the thin film while trapping and reflection events occur primarily in the undoped layer (the rigid transparent substrate).

Light emitted into the undoped layer will travel to the plate edges by total internal reflection (TIR) with a greatly reduced chance of being reabsorbed. Absorption by the host material can also be minimized since pure materials with high optical clarity can be used. In

order to reduce light reflection by the film-substrate interface, glass substrates were used as rigid transparent substrates, as glass presents refractive index similar to that of PMMA.

III.2.2.Fabrication Procedure

In order to fabricate OLSCs, chloroform solutions containing PMMA concentrations at 10% w/w on $CHCl_3$ and dye at different concentrations were performed. These solutions were spincoated onto rigid transparent glass substrates. Such thin film OLSCs were then coupled to a Si solar cell so that one edge of the rigid glass substrates was connected to the active surface of the cell. The bonding was performed by using a commercial thermosoftening adhesive (Krystalflex PE399 by Huntsman Polyurethanes). Heated to 130°C, the adhesive (softening range from 80 to 140°C) melts, becomes transparent and matches its refractive index to a value similar to the refractive index of glass.

The cell firstly was placed on hotplate set to room temperature. An area of Krystalflex PE399 of the size of the SLSD-71N4 Si cell top face was cut and placed on the cell. The hotplate was then switched on and set to reach the 130°C temperature. In order to allow the Krystalflex PE399 to soften sufficiently, the temperature was kept at 130°C for at least 2 minutes. One edge of the OLSC was then manually pressed onto the cell with the Krystalflex film on it, until a good optical contact was achieved. Finally, in order to ensure a strong bonding between the LSC and the cell, the device was allowed to cool down to room temperature. After the fabrication of the OLSC device, its performance was characterized with I-V measurements under simulated solar light irradiation.

In order to optimize the transport of photons within the transparent polymeric carrier, perfect perpendicularity between the OLSC and the cell is needed. To confirm this observation, preliminary tests were carried out on OLSC devices coupled to Si solar cells without paying much attention to the bonding process. Indeed, it was found that I-V measurements were inaccurate and non-reproducible. A holder that could guarantee almost perfect perpendicularity between cell and OLSC during the bonding stage was needed. In particular a steel square was used for this aim, so that good heat tranfer could be ensured between hot plate and the thermosoftening adhesive together with excellent control of the planarity of the system.

III.2.3.Parametric Study

The OLSC performance was estimated by comparing the efficiency of the illuminated PV cell alone with the efficiency of the system including PV cell connected to the OLSC thin film. Efficiency values were calculated by means of I-V measurements on the individual

SLSD-71N4 cells and on the OLSC mounted devices, both illuminated under simulated solar light.

FigureIII. 53 shows the I-V curve of a typicall SLSD-71N4 cell.

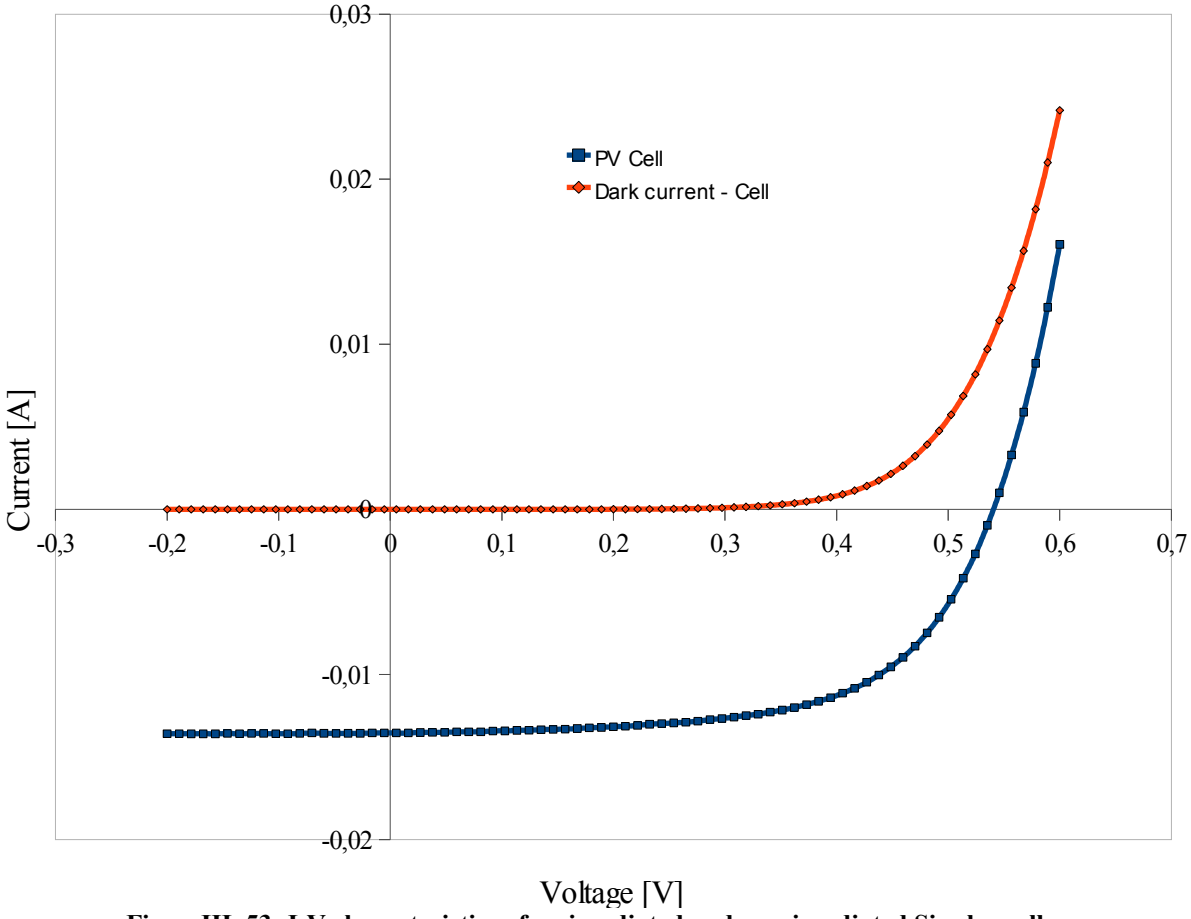

FigureIII. 53- I-V characteristics of an irradiated and non-irradiated Si solar cell

According to the manifacturer, the SLSD-71N4 solar cell exposed to 25 mW/cm^2 shows the V_{OC} around 0,5 V and the I_{SC} within 1,4 and 2,3 mA. As shown in FigureIII. 53, the performed experimental tests showed an efficiency of about 9,55±0,4, with a V_{OC} of 0,53 V and an I_{SC} of 13,64 mA. Differend values are observed, as the cells in this research were exposed to 100 mW/cm^2.

The solar cell efficiency was calculated according to the following equation:

$$\eta_{CELL} = \frac{P_{m,CELL}}{P_{ph}} = FF_{CELL} \frac{J_{SC,CELL} V_{OC,CELL}}{P_{ph}}$$

where $J_{SC,CELL}$ is the short circuit current density calculated on the active surface area of the cell alone (A_{CELL} = 0,452 cm^2).

The I-V curve of a typical OLSC mounted device is shown in FigureIII. 54.

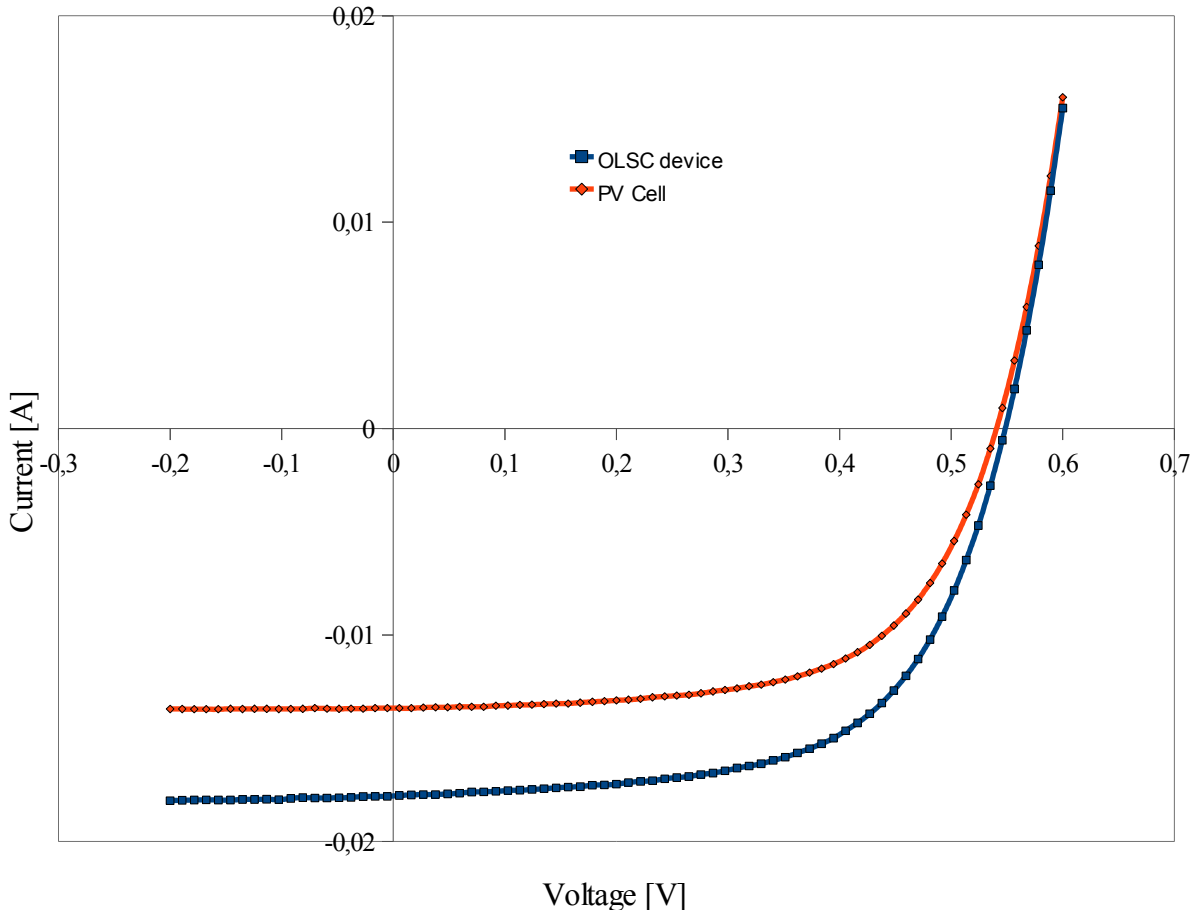

FigureIII. 54- I-V characteristics of a cell before (PV cell) and after bonding (OLSC device)

The behaviour of an illuminated OLSC mounted device is similar to that of a Si solar cell, however an increase in efficiency can be clearly distinguished, mainly due to an increase in I_{SC} occurring by the incorporation of the OLSC thin film. In particular, in FigureIII. 54 the I_{SC} changes from 13,37 mA measured on the bare cell to 18 mA measured on the OLSC mounted device.

In order to estimate the efficiency of the OLSC mounted device, two different approaches were used. A first estimate was given by calculating the power conversion efficiency (PCE) of the OLSC, according to the followinf formula [13-15]:

$$\eta_{OLSC} = \frac{P_{m,OLSC}}{P_{ph}} = FF_{OLSC} \frac{J_{SC,OLSC} V_{OC,OLSC}}{P_{ph}}$$

where $J_{SC,OLSC}$ is the short circuit current density calculated as the ratio between $I_{SC,OLSC}$ and the actual active surface area of the solar concentrator (A_{OLSC} = 13,45 cm^2). This parameter represents the OLSC power conversion efficiency and it can be related to the External Quantum Efficiency (EQE) of the coupled system, as the EQE is defined as the conversion to electrons of the photon flux incident on the OLSC surface. In addition, η_{OLSC} takes into account the contribution of the surface area of the OLSC, thus allowing comparisons between

devices with different dimensions.

Due to the incorporation of an OLSC onto a solar cell, a relative efficiency improvement Δη(LSC) due to the presence of the OLSC can be also calculated according to the following equation:

$$\Delta\eta(\mathrm{LSC}) = \frac{\eta_{CONC} - \eta_{CELL}}{\eta_{CELL}} = \left(\frac{FF_{OLSC}}{FF_{CELL}}\right)\left(\frac{I_{SC,OLSC}}{I_{SC.CELL}}\right)\left(\frac{V_{OC,OLSC}}{V_{OC.CELL}}\right) - 1$$

where η_{CONC} is the efficiency of the OLSC mounted device calculated by considering the JSC as the ratio between $I_{SC,OLSC}$ and the surface area of the cell (A_{CELL}=0,452 cm^2)over the cell surface area:

$$\eta_{CONC} = FF_{OLSC} \frac{\frac{I_{SC,OLSC}}{A_{CELL}} V_{OC,OLSC}}{P_{ph}}$$

As this efficiency is calculated on the cell area, it indicates how efficiently the cell active surface area is used in the power conversion. The percentage growth in efficiency (Δη(LSC)) is considered in order to evaluate the variation in the electrical properties of the cell after the OLSC coupling. As long as Δη(LSC) is a positive value, the mounting of the OLSC onto the cell yields to an efficiency gain.

In order to ensure a high level of accuracy during measurements, tests on each chosen condition were carried out on three different devices, and for each device, I-V measurements were repeated five times. In conclusion, each condition was defined by averages of 15 measured values.

In order to avoid light losses from the back of the OLSC under simulated solar light, a distributed Bragg backreflector is needed. In order to fulfil such requirement, the OLSC was placed onto a white mat cloth acting as a distributed Bragg backreflector, as white surfaces ensure diffuse reflection with no absorptions of radiation in the visible region.

In order to optimize the OLSC-mounted device efficiency, several device parameters can be independently studied. In this work changes in efficiency were measured as a function of dye concentration and PMMA concentration.

The dye concentration was varied from 2% to 12% w/w on PMMA, as at 12% a negative Δη(LSC) was reached. The negative value of Δη(LSC) may be attributed to an excess of reabsorption losses. Tests were performed on samples obtained by seven different solutions containing PMMA concentration at 10% w/w on $CHCl_3$ and 2,4,5,7,8,10,12% of dye in weight of PMMA. Each condition was tested on three samples and each test was repeated five times, as mentioned above. Employed samples exhibited a thickness of about 5 μm at any dye

concentration. Therefore the concentration of the dye do not affect the film thickness, as expected.

Firstly, bare cell performance was analyzed. Table III.1 collects the average electrical parameters resulting from I-V tests performed on the cells. The 21 cells employed in this first study were divided into 7 groups of three cells each. Each cell was coupled to an OLSC containing a given dye concentration. Each group was named after the dye concentration present in the solution used to fabricate the thin film OLSC, as S stands for "series" and the number for the dye concentration.

	PV Cell			
	$I_{SC,CELL}$	$V_{OC,CELL}$	FF_{CELL}	η_{CELL}
S2	13,86±0,44	0,54±0,005	59,74±0,70	9,80±0,49
S4	13,56±0,05	0,54±0,002	61,39±0,33	9,92±0,10
S5	13,83±0,27	0,54±0,001	59,18±0,62	9,67±0,19
S7	13,49±0,14	0,54±0,010	59,83±2,17	9,53±0,42
S8	13,57±0,15	0,52±0,003	58,54±0,61	9,21±0,20
S10	13,53±0,20	0,52±0,002	58,53±0,37	9,14±0,18
S12	13,68±0,36	0,53±0,010	59,66±1,88	9,59±0,74

Table III.1 – Characteristics of the cell alone

Each value is obtained by the average of the fifteen measured values in the electrical analysis of each group, and in order to consider the reproducibility of measurements, the standard deviation is also calculated. Special attention was given to V_{OC} and FF, as these are characteristic parameters related to the quality of the PV cell.

As the V_{OC} parameter is closely related to the quality of the cell material, and standard deviation values calculated on its measurements can be approximated to zero, homogeneity in the material properties can be assumed.

On the other hand, the FF is strictly related to the fabrication procedure of the cell, as the Fill Factor indicates how well a pn junction is made. Fill Factor standard deviation values shown in Table III.1 suggest that the provided cells are not high precision products. Accordingly, efficiencies and short circuit current standard deviations were generally found to be higher in groups characterized by higher FF standard deviations values.

Table III.2 collects the average characteristics obtained by measurements performed on the cell alone and on OLSC mounted devices.

The devices are named after the name of the deposited solution, as P stands for

PMMA, L for Lumogen and the number indicates the dye concentration by weight of PMMA.

	OLSC device					
	$I_{SC,OLSC}$	$V_{OC,OLSC}$	FF_{OLSC}	η_{OLSC}	η_{CONC}	$\Delta\eta$(LSC)
PL2	18,42	0,55	58,09	0,43±0,01	13,00±0,24	32,89
PL4	18,42	0,55	60,33	0,44±0,02	13,47±0,50	35,81
PL5	18,95	0,55	59,05	0,45±0,04	13,58±1,33	40,29
PL7	17,57	0,54	59,08	0,41±0,05	12,47±1,38	30,48
PL8	17,59	0,53	58,11	0,39±0,01	12,00±0,24	30,37
PL10	14,85	0,52	58,27	0,33±0,02	9,96±0,74	8,94
PL12	13,29	0,52	58,96	0,3±0,05	9,14±1,48	-5,05

Table III.2 – Characteristics of the OLSC mounted devices

Similarly to what performed in the case of bare cells analyses, standard deviations were calculated and reported in Table III.2. The inhomogeneity in electrical properties measured from electrical analyses of the bare cells, appears to be amplified after the bonding of OLSCs on the surfaces of the cells. This increase in the standard deviations is probably due to the amplification of the related signals after the mounting of the OLSC on the PV cell.

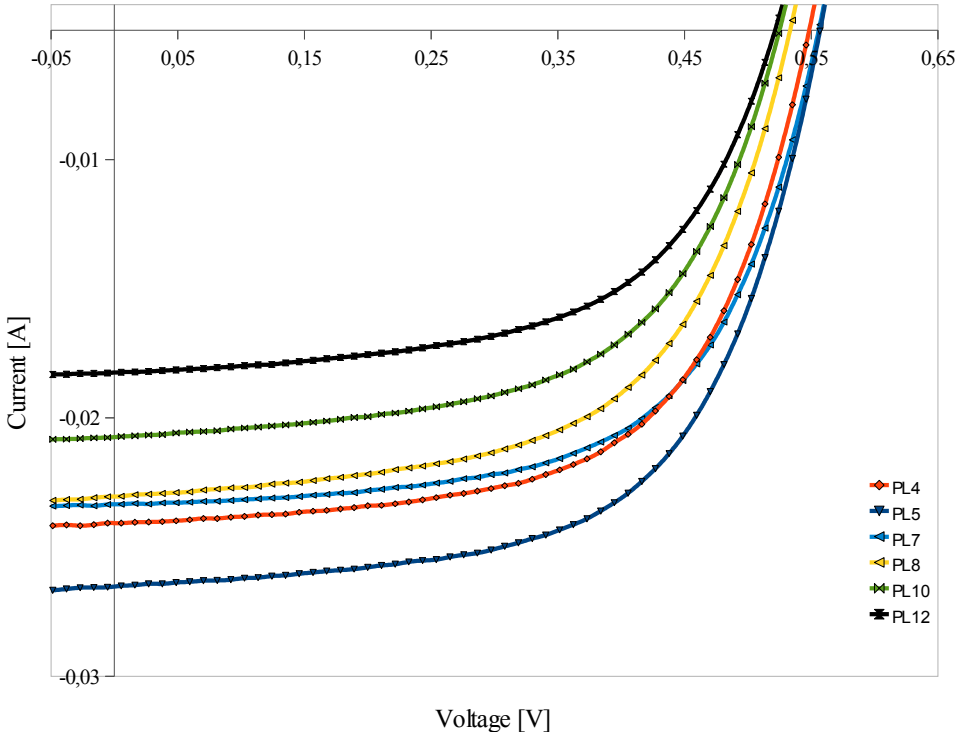

FigureIII. 55- I-V characteristics of OLSC devices at different dye concentrations.

In conclusion, OLSC device fabricated in the conditions described above shows low reproducibility of electrical measurements, which is probably due to the inhomogeneity in the

electrical measurements caused by the commercial grade of the provided cell, and to inaccuracies that may occur in the bonding stage.

However, referring to data shown in Table III.2, a maximum in efficiency was found. The best performance is obtained by a PL5 OLSC device. This finding is also shown in FigureIII. 55 as higher I_{SC} was measured for PL5 OLSC device compared to the other OLSC.

By the observation of the curves in FigureIII. 55, no significant changes in V_{OC} and FF are visible at increasing I_{SC}, as V_{OC} is the value in V corresponding to the intersection between the curves and the horizontal axis and the FF is a measure of sharpness of the knee in an I-V curve. This result verifies the theory, as both V_{OC} and FF do not depend on the current generated.

Referring to efficiencies related to different dye concentrations, curves in FigureIII. 56 were plotted. The efficiency of OLSC devices versus dye concentration and the relative efficiency gain with OLSC devices are presented in FigureIII. 56.

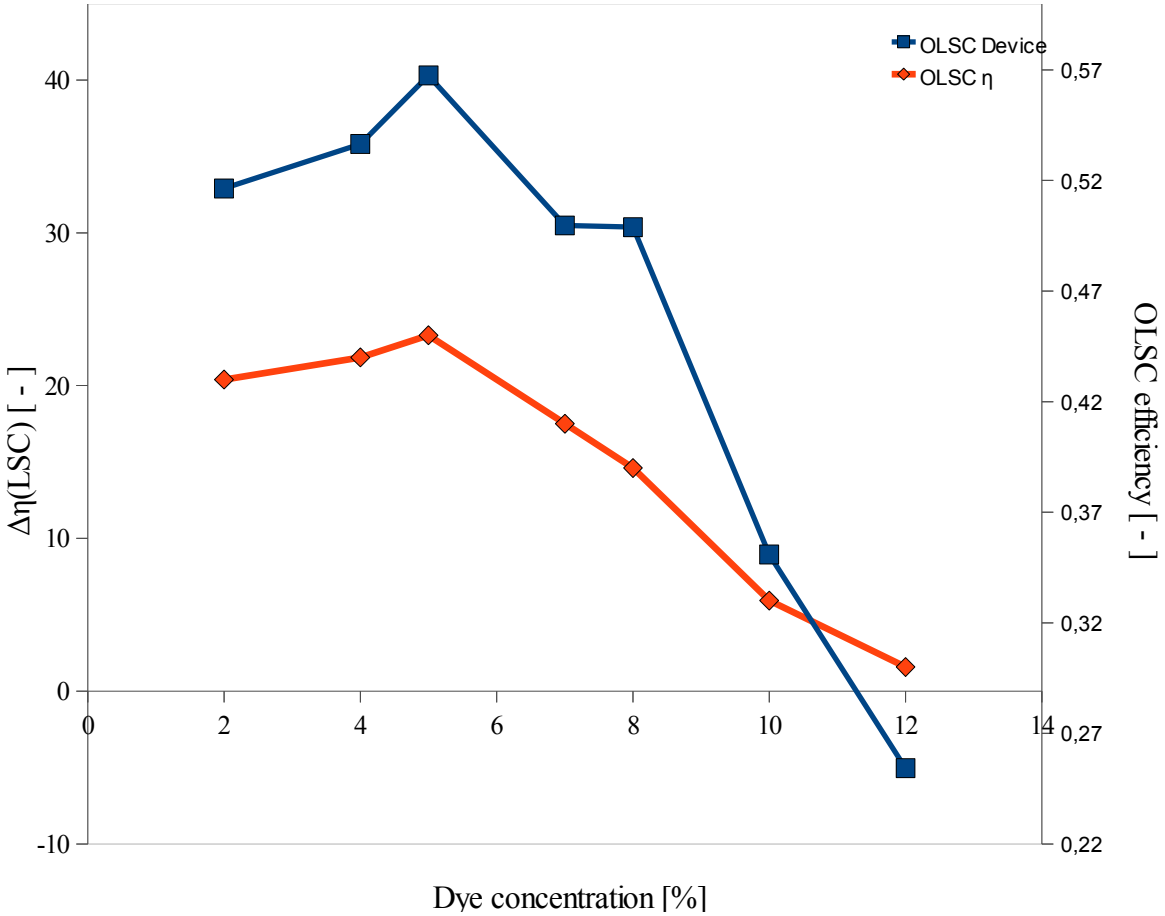

FigureIII. 56 - Δη(LSC) curve and η_{OLSC} curve in dye percentage

In FigureIII. 56 two efficiencies are plotted, and both present a maximum at the same dye concentration. According to the theory, two divergent trends are responsible for this behaviour. The increase of the dye concentration permits the conversion of a higher quantity

of photons, corresponding to an increase in efficiency until it reaches a maximum in efficiency. The decreasing trend is due to reabsorption losses, as an increase of dye particles in the carrier matrix leads to a growing probability of reabsorption.

Both blue and red curves present an efficiency maximum corresponding to the luminescent thin film which contains 5% of dye.

A preliminary study on the luminescent film thickness has been also carried out, fixing at 5% the dye concentration as it showed best performance in the dye concentration studies.

The effect of film thickness on OLSC device performance can be analyzed by varying the PMMA concentration in the chloroform solution or by changing the spincoating speed. As changes in spincoating speed may also change surface morphology of the film, modifications of OLSC thickness have been performed by varying the solution concentration.

Solutions with 1%, 5% and 10% by weight of PMMA in chlorofrom and with 5% of dye in PMMA were prepared, and then deposited onto glass substrates by employing the same conditions as those used in the previous study. Firstly, bare cell performance was analyzed by collecting the average electrical parameters resulting from I-V tests performed on the cells (Table III.3). The 9 cells employed in this first study were divided into 3 groups of three cells each. Each cell was then coupled to an OLSC containing a given PMMA concentration. Each group was named after the PMMA concentration present in the solution used to fabricate the thin film OLSC. OLSC devices were then coupled to a Silicon cell mounted on an OLSC edge and I-V measurements were carried out.

	PV Cell			
	$I_{SC,CELL}$	$V_{OC,CELL}$	FF_{CELL}	η_{CELL}
S1%	13,3±0,36	0,52±0,01	57,17±2,33	8,75±0,41
S5%	13,34±0,24	0,51±0,03	55,70±4,76	8,42±1,51
S10%	13,83±0,27	0,54±0,04	59,18±0,62	9,67±0,19

Table III.3 – Characteristics of the cell alone

Standard deviations were also calculated as the values reported in Table III.3 are average values.

After characterization of the PV cells alone, I-V measurements were extended to the device combining PV cell and OLSC. Table III.4 shows the electric parameters obtained by I-V measurements performed on the bonded system.

In addition, OLSC thicknesses were calculated by profilometry. The values obtained are collected in Table III.4.

		OLSC device					
	Thickness	**$I_{SC,OLSC}$**	**$V_{OC,OLSC}$**	**FF_{OLSC}**	**η_{OLSC}**	**η_{CONC}**	**$\Delta\eta$(LSC)**
P1L5	**100 nm**	9,27	0,51	57,29	0,20±0,05	5,94±1,66	-32,03
P5L5	**200 nm**	15,64	0,51	55,02	0,32±0,05	9,81±1,51	16,5
P10L5	**5 µm**	18,95	0,55	59,05	0,45±0,04	13,58±1,33	40,29

Table III.4 – Characteristics of the bonded system

The efficiency of the coupled device was calculated as the efficiency in the previous study.

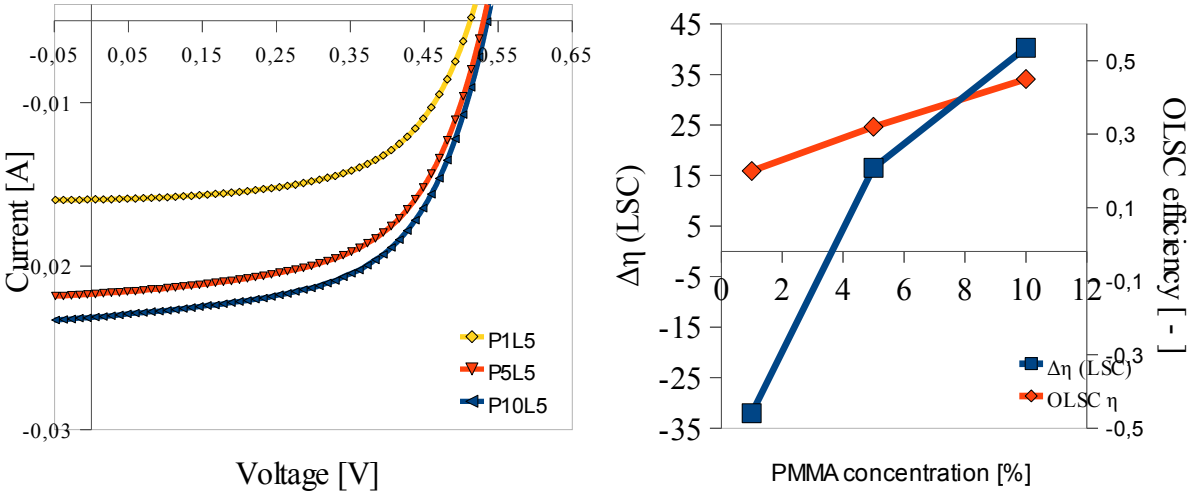

FigureIII. 57- I-V characteristics (a) and efficiency curves (b) obtained by OLSC devices with different thickness of the fluorescent layer

FigureIII. 57 shows the I-V curves. As it presents higher I_{SC} while V_{OC} and FF remain constant, according to theory, a maximum in efficiency can be identified in the P10L5, as also shown in Table III.3.

FigureIII. 57 shows the trends of the efficiencies η_{OLSC} and $\Delta\eta$(LSC). P10L5 exhibits the maximum in both the efficiencies. The reduction in the film thickness also involves a reduction in the quantity of luminescent particles within the film.

In order to characterize more in detail the dependence of OLSC efficiency on PMMA concentration, a higher range of PMMA concentrations would need to be explored, although a first trend can be clearly noticed from this study.

The measurements presented in this section represent a preliminary study on different device parameters aiming at the optimization of OLSC efficiency. Further tests will need to be carried out to take into account the effects on OLSC efficiency of variables such as geometry of the OLSC plate, deposition technique, different type of backreflecting coatings.

Bibliographic References

1. Brenda C. Rowan, Lindsay R. Wilson, and Bryce S. Richards "Advanced Material Concepts for Luminescent Solar Concentrators", IEEE Journal of selected topics in quantum electronics, vol.14, no.5, 2008
2. J. M. Drake et al. "Organic dyes in PMMA in a planar luminescent solar collector: A performance evaluation", Appl. Opt., vol. 21, no. 16, pp. 2945–2952, 1982.
3. A.B.F Duncan, Walter Gordy, R. Norman Jones, F.A. Matsen "Chemical Applications of Spectroscopy", New York: Interscience publishers (1956)
4. G. Socrates "Infrared characteristic group frequencies", ed.Wiley (2001)
5. T. Ceaykara, O. Guèven "UV degradation of poly(methyl methacrylate) and its vinyltriethoxysilane containing copolymers",. Polymer Degradation and Stability 65 225±229 (1999)
6. Halina Kaczmarek, Alina Kaminska, Alex van Herk "Photooxidative degradation of poly(alkyl methacrylate)s" European Polymer Journal 36 767±777 (2000)
7. R. Srinivasan, Bodil Braren, and Kelly G. Casey "Ultraviolet laser ablation and decomposition of organic materials" Pure &App/. Chem., Vol. 62, No. 8, pp. 1581-1584,(1990)
8. C. Wochnowski, M.A. Shams Eldin, S. Metev "UV-laser-assisted degradation of poly(methyl methacrylate)", Polymer Degradation and Stability, (2005)
9. N. Nagai, T. Matsunobe, T. Imai "Infrared analysis of depth profiles in UV-photochemical degradation of polymers", Polymer Degradation and Stability 88 224e233 (2005)
10. Prelini Carlo "Studio di fenomeni di autoaggregazione in molecole policoniugate: contributo della spettroscopia ottica", thesis, (2004/2005)
11. Alex A. Granovsky, Firefly version 7.1.G, http://classic.chem.msu.su/gran/firefly/index.html
12. M.W.Schmidt, K.K.Baldridge, J.A.Boatz, S.T.Elbert, M.S.Gordon, J.H.Jensen, S.Koseki, N.Matsunaga, K.A.Nguyen, S.Su, T.L.Windus, M.Dupuis, J.A.Montgomery J.Comput.Chem. 14, 1347-1363 (1993)
13. L. H. Slooff, E. E. Bende, A. R. Burgers, T. Budel, M. Pravettoni, R. P. Kenny, E. D. Dunlop, A. Büchtemann, "A luminescent solar concentrator with 7.1% power conversion efficiency", p hys. stat. Sol. 6, 257–259 (2008)

14. W. G.J.H.M. van Sark, K. W.J. Barnham, L. H. Slooff, A. J. Chatten, A. Büchtemann, A. Meyer, S. J. McCormack, R. Koole, D. J. Farrell, R. Bose, E. E. Bende, A. R. Burgers, T. Budel, J. Quilitz, M. Kennedy, T. Meyer,C. De Mello Donegá, A. Meijerink, D. Vanmaekelbergh, "Luminescent Solar Concentrators – A review of recent results", Optical Society of America (2008)

15. L.H. Slooff, R. Kinderman, A.R. Burgers, A. Büchtemann, R. Danz, T. Meyer, A.J. Chatten, D. Farrell, K.W.J. Barnham, J.A.M. van Roosmalen, "The luminescent concentrator illuminated", Proceedings of the society of photo-optical instrumentation engineers, 6197 (2006)

Chapter IV
Conclusions and Future developments

IV.1 Conclusions

The research described in this thesis was focused on the the study of the degradation under UV exposure of an OLSC, and on the fabrication of an OLSC device. The degradation process was performed by the exposure of the samples under UV light, and then monitored through spectroscopic techniques. Such analyses were performed on samples obtained by the deposition through spicoating of the carrier matrix (PMMA), of dye alone and of the dye mixed in PMMA.

In order to produce a short term degradation process on the samples, a 500W UV lamp was adopted.

UV-vis and FTIR spectra of degraded PMMA samples were collected.

UV-vis technique showed an increase of absorbance at 250-350 nm range in the spectra of the degraded samples. Around 275 nm a new absorption band is formed after UV exposure and can be explained by the formation of an unsaturated group in combination with carbonyl groups. The main peak centered at about 230 nm in the spectrum of pristine PMMA undergoes a blue shift increasing at longer exposure times. An increase in intensity in the spectrum of PMMA after 1h of UV exposure is observed. This feature may be attributed to changes in optical properties of the thin film. For longer UV irradiation times, spectra exhibit a decrease in absorbance. This may be due to partial loss of material during irradiation.

The UV exposure effects on PMMA samples were also studied through FTIR spectroscopy. Although a general reduction of all peak intensities is found in the whole spectrum, the formation of new species can be observed at about 3500 cm^{-1} and from the broadening of carbonyl region (1900-1600 cm^{-1}) adjacent to the main peak centered at 1731 cm^{-1}. The absorbance of the main carbonyl peak centered at 1731 cm^{-1}, attributed to the stretching of C=O bond, decreases continuously during irradiation but simultaneously the development of carbonyl shoulder at 1754-1760 cm^{-1} takes place.

The organic dye (Lumogen F Red 305) was deposited alone as thin film and also

analyzed by spectroscipic techniques. Through the comparison with UV-vis and FTIR spectra of similar molecules, peaks related to the perylene core and to the lateral substituents were identified.

UV-vis spectra of degraded dye samples were collected. A decrease of intensity for the absorption peaks attributed to the perylene core absorption and to the lateral substituents absorption can be observed. In addition, a 5 nm red shift is found for the main absorption peak from 568 nm to 573 nm. As the main absorption peak was attributed to the perylene core absorption, the observed red shift is probably due to a loss of conjugation.

In addition, FTIR spectra of dye-only samples exposed to UV light were also collected. A general decrease of all peak intensities is found in the whole spectrum. In addition, in the carbonyl region degraded dye-only samples exhibit a wide band at around 1775 cm^{-1} whose intensity progressively increases upon UV-exposure time. As this band is still in the carbonyl region, it may be assigned to stretching vibrations of C=O bonds of new oxidized species formed during irradiation.

Spectroscopic analyses were performed on the OLSC luminescent material, obtained by mixing the fluorescent dye in PMMA, and named in degradation studies PL6. UV-vis spectra of PL6 samples exposed to UV light show, according to dye-alone UV-vis spectra, a general decrease in absorption intensity. In addition, the peak attributed to the absorption of the perylene core undergoes a 8 nm red shift with respect to the spectrum of dye-only as the maximum in the spectrum of the dye alone is at 568 nm while in PL6 is at 576 nm.

The comparison between the FTIR spectra of pristine PMMA and of pristine PL6, three peaks attributed to the dye were found. The degradation of the PL6 films leads to an increase of the signals in the 3500 cm^{-1} region accompanied by the appearance of two bands in the carbonyl region adjacent to the main peak (1731 cm^{-1}), as also found in the degradation of PMMA. In addition, a general decrease of the peaks associated to band vibrations in the PMMA molecule is observed. The peaks attributed to vibrations in the dye molecule exhibit a progressive decrease of intensity at increasing exposure to UV-light, as also reported for the dye-only films. However, different rate of intensity decay are observed.

Fluorescence spectra of both dye-only and PL6 thin films showed a decreasing in intensity with increasing exposure times. In addition, the structure of the spectra of both pristine materials excited at 445 nm and 540 nm were similar, suggesting that only one group is responsible for the emission phenomenon. This feature was also verified by the analyses of the ratios calculated between the emission intensity maxima of degraded samples whether excited by 445 nm light or by 540 nm light, as no different degradation trends are observed.

In UV-vis and FTIR spectra analyses, degradation processes can be monitored by examining the ratios between characteristic bands. In particular, a faster decay was observed for the signals attributed to the lateral substituents with respect to the perylene core. In addition, abrupt changes in the spectroscopic characeristics were observed for the dye mixed with the polymer matrix. Conversely, a much slower degradation was exhibited in the dye-only films.

Additionally results by UV-vis PL6 spectra that could further confirm the supposed degradation mechanism were obtained by subtracting spectra of the sample degraded at different irradiation times from the pristine spectrum of the dye.

Finally, the spectroscopic analyses suggest stability of Lumogen F Red 305 to UV irradiation when exposed as dye-only film and instability of the dye when dispersed in the polymeric matrix. The hypothesis of the stability of Lumogen in dye-only samples was also verified by DSC and 1H-NMR analyses performed on dye-only samples. The reason of the instability of the dye mixed in the polymer matrix may be the absence of crystalline order of the dye molecule when mixed in the binder. Indeed, the amorphous phase of the dye, present in higher amounts in dye doped polymer films, may undergo a faster degradation process. Conversely, due to higher crystallinity, dye-only films are able to exhibit relatively high stability to UV-exposure.

In conclusion, the comparison between the spectra of degraded PMMA thin films and the spectra of degraded PL6, suggest that the organic dye acts as UV-absorber during the irradiation process of the OLSC thin film, thus protecting the polymer matrix, as PMMA thin films degrade faster than PL6 films.

The fabrication of the OLSC mounted device was performed by coupling an OLSC to a Si PV cell, by a thermosoftening adhesive. The fabrication presented several realization inaccuracies. Firstly, the provided cells showed low and variable values of FF. In order to obtain repeatability in efficiency values, higher quality PV cells are needed.

In order to obtain perfect perpendicularity between the OLSC and the cell, a steel square was used. Good heat tranfer could be ensured between hot plate and the thermosoftening adhesive together with excellent control of the planarity of the system.

Electrical measurement firstly on bare cells and then on OLSC mounted devices were collected in order to evaluate the gain in efficiency due to the addition of the OLSC. In order to optimize the OLSC-mounted device efficiency, dye concentration and thickness of the luminescent thin film were independently studied.

A complete analysis was performed in the study of the dependence of the electrical efficiency on the OLSC mounted device. According to the theory, two divergent trends are observed. For lower dye concentrations, an increasing efficicency at increasing dye concentration was observed. The increase of the dye concentration permits the conversion of a higher quantity of photons, corresponding to an increase in efficiency until it reaches a maximum in efficiency. Secondly, an decreasing trend is found. It is due to reabsorption losses, as an increase of dye particles in the carrier matrix leads to a growing probability of reabsorption.

The analyses on the dependence of the electrical efficicency of the OLSC mounted device on the luminescent film thickness were preliminary, as only the initial increasing trend is observed.

IV.2 Future developments

The results obtained in this work represent a starting point for further investigations.

FTIR spectra of the three analyzed samples (PMMA, dye-only and PL6) after UV exposure, show new peaks in the carbonyl region. This feature suggests the appearance of new oxidized species, which may be due to the presence of O_2. Therefore, in order to better define the degradation process, the investigation of the role of O_2 may represent a key feature.

In this research all the reported tests were carried out in air, without O_2 control. In order to understand the role of O_2, degradation tests in N_2 were also performed (data not shown), although no significant differences were found. The samples during UV exposure were contained in a metal box. As tests of the leakage of the metal box were not carried out, the similarity between the degradation trends do not represent an indicator of the indipendence of the degradation process on the presence of O_2.

As the dependence on the presence of O_2 can be an important feature in the degradation process several applications can be adopted in order to ensure the impermeability from O_2. Preliminar studies were carried out. In particular, SiO_2 thin films were deposited onto the PL6 thin film. The sol-gel method was used to prepare the SiO2 thin films. The precursor solutions were obtained by solving various concentrations of TEOS and 3-aminopropyltrimethoxysilane (APTMS) in ethanol. A solution of H_2O and HCl was added in different amounts as a catalyst for the hydrolysis. After 30 minutes of magnetic stirring, the transparent solutions were spincoated onto the PL6 thin films and cured at 120°C for 1h. Neverthless an evident surface cracking of the PL6 films due to a fast solvent evaporation was observed. In order to avoid this behaviour, further investigations will be needed, in particular

focusing on the optimization of the components relative amounts in the precursor solution.

In order to prevent the radicalic photodegradation of PMMA exposed to UV light, the Tinuvin 123 and Tinuvin 292 HALS compounds were adopted in this work. According to the manifacturer, both can be used for the protection of termoplastic acrylics, and therefore both were used as potential stabilizing agents for the polymeric binder. Firslty was verified their solubility in CHCl3 then were mixed in low concentrations in the $CHCl_3$ solutions of PL6 and PMMA. Thin films were then realized by spincoating and exposed to UV light at increasing times, and spectroscopic analyses were carried out. As a result, no differences in degradation trends collected on the samples containing HALS comparated to those of PL6 and PMMA without additives are found. This is probably due to the chosen photodegradation source, which probably leads to an abrupt photodegradation of the material in shorter times than the HALS activation times. In order to take advantage of the radical scavenging realized by HALS, longer times may be necessary, which requires therefore a less pronounced degradation and then a different light source.

The efficiency measurements of an OLSC mounted device showed low repeatability. This was ascribed to the commercial grade of the employed solar cells and to the inaccuracies that may occurr in the bonding stage. In order to overcome the low repeatability, firstly higher quality solar cells are needed in order to obtain more accurate electrical values. Secondly, optimizations of the linkage stage should be implemented. In this work, due to the application of the steel square almost perfect perpendicularity was reached. Special attention could be given to the thickness of the thermosoftening film employed as adhesive as it can be responsible for photon losses before the light collected by the OLSC reaches the active surface of the solar cell.

The performed study on the dependence of the electrical efficiency on the dye concentration and the thickness of the luminescent layer represent the basis for further more in-depth analyses. The OLSC realized can be optimized in relation with the active surface area of the OLSC, the application of backreflectors and side coatings on the glass substrate.

Side coatings on the glass substrate edges which are not linked to the cell, must provide almost complete reflection to light, in order to promote the total internal reflection of light within the thickness of the glass substrate.

Conversely, backreflectors must provide wider reflections which can lead to enhanced light confinement within the glass waveguide. In this work a white mat cloth was employed as backreflector. White paints or high efficiency resins with TiO_2 pigments dispersed in it.